AN INVESTIGATION INTO STRAIGHT PIPE PRESSURE DROP AND FLOW-MODE TRANSITION CRITERIA FOR FLUDISED DENSE-PHASE PNEUMATIC CONVEYING SYSTEMS

A

THESIS

Submitted in partial fulfillment of the requirement for the award of degree of

Master of Engineering

In

Thermal Engineering

Submitted by

ANUJ BANSAL

(ROLL NO. 801083004)

UNDER THE GUIDANCE OF

Dr. S.S. MALLICK

(ASSISTANT PROFESSOR)

DEPARTMENT OF MECHANICAL ENGINEERING

THAPAR UNIVERSITY, PATIALA

JULY 2012

CERTIFICATION

I, Anuj Bansal, declare that this thesis, submitted toward fulfillment of the requirements for the award of Master's degree in Thermal engineering, in the Mechanical Department, Thapar University, Patiala, is wholly my own work. This document has not been submitted for any degree at any other institution.

Date: 10/7/2012

Place: PATIALA

Anuj Bansal

801083004

Thapar University, Patiala

This is to certify that the above statement made by the candidate is correct and true to the best of my knowledge

10/7/12

Supervisor:
Dr. S.S. Mallick
Assistant Professor
Mechanical Engineering Department
Thapar University, Patiala

Countersigned by

Prof. Ajay Batish
Head of the Mechanical Engineering Department
Thapar University, Patiala

Prof. S. K. Mahopatra
Dean of Academic Affairs
Thapar University, Patiala

ACKNOWLEDGEMENT

I wish to express my deep sense of gratitude and indebtedness to Dr. S.S. Mallick, Department of Mechanical Engineering, Thapar University, Patiala, for introducing the present topic and for his inspiring guidance, constructive criticism and valuable suggestion during this work.

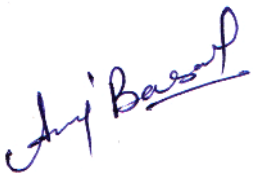

Anuj Bansal

801083004

Thapar University, Patiala.

ABSTRACT

This thesis presents results from an investigation into the pneumatic conveying characteristics (PCC) for horizontal straight pipe sections for fluidised dense-phase pneumatic conveying of powders. Two fine powders (median particle diameter: 30 and 55 μm; particle density: 2300 and 1600 kg m^{-3}; loose-poured bulk density: 700 and 620 kg m^{-3}) were conveyed through 69 mm I.D. × 168 m, 69 mm I.D. × 148 m, 105 mm I.D. × 168 m and 69 mm I.D. × 554 m pipelines for a wide range of air and solids flow rates. Straight-pipe pneumatic conveying characteristics obtained from two sets of pressure tappings installed at two different locations in each pipeline have shown that the trends and relatively magnitudes of the pressure drops can be significantly different depending on product, pipeline diameter and length and location of tapping point in the pipeline (indicating a possible change in transport mechanism along the flow direction). The corresponding models for solids friction factor were also found to be different. There was no distinct Pressure Minimum Curve in any of the straight pipe PCC, indicating a gradual change in flow transition (change in flow mechanism from dense- to dilute-phase). For total pipeline conveying characteristics, the shapes of the PCC curves and the location of the Pressure Minimum Curve were found to be significantly influenced by pipeline layout (e.g. location and number of bends) and not entirely by the dense- to dilute-phase transition of flow mechanism. One existing dilute phase model has been modified by taking into account the particle-particle collision effect and it has been evaluated under different scale–up conditions (for diameter and pipe length scale-up conditions).

Keywords: dense-phase, pneumatic conveying, pressure drop, straight pipe conveying characteristics, pressure minimum curve

TABLE OF CONTENT

CHAPTER 1: Introduction and Objectives

1.1 Introduction

A pneumatic conveying system is a technique by which bulk materials of almost any type are transferred using a gas/air as the conveying medium from multiple sources to multiple destinations (Ratnayake, 2005). Air is the most commonly used transporting medium. Pneumatic conveying is done either by positive pressure system: in pressure system solid particles are conveyed using positive pressure or by suction/vacuum system: in vacuum system solid particles are conveyed using negative pressure system. Pneumatic systems are completely enclosed (Mallick, 2010). Product contamination, material loss and dust emission (thus, environment pollution) are reduced or eliminated. In general, pneumatic conveying system falls into two main categories on the basis of flow mechanism: dilute phase, dense phase. Dilute-phase conveying is the process of conveying air-suspended materials by maintaining a sufficient gas velocity. Dilute phase conveying is characterized by low product to air mass flow ratio. Dense-phase system is characterized by low velocity and high product to air ratio (Ratnayake, 2000). Pneumatic conveying of fine powders, especially for fluidised dense-phase is becoming increasingly popular in various industries such as power, cement, chemical, pharmaceutical, alumina, limestone, refinery, due to the reasons of high efficiency, reduced gas flows and power consumption, improved product quality and increased workplace safety (Mallick, 2010). A list of industrial fields where it has extensively been used is chemical process, pharmaceutical, mining, agricultural, mineral and food processing industry (Ratnayake, 2005; Kalman and Rabinovich, 2010).

However in spite of such potential use or merits of fluidised dense-phase mode of conveying wide spread use of such technology is still limited as fundamentally understanding the flow

mechanisms (and design) have made only limited progress so far due to the highly complex and turbulent nature of the moving bed of fine powders. One important parameter which the designer must know before designing an industrial system is the material flow characteristics (such as the minimum conveying condition, pressure drop for different gas and dense to dilute transition criteria). Such information (dense to dilute transition) is represented using straight-pipe PCC (Mallick, 2010).

Pneumatic conveying characteristic (PCC) is a representation of a given product that is being conveyed pneumatically through a particular pipe i.e. variation of pressure drop for a given flow rate. It may be considered as the "performance curves" similar to pump, fan and blowers (Wypych, 2005).

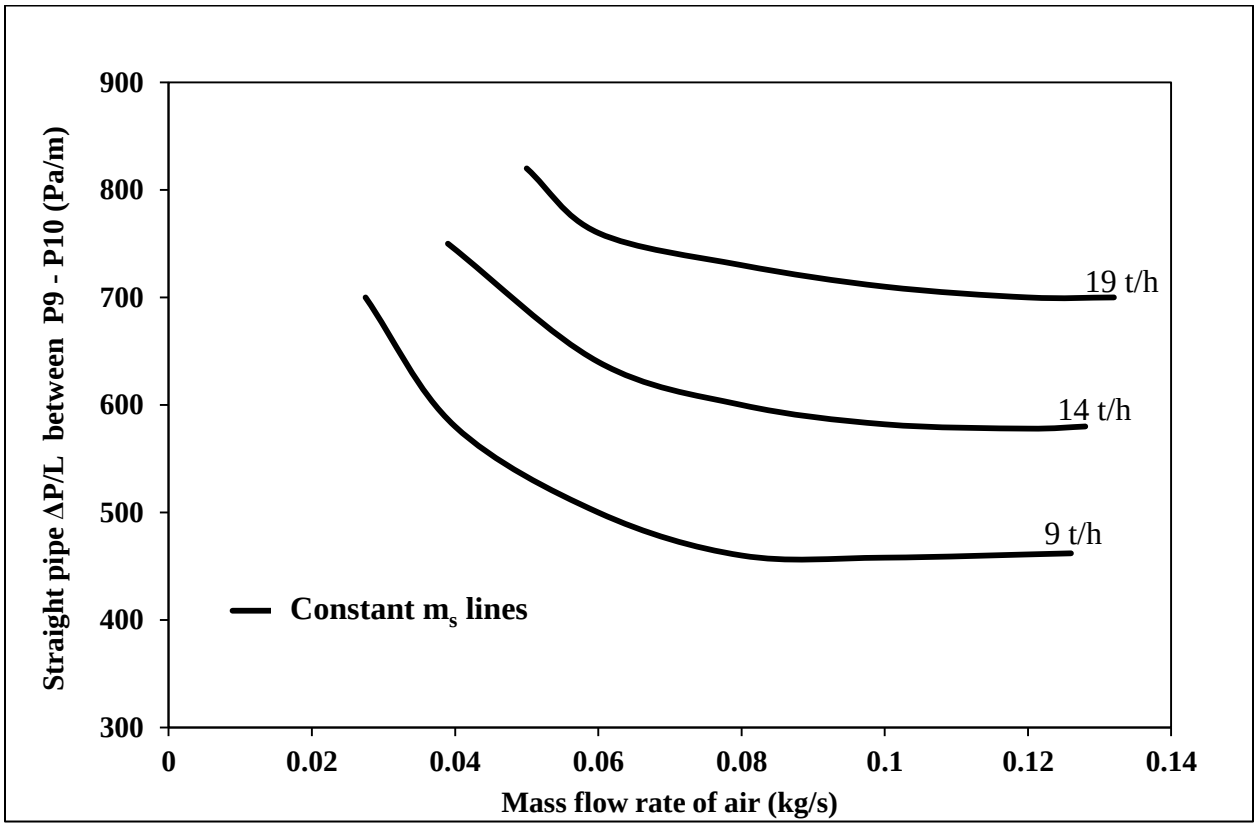

Figure 1.1: Typical straight pipe PCC for Fly Ash and 69 mm ID × 168 m Pipe (Mallick, 2010)

The PCC drawn for a pipeline is a plot of the pipeline pressure drop (ΔP) or pressure gradient (ΔP/L) for horizontal straight pipe section or total pipe in y-axis versus the mass flow rate of gas (m_f) or superficial gas velocity (V_f) in x-axis. The Figure 1.1 shows a typical "straight pipe" PCC, pressure drop per unit length (ΔP/L) versus mass flow rate of fluid (m_f) for fly ash and 69 mm ID × 168 m pipe test rig (Mallick, 2010). Pneumatic conveying characteristics (PCC) constitute an essential requirement for the reliable design of pneumatic transportation systems (Wypych and Arnold, 1985; Mallick, 2010). Steady state pipeline conveying characteristics can provide valuable information, such as: the expected mode of flow condition (dilute/dense-phase) for a particular combination of m_s and m_f, minimum conveying air velocity (either for dense- or dilute-phase) and the optimal operating conditions for a given product (e.g. based on the location of the pressure minimum curve) (Mallick, 2010). PCC is also used to analyse the properties of different powders (like particle diameter and velocity) in powder technology (Kalman and Rabinovich, 2008, 2009). Further details of the importance of PCC to design or evaluate a proposed plant or for troubleshooting existing pneumatic conveying systems are provided in Wypych and Arnold s(1985) and Wypych (1989).

Although numerous PCC for the total pipe line have been published over the years by various researchers (Wypch, 1989 to Mallick, 2010), only limited work have been carried out to study the straight-pipe PCC or modelling the dense to dilute transition criteria for fine powders in FDP (Mallick, 2010). Therefore further studies are to be carried out to determine the dense to dilute transition criteria (e.g. using "straight-pipe" PCC) for FDP.

1.2 Objectives

Specific objectives include:

i) To examine the variation of PCC with the change in pressure tapping locations along the line (i.e. change in flow mechanism along the flow direction).

ii) To develop a model to determine dense (non-suspension to suspension) flow mode transition criteria

iii) In the later part of this thesis, efforts were made to develop straight pipe pressure drop model.

CHAPTER 2: Literature Review

The purpose of this chapter is to present a review of the various studies conducted over the years (by different researchers) on the subject of flow mode transition criteria for pneumatic conveying system or related to the pneumatic conveying characteristics and pressure drop. Initial studies conducted during the thesis work were related to the general concepts and design considerations of pneumatic conveying systems. Afterwards the studies regarding flow mode transition criteria, minimum conveying velocity and pressure drop (expression for solid friction factor) were carried out in the mean while. The brief details about these studies are listed underneath:

2.1 Pneumatic conveying and its components

Pneumatic conveying is a technique by which bulk materials (almost any type) are transferred using a gas flow (conveying medium) from multiple sources to multiple destinations (Ratnayake, 2005). The materials to be transported are forced through closed pipes by conveying medium (provided by positive or negative pressure) and finally separated (with the help of cyclones, bag filters, electrostatic precipitators) from gas and gathered at final destination (Ratnayake, 2005). The bulk materials exist in different forms including lump, powder, granules, chips, and pallets. These materials require reliable material handling systems during their transportation. Coal and fly ash in thermal power plants, sugar, flour, and chocolate powder in food processing plants, zircon and zirconium hydro-oxide in nuclear power plants are well-known bulk materials (Mallick, 2010).

The pneumatic conveying system are totally enclosed, as a result relatively clean, more secured, more environmental friendly, flexible in terms of rerouting and expansion (i.e. products can be coved through bend and vertical lengths) (Mallick, 2010). Pneumatic conveying system as

explained by Ratnayake (2005) comprises of four different zones where distinct operations are carried out. In each of these zones, some specialised equipments are required for the successful operation of the plant. These components are discussed below:

- Conveying gas supply: Various types of compressors, fans, blowers and vacuum pumps are used as the prime mover for providing necessary energy to the conveying gas (Ratnayake, 2005).
- Feeding mechanism: To feed the solid to the conveying line, a feeding mechanism such as Venturi feeder (very low pressure < 20 kPa), rotary valve (Low pressure < 100 kPa), screw feeder (Medium pressure: 100 to 300 kPa), Vacuum nozzle (negative pressure) and Blow tank (High pressure: 300 to 1000 kPa) are used (Ratnayake, 2005).

- Conveying line: This consists of all straight pipe lines of horizontal and/or vertical sections, bends and other auxiliary components such as valves.
- Separation equipment: Cyclones, bag filters, electrostatic precipitators are usually used in the separation zone to separate solid from the gas stream in which it has been transported (Ratnayake, 2005).

2.2 Types of Pneumatic Conveying

The pneumatic conveying can be classified into two main categories, on terms of flow mechanism: namely the dilute and dense phase (Mallick, 2010).

Dilute Phase

This process uses a relatively large amount of air or gas to convey a relatively small amount of material (Wypych, 2006). The dilute phase is characterized by relatively high velocities (approx. more than 8 m/s) and low mass load ratios. In this mode, the bulk material is carried by an air stream of sufficient velocity to entrain and re-entrain it for a distance, which depends on the available pressure (Ratnayake, 2000). There is virtually no limit to the range of materials that can be conveyed with dilute phase system. Products commonly conveyed in dilute phase systems include flour, resins, specialty chemicals, ground feeds, and granular and palletized products. A dilute phase system will generally be lowest in capital cost as compared to other systems. The schematic diagram of dilute phase is shown in Figure 2.1.

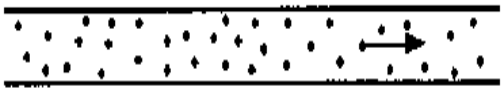

Figure 2.1: Dilute-phase pneumatic conveying

Dense Phase

In a dilute phase conveying system, the product is transported by lift, or suspension of the individual particles in the gas stream. As the velocity is subsequently reduced, the larger particles cannot sustain this lift and they begin to fall from suspension to the bottom of the pipe. The

velocity at which particles fall from suspension from the air stream is "saltation velocity" (Wypych, 2006). Unlike dilute-phase conveying systems that typically use larger amounts of air to move relatively small amounts of materials at high velocities in suspension, dense-phase offers the advantage of efficiently "pushing" a much denser concentration of bulk solids at relatively low velocities through a conveying line. The best, single description for identifying if a system is dense phase is whether the product velocities in the pipe are designed to be operating below the saltation velocity. The dense phase pneumatic conveying systems uses low volume, medium pressure air stream and relies on a continuously expanding volume of air pushing cohesive slugs of material along the pipe (Ratnayake, 2000). The schematic diagram of dense phase is shown in Figure 2.2.

Figure 2.2: Dense-phase pneumatic conveying

Dense phase is very popular as it has advantages like high efficiency, reduced gas flows and power consumption, improved product quality and increased workplace safety (mallick, 2010). Dense phase is further classified into following different modes:

- Fluidized dense phase: Fluidised dense-phase, is considered often as the most reliable and efficient method of conveying certain powders or fine granular bulk solids over distances ranging from only a few metres up to 2 km. It takes advantage of the fluidisation and air retention properties of the bulk material (Mainwaring et al., 1987).

- Low velocity slug flow: This mode of dense-phase pneumatic conveying (Wypych et al., 1990), has been developed to allow friable and/or granular products to be conveyed with extremely low levels of particle damage (e.g. sugar, poly pellets, wheat and duralina) and also system damage (e.g. bend wear) (Pan et al., 1994).
- Low velocity plug flow: The low velocity conveying systems typically transport the product as a series of discrete plugs. At first glance, this mode of flow (Wypych et al., 1990) appears similar to low velocity slug flow. However, the main differences are that low velocity plug flow does not produce a stationary layer of material. It is most suited to cohesive or sticky powders
- Bypass conveying: The gritty bulk materials (e.g. alumina, poly powder, fine sand, coarse fly ash) usually display good fluidisation behaviour, they also dearate quite quickly (especially compared with the powders suited to FDP) and generate high friction forces when allowed to build up inside the pipeline. Hence, it is usually necessary to employ dilute-phase for such materials and also purge the pipeline prior to any shut-down operation. However, by employing specially designed bypass technology, it is still possible to convey such materials in dense-phase. Various types of bypass technology are available (Klintworth and Marcus, 1985).
- Single slug conveying: This dense-phase mode involves the transportation of a limited batch of material per conveying cycle. A detailed description of this method of transport together with typical performance results has been presented by Wypych and Arnold (Wypych and Arnold, 1989).
- Extrusion flow: Occasionally, it may be beneficial to maintain the total conveying pipeline full of material and produce an extrusion mode of flow. Usually,

specially designed blow tank feeders are employed for this purpose. It is used to convey meat lumps for canned dog food, chopped fish chunks and gravy (Wypych and Arnold, 1989).

- Air assisted gravity conveying: Air-assisted gravity conveying (Ashenden et al., 1995) is actually one of the most efficient modes of dense-phase due to its relatively high solids loadings, low conveying velocities and low specific air power requirements. For example, a Roots-type blower or even a centrifugal fan is only required, as opposed to a compressor that quite often is selected for the other modes of dense-phase

2.3 Design Consideration of pneumatic conveying.

Two parameters, "pressure drop along the line" and "minimum conveying velocity" play major roles during the design of reliable pneumatic conveying systems. So, one should accurately determine the above two parameters, prior to the design of pneumatic conveying system. The literatures related to the above two parameters were studied during the thesis and discussed underneath:

In order to calculate the compressor sizing (pressure developed) for the pneumatic conveying system, one has to calculate the pressure drop along the line of the pneumatic conveying system. Barth proposed a relation for calculating the pressure drop along the straight pipe.

$$\Delta p = \frac{(\lambda_f + m^* \lambda_s) L \rho V^2}{2D} \qquad (2.1)$$

The above equation 2.1 was also used by Stegmaier (1978), Rizk (1976,1982), Wypych (1989), Pan (1992), Pan and Wypych (1998) Jones and Williams (2003), Williams and Jones (2004) and Mallick (2010).

Rao (1975) proposed a simple and reliable correlation for predicting the gas-solids flow pressure drop under dispersed phase flow conditions using the principle of similarity and model theory. They developed the equation for the gas-solids friction factor, as per the requirement for dynamic similarity for two phase flow and the validity of this approach had been checked by utilizing the available pressure drop data. The gas-solid friction factor model obtained by him using power function method is as given below:

$$f_{g-s} = 0.046Re^{-0.2}(1 + \overline{m^*})^{0.296} \tag{2.2}$$

The proposed correlation could be used to calculate the pressure drop of a solids-laden gas stream flowing in the pipe, knowing the Reynolds number and the solid-gas loading ratio.

Stegmaier (1978) had worked on an innovative idea of using the power function type formats to represent solids friction factor. His work was further considered by Weber (1981) and other researchers. Stegmaier investigated a number of fine and coarse particles, including fly ash, alumina, quartz powder, sand, catalyst for horizontal transport (with particle size and particle density ranging from 15 to 112 μm and 1500 to 4100 kg/m^3, respectively) and established a correlation for solids friction factor, expressed as:

$$\lambda_s = 2.1m^{*-0.3}Fr^{-1}{Fr_s}^{0.25}(D/d)^{0.1} \tag{2.3}$$

From the range of values of Fr shown in the plot of $\lambda_s m^{*0.3} Fr Fr_s^{-0.25} (D/d)^{-0.1}$ versus Fr (Stegmaier, 1978), it seems that Stegmaier had conveyed the products from dilute to dense-phase. However, there appear to be some uncertainties in the definition of Fr_s. Stegmaier (1978) and Weber (1982) used $Fr_s = W_f/(dg)^{0.5}$, whereas Weber (1981) used $Fr_s = W_f/(Dg)^{0.5}$.

Rizk (1982) mentioned that the first pneumatic conveying was used in 1887 to transport the agriculture products and then the pneumatic conveying was developed and used in many industries. The pneumatic conveying on the basis of mass load ratio can be divided into two main type's namely dense and dilute phases. Rizk (1982) explained that the dilute-phase is characterised by relatively high velocity and low mass load ratio and the pressure drop per unit length along the line was low. Dense phase was described by low velocity, high mass loading ratio and having high pressure drop per unit length along the line. According to him, these two can be distinguished using the pressure minimum curves in the PCC plots. The pressure minimum curves were drawn by connecting all the minima values for different mass flow curves in the PCC. Rizk (1982) attempted to identify the factors that contributed to the overall solids friction factor (λ_s). He mentioned λ_s can be separated into two terms:

$$\lambda_s = \lambda_s{}^* \frac{C}{V} + \frac{2\beta}{Fr^2 C/V} \tag{2.4}$$

Where, $\lambda_s{}^*$ is related to the impact and friction of the solid particles (particle to particle/wall). The term $[2\beta/\{(C/V)Fr^2\}]$ takes into account the influence of weight (i.e. energy loss due to keeping the particles in suspension). β refers to the particle fall velocity in a cloud of particles.

This indicates Rizk (1982) considered the individual particles in suspension to be influenced by its surrounding particles. This model (equation 2.4) was originally proposed by Weber.

Chambers and Marcus (1986) presented a procedure to predict the total pipeline pressure drop by dividing the whole pipe-line into components, i.e. by individually calculating pressure drop in straight pipes, bend loss, vertical lift loss and losses due to the initial acceleration and finally adding the all components to find out the total pressure drop. They presented the following relationships for different components:

Acceleration loss: $$\Delta P_{accel} = \frac{\rho V^2(1+2m^*C/V)}{2} \quad (2.5)$$

Vertical loss: $$\Delta P_V = \frac{m^*\rho g L_V V}{C} \quad (2.6)$$

Straight pipe loss: $$\Delta P = \frac{(\lambda_f+m^*\lambda_s)L\rho V^2}{2D} \quad (2.7)$$

Bend loss: $$\Delta P_b = \frac{NB(1+m^*)\rho V^2}{2} \quad (2.8)$$

Total loss: $$\Delta P_T = \Delta P_{accel} + \Delta P_V + \Delta P + \Delta P_b \quad (2.9)$$

They proposed Stegmaier (1978) model for calculating solid friction factor:

$$\lambda_s = 2.1 m^{*-0.3} Fr^{-1} Fr_s^{0.25} (D/d)^{0.1} \text{ for } d < 0.5 \text{ mm} \quad (2.10)$$

Chambers and Marcus (1986) did not provide any derivation or reference for the bend model. It was stated that the model predicts pressure drop in the straight pipe for wide range of m^* from 2 to 530. However, with increasing value of pipe length, the model performance was observed to get decreased. So it was prescribed to use model for pipe, having length less than 500m. It was

claimed that using $Fr_s = \frac{U_{to}}{\sqrt{gD}}$ instead of $Fr_s = \frac{U_{to}}{\sqrt{gd}}$ may introduce some improvement. In any case, an uncertainty factor of 2 (even within 500 m length) (i.e. error of 500±2 m) cannot be acceptable as a reliable design procedure.

Klinzing et al. (1989) developed a new correlation for solid friction factor in horizontal pneumatic conveying, based on the unified theory of Yang-Mills (it is a classical field theory generalizing Maxwell's equations). They conveyed three types of glass particles (two spherical and one crushed; d 67,450 and 900 μm; ρ_p 2470, 2395 and 2464 kg/m^3) and iron ore flake (d 400 μm; ρ_p 5004 kg/m^3) through two horizontal pipes with ID 0.0266 m and 0.0504 m. Using Yang's unified theory and having the particle velocity as a function independent of λ_s, they proposed following model:

$$\lambda_s = \frac{3C_{ds}\varepsilon^{-4.7}\rho(V-C)^2D}{4(\rho_p-\rho)dC^2} \tag{2.11}$$

Here as per the Newton's regime drag coefficient (C_{ds}) is 0.44 and pressure drop is obtained as:

$$\frac{\Delta P_s}{L} = \frac{2\lambda_s\rho_pC^2(1-\varepsilon)}{D} \tag{2.12}$$

The results from above models were compared with the experimental data and the overall standard relative deviation (SRD) is obtained as 42.1%, which was reported to be better than the original Yang's model.

Keys and Chamber (1995) described the scaling up of pneumatic conveying characteristics. They conveyed different fly ash samples as the test material using different test rig configurations. They used two scaling methods: in the first method the friction loss was calculated using the friction loss for fluid alone and by eliminating the bend effects (calculated as per Chambers and Marcus, 1986) from the total pipeline pressure loss (see equation 2.13). The correlation for λ_s was derived using power function modelling approach with different fly ash samples as the test material using different test rig configurations. The relation is provided in equation 2.14:

$$\lambda_s = \frac{2.\Delta P_e.D}{\rho.L.V^2 m^*} - \frac{\lambda_f}{m^*} \tag{2.13}$$

$$\lambda_s = 1.24\ m^{*-0.3} Fr^{-0.73} \tag{2.14}$$

In the second scaling method, they also included the effect of bends using a bend model. For the horizontal pipe line, the material friction factor was calculated using equation 2.15 and by considering the bend pressure loss the correlation for λ_s was derived as in equation 2.16:

$$\lambda_s = \frac{2.(\Delta P_e - \Delta P_b).D}{\rho.L.V^2 m^*} - \frac{\lambda_f}{m^*} \tag{2.15}$$

$$\lambda_s = 0.75\ m^{*-0.3} Fr^{-0.58} \tag{2.16}$$

Using the above correlation, the predicted values of the pipeline friction drop were calculated within 10% of the measured pipeline pressure loss. Incorporating the effect of d/D, the above correlation was modified to:

$$\lambda_s = 1.24\ \mathrm{m}^{*-0.3}\mathrm{Fr}^{-0.73}(d/D)^{0.1} \tag{2.17}$$

They did not validate their models for length and/or diameter scale-up conditions.

Pan and Wypych (1998) conducted different experiments by conveying four different samples of fly ash (ρ_p from 2197 to 2540 kg/m3; ρ_{bl} from 634 to 955 kg/m3; d_{50} from 4 to 58 μm) in various test rig combinations (D = 52.5 to 105 mm; L = 70 to 564 m) for further research on scale-up test design procedures. It different conveying characteristics were produced by different fly ash samples. Also, the corresponding models for solids friction for horizontal straight pipes and bends proposed earlier (in the form of equations 2.18 and 2.19, respectively) were also found to be different.

$$\Delta\lambda_s = \mathrm{X1}\ (\mathrm{m}^*)^{\mathrm{X2}}\ (\mathrm{Fr_m})^{\mathrm{X3}}\ (\rho_\mathrm{m})^{\mathrm{X4}} \tag{2.18}$$

$$\Delta\lambda_{bs} = \mathrm{Y1}(\mathrm{m}^*)^{\mathrm{Y2}}(\mathrm{Fr_{bo}})^{\mathrm{Y3}}(\rho_{\mathrm{bo}})^{\mathrm{Y4}} \tag{2.19}$$

Where, X1, Y1 are the constants and X2, X3, X4, Y2, Y3, Y4 are the exponents of power function. Combining the data of all four fly ash samples, the following correlations were derived (exponents are quoted up to 2 significant figures):

$$\Delta\lambda_s = 3.2343\,(m^*)^{-0.47}\,(Fr_m)^{-1.56}\,(\rho_m)^{-0.43} \quad (2.20)$$

$$\Delta\lambda_{bs} = 0.0097(m^*)^{0.57}(Fr_{bo})^{0.97}(\rho_{bo})^{-0.62} \quad (2.19)$$

Datta et al. (2003) proposed the pressure drop model for pneumatic conveying by modifying the Darcy's equation (equation used to find, net head loss along the straight pipe due to friction). The pressure drop model proposed comprises of two things (pressure drop due to solids particles and that of gas) as per equation 2.20.

$$\Delta P = \Delta P_f + \Delta P_g \quad (2.20)$$

For straight pipe Darcy equation is modified as:

$$\Delta P = \frac{KL\rho_{sus}V_i^{\,2}}{2D} \quad (2.21)$$

Here K is a constant and its values were calculated using the test data. They conveyed barite (d 12 μm, ρ_s 4200 kg/m^3), cement (d 15.5 μm, ρ_s 3100 kg/m^3) and ilmenite (d 9.5μm, ρ_s 4600 kg /m^3) through three horizontal pipe-lines with pipe diameters: 80, 100 and 120 mm and 70, 66 and 68 m long respectively. The claimed that, the prediction pressure values matched with the test data reasonably well. These models were evaluated by Mallick (2010), the predictions were not coming good.

Williams and Jones (2003) explained the use of the solid friction factor for dense phase pneumatic conveying system. They concluded that the solid friction factor provides a reliable empirical model for predicting the pressure drop along the pneumatic conveying line. They plotted the $\lambda_s m^{*0.9}$ versus the inlet Froude number and provided a relation between them as shown in equation 2.22. They conveyed various powders, such as pulverised fuel ash, iron powder, copper ore and flour (ρs: 1470 to 5710 kg/m3; "mean diameter": 42 to 90 μm) in a test rig (L = 50 m, D = 53 mm, 9 bends), Calculated values of total pipe pressure drops, using the above expression for λ_s, when compared with the measured values, resulted in an average error of only 2% and an associated standard deviation of 12%. This model was evaluated by Mallick (2010), large over-prediction were noted by him.

$$\lambda_s = \frac{83}{m^{*0.9} Fr_i^2} \tag{2.22}$$

Williams and Jones (2004) had done further studies to model solids friction for cement, having diameter of solid particles: 22μm, and fluidised bulk density: 930 kg/m^3. They conveyed the cement in a 50 mm nominal bore pipeline, having length of 176 m with 14 short radius bends. The pressure drop of the system was expressed by the following equation 2.23. Williams and Jones (2004) opted for a combined single friction factor (λ_e) representing losses due to both air and solids. Using a back calculation method, the following model was obtainedas in equation 2.24. Again, it can be observed that the magnitude of "constant" term of the above power function model appears large. Similar modelling using "back calculation" method was further pursued by Williams and Jones (2006), but the above modelling is valid for the dilute phase system. Mallick (2010) had tested these models.

$$\Delta P = (m^* \lambda_e)\, \rho_m\, V_m^2 L/2D \quad (2.23)$$

$$\lambda_e = 104\, m^{*-0.9} Fr^{-2.2} \quad (2.24)$$

Datta and Ratnayaka (2005) presented the experimental findings to show that the pressure drop coefficient (K) for vertical and horizontal pneumatic conveying for a given bulk material follows a certain pattern (i.e. hyperbolic type curve was seen). The pressure drop coefficient for vertical pneumatic conveying for a given material had been claimed to be independent of any variation of particle size distribution, within experimental limits. The model represented in Datta and Ratnayaka (2003) had been tested for eight different quantities of bulk materials. The technique discussed in the paper worked well for both dense-phase and dilute-phase pneumatic conveying situations, as there test results ranged from dense-phase to dilute-phase flow conditions (air velocity ranging from 8 to 20 m/s). The technique discussed did not work well in complete dense-phase situation (air velocity ranging lea than 8 m/s).

Rabinovich and Kalman (2009) proposed a theoretical analysis of the force and moment balance during incipient motion of a single particle, Vander-wall force, drag force and lift forces. The analysis showed that large particles start their motion by rolling for spherical particles and by sliding for non-spherical particles. It was shown that fine spherical or near spherical powders starts their motion by rolling. The theoretical analysis showed that the velocity of individual particles for all fluid, system and particle properties could be presented as power relationships between the Reynolds and Archimedes numbers. The incipient motion velocity of single particles was theoretically investigated. The theoretical analysis was done by comparing the

force and moment balance for different particle size, fluid and conveying system properties. The velocity profile and the pipe diameter effect were obtained using the above calculated forces. The particles like large spherical particles (glass (0.15 to 3.30 mm), zirconium (1.0 to 3.5 mm) and alumina (1.6 to 1.8 mm)) and non-spherical particles (salt (1 to 3.35 mm) and sand (up to 2 mm)) in air and water were examined for the different forces.

Cai et al. (2011) studied the influence of moisture content on conveying characteristics in an experimental test facility. His conveying pressure limit was up to 4 MPa. In their experimental test facility, they took lignite and soft coal with similar particle size and density. With increase in moisture content, decrease in the mass flow rate for lignite (i.e. $3.24\% < M < 8.18\%$) and for soft coal, it first increased and then decreased (i.e. $0.4\% < M < 6.18\%$). They explained the flow ability of the soft coal was worse because of low moisture content than lignite. They emphasised on electrostatic forces that decreased with in the increasing moisture content, because of the conductive properties of water and liquid bridge of coal particles decrease flow ability. Pressure drop of soft coal predicted was larger than that of lignite at similar operating parameters, material properties and mass flow rate.

"Minimum Conveying Velocity" is very useful in appropriately choosing, parts with desired strength and required rated compressor. The literatures studied regarding the minimum conveying velocity are listed below:

Mills (2004) explained that for fine powdered materials, which were capable of being conveyed in dense phase, a conveying region exists in which instability in flow and pipeline blockage

could occur if the pressure gradient available was insufficient to maintain a minimum value of solids loading ratio. He also said that the reduction in material flow rate could also lead to pipeline blockage in this region. He said that for low velocity dense phase conveying, with low pressure gradient values, the location of the conveying limit in the transition region between dilute phase, and the ultimate dense phase limit at 3 m/s, was an essential requirement. In commenting on a blow tank system conveying 120 tonne/h of cement over a distance of 850 m, Schaberg and Mehring (1987) stated that the material was conveyed at a solids loading ratio of 32 and with a conveying line inlet air velocity of 3·72 m/s, which was well below the minimum limit but this was due to the difference in pipeline bore related to a 257 mm single bore pipeline.

Mallick and Wypych (2009) explained that the existing method of representing minimum transport criteria (using V_i as a function of m^*) had been found inadequate of accurately scaling up the unstable boundary. They proposed newly validated improved design criterion based on the Froude number values at the pipe inlet. from the experimental data of eight different samples of fly ash (ρ_s: 2300 kg/m3; "mean diameter": 30 μm), ESP dust (ρ_s: 3637 kg/m3; "mean diameter": 7 μm), "white powder (ρ_s: 1600 kg/m3; "mean diameter": 55 μm)", pulverised coal and cement, conveyed over a wide range of pipe lengths (71 to 554 m) and diameters (52 to 105 mm ID), they found that $Fr_{i,\ min.} \approx 5$ predicts minimum transport limits quite well for products which had "good" fluidised dense-phase characteristics. However they were not sure that the above work is going to be valid for other fine powders.

2.4 Flow mode transition criteria

The flow is changing from dense to dilute phase along the line. So flow mode transition criterion (i.e. dense-to-dilute phase flow transition) is to be specified (Mallick, 2010). The literatures studied regarding the flow mode transition criteria are discussed in the following:

Riez (1982) plotted a PCC for granular products and wrote that the transition from dilute to dense phase conveying was rather smooth, i.e. there was no clear limit in the state diagram drawn by him. According to him, when moving towards the lower velocity end of fluid flow, the dilute-phase changed into the plug flow. In some exceptional cases, it was possible to have a continuous plug flow all through the pipe-line at extreme low velocities, which dissolved then into shorter parts with increase in velocity and it was very hard to obtain a continuous plug flow i.e. one moving part in the pipe (Welschof, 1961; Schroter, 1965).

Pan, Mi and Wypych (1994) conveyed different samples of coal and fly ash (ρ_s 1390 to 2197 kg/m^3; ρ_{bl} 541 to 634 kg/m^3; d_{50} 16 to 41 μm) in various test rig combinations (D = 25.4 to 105 mm; L = 48 to 553 m) to study the conveying characteristics. They explained that fine and granular products have significantly different pneumatic conveying characteristics. According to them, fine products could be usually transported smoothly and reliably from dilute to dense phase, On the other hand, when granular products were conveyed between dilute and dense phase, significant fluctuations in pressure and vibration could occur along the pipeline. They provided correlations to determine the pressure minimum curve (PMC) for fine powders and boundaries between dilute-phase, unstable zone and dense–phase regions for granular products. These correlations were further used for predicting pressure drop along horizontal section of the pipe. The shape of total pipeline PCC (and hence position of PMC) is significantly influenced by the numbers, types and location of bends and verticals in the pipeline. In other words, PMC

based on the total pipeline PCC is very much layout dependent of the particular test rig. Hence, the usefulness of deriving such a correlation for PMC is not very clear. Similar concerns were also raised by Mason et al. (1998).

Rabinovich and Kalman (2010) after performing numerous experimental and theoretical studies defined and characterized possible flow regimes for vertical pneumatic conveying and fluidised dense phase systems. They found that the non-dimensional groups of the Reynolds and Archimedes numbers, the void fraction and the volume concentration of circulating solids were relevant parameters for defining the transition velocities in vertical pneumatic conveying systems. They also empirically derived the operating conditions of classical choking, accumulated choking, minimum pressure, minimum fluidization, minimum bubbling and minimum slugging velocities in order to understand the transitions between various flow regimes. Based on their results, they concluded that all transition velocities follow power law relationships between the modified Reynolds number and Archimedes numbers (Ar), which are as given below.

$$Re_c = 1.24Ar^{0.45} \qquad (2 < Ar < 10^8) \tag{2.26}$$

And

$$Re_{se} = 1.53Ar^{0.5} \qquad (2 < Ar < 4.10^6) \tag{2.27}$$

Here Re_c is related to the fluid velocity for which standard deviation of differential pressure fluctuations reach a maximum value and Re_{se} is related fluid velocity for which the particles are entrained.

Mallick (2010) had drawn a typical PCC. On the basis of PCC he shown that the flow transition from suspension to non-suspension mode for fly ash (suitable for fluidised dense-phase conveying), was relatively gradual, i.e. without any sudden changes in the flow mechanism causing instability, unlike the low-velocity slug-flow of granular products (Wypych and Yi, 2003), where flow transition occurs with large flow/pipe vibrations.

Existing models for PMC (Rose and Duckworth, 1969; Matsumoto, 1974; Rizk, 1976; Weber, 1981; Schade, 1987; Cabrejos and Klinzing, 1994; Kalman et al., 2005) were evaluated for straight pipe PCC and discussed in the appropriate chapters.

From above discussion it was seen that, many researchers (Weber, 1981; Mills, 2004; William and Jones, 2004; Mallick, 2010) worked on calculating pressure drop along the line of pneumatic conveying using the solid friction factor, scaling up pneumatic conveying characteristics for pipe-line, pressure minimum curve and minimum conveying velocity, but very few people investigated into the transition from dense to dilute phase in the case of the fine powders like fly ash, ESP dust etc., also the variation in the PCC with change in flow mechanism along pipe-line (i.e. along flow direction) was not still compared. Riez (1982), Pan, Mi and Wypych (1994), (Wypych and Yi, 2003) and Rabinovich and Kalman (2010) explained the transition from dilute to dense phase but they had done this from granular products not for fine powders.

CHAPTER 3: Evaluation of Existing Model for Flow Mode Transition Criteria

Over the years, most of the conveying characteristics that have been published in the literature for fine powders are based on total pipeline pressure drop (Wypych, 1989; Mills, 2004; Ratnayake and Datta, 2007). Very few work has been reported for straight-pipe conveying characteristics for fine powders in fluidised dense-phase, which may reveal useful information on the flow mechanism (such as dense-to-dilute phase flow transition). The existing method of flow transition (from dense to dilute-phase) seems to be rather general, e.g. 13 – 15 m/s for a wide range of products (Mills, 2004). Such type of generalised approach appears to be questionable considering the significant changes in total pipeline conveying characteristics that the products can exhibit (Wypych 1989, Pan 1992, Ratnayake 2004, Mallick 2010). Most of the existing literature provides pressure drop characteristics for the total pipe line (Wypych 1989, Pan 1992, Ratnayake 2004). Comparatively, limited amount of studies have been conducted till date on the straight-pipe conveying characteristics – where the pressure minimum curve would represent the dense-dilute transition criteria (Marcus et al. 1990, Mallick 2010). Therefore, there is a need for a more in-depth study of the pressure drop characteristics of solids-gas flow through straight-pipe sections (or the straight-pipe pneumatic conveying characteristics, PCC). With such background, the main purpose of this chapter is to investigate the straight-pipe conveying characteristics for different powders, pipelines and pipeline tapping points (different diameter and lengths of pipe and location of tapping points in the pipeline) and achieve a better understanding of the flow characteristics of fluidised dense-phase pneumatic conveying of fine powders also the evaluation of seven existing models for pressure minimum curve for straight-pipes has been done against experimental data.

3.1 Experimental data used in this study:

Test data from the following products were used in this study:

a) Fly ash (Wypych et al., 2005; Mallick, 2010)

b) ESP Dust (Wypych et al., 2005; Mallick, 2010)

c) White powder (Mallick, 2010)

Table 3.1 lists some physical properties of these products:

Table 3.1: Some Physical Properties of the Powders (Mallick, 2010)

Product	ρ_s **(kg/m^3)**	ρ_{bl} **(kg/m^3)**	d_{50}^* **(μm)**
Fly ash (Wypych et al., 2005)	2300	700	30
ESP ash (Wypych et al., 2005)	3637	610	7
White powder	1600	620	55

d_{50}^* = medium particle size.

Power station fly ash and ESP dust were conveyed through 69 mm I.D. × 168 m, 105 mm I.D. × 168 m and 69 mm I.D. × 554 m long pipelines at the Bulk Material Handling Laboratory of the University of Wollongong, Australia by Wypych et al (2005). A schematic of the test set up for the 69 mm I.D. × 168 m long pipeline is shown in Figure 3.1. This test rig comprised:

- Tandem 0.9 m^3 bottom-discharge blow tank feeding system;
- 69 mm I.D. × 168 m long mild steel pipeline, including 7 m vertical lift, five 1 m radius 90° bends and 150 mm N.B. tee-bend connecting the end of the pipeline to the feed bin;
- 6 m^3 receiving bin with insertable pulse-jet dust filter;
- All necessary instrumentation: load cells on feed bin and receiving bin, annubar with differential pressure meter, static pressure measurements via two sets of tapping locations on the straight pipe lengths: P9-P10 (52.68 m apart) and P11-P12 (40.41 m apart).
- Data acquisition unit for data recording and analysis

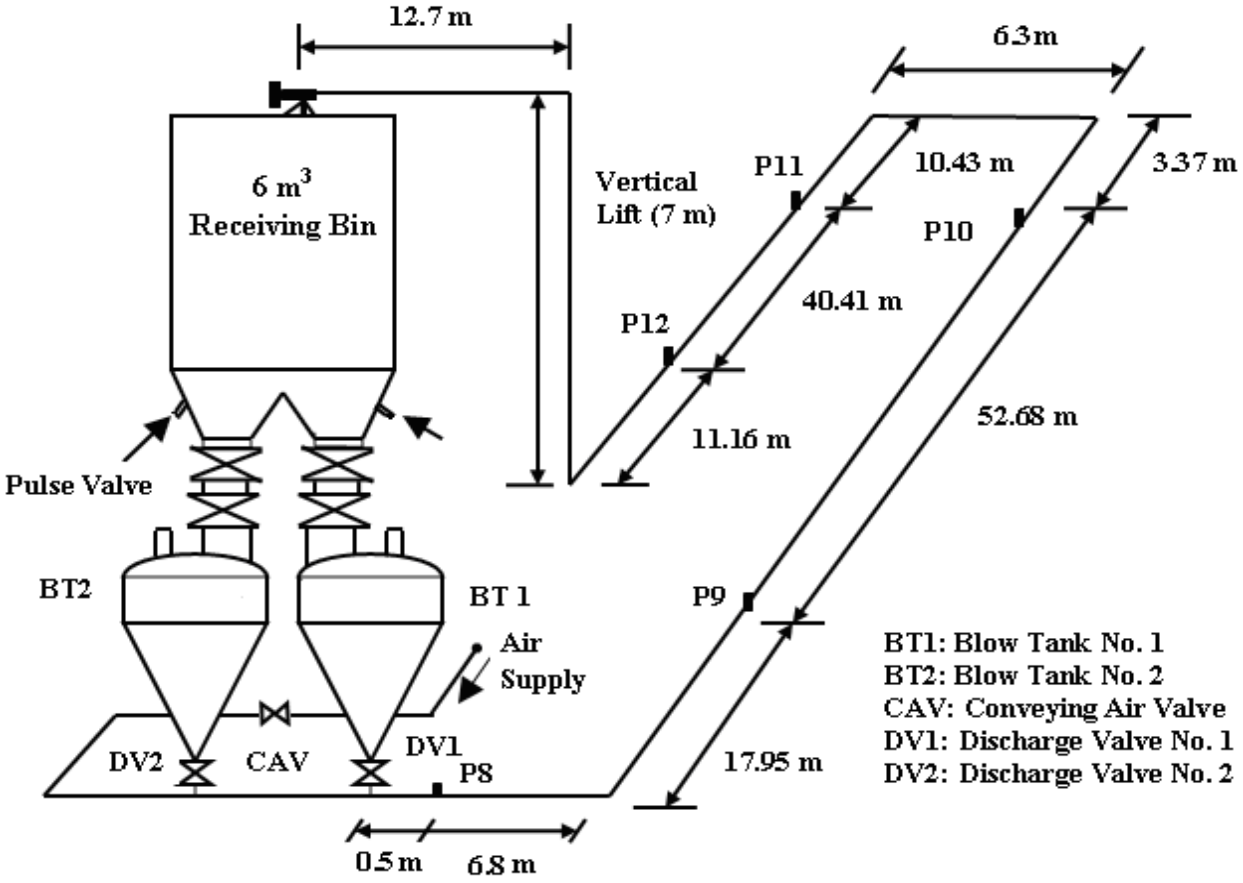

Figure 3.1: Layout of the 69 mm I.D. × 168 m Long Test Rig (Mallick, 2010 and Wypych et al, 2005)

A schematic of the test set up for the 105 mm I.D. × 168 m and 69 mm I.D. × 554 m long pipes (Mallick, 2010 and Wypych et al, 2005) are shown in Figures A1 and A2 (see Appendix A).

The fine "white powder" was conveyed through another test rig (as shown in Figure A3) (Mallick, 2010).

The test facility comprised:

- 0.5 m^3 bottom-discharge blow tank feeding system;
- 69 mm I.D. × 148 m long mild steel pipeline, including 4 m vertical lift, 6 no. 1 m radius 90° bends;
- Static pressure measurements via two sets of tapping locations on the straight pipe lengths: P9-P10 (53.1 m apart) and $P11^+$-P12 (19.9 m apart). The tapping locations were similar to that of the fly ash test rig (described previously), except the new tapping $P11^+$ was introduced almost mid-way between P11 and P12.
- "Sight glass" just after the P12 location (approximate length of 1 m) for flow visualisation. Other arrangements were similar to that of the fly ash rig.

3.2 Pneumatic Conveying Characteristic (PCC)

3.2.1 Method used for plotting the PCC:

Using the steady state conveying data obtained above from the different static pressure tapping points installed along the test rigs for fly ash and white powder, PCC for the pressure drop per unit length were obtained. The format of presentations of PCC's throughout used are plots of

pressure drop per unit length (y-axis) versus mass flow rate of conveying air (x-axis) for different solids flow rates or in some cases the average superficial air velocity is also considered on the x-axis. While drawing the PCC different constant properties (mass flow rate of solid (m_s), Froude number (Fr), velocity of fluid (V_f)) were drawn by using the experimental data. For drawing these constant property lines, the data points were obtained by modifying the actual experimental points. The final PCC were obtained using an interpolation relationship technique used by (Mallick, 2010). In this technique, the experimental data points are first plotted having the axis as shown in Figure 3.2. The experimental data points may not be on constant solids flow lines because even if the solids discharge rate of the blow tank is set to a constant value during experimental work, the actual discharge values may vary to some extent for every test. Interpolation relationship is used with m_f and ΔP_t values of data points, which are close to each other and up/down (i.e. vertically orientation) to get intermediate points for a selected m_s value. Figure 3.2 shows typical examples of some experimental data points. The numbers, such as 19.7, 15.6 etc are the 78 experimental m_s values in t/h. For example, we are using two points as E and F for interpolating a point of m_s as 19 t/h. The point is named as H and lies on the line joining from E to F as shown in Figure 3.3. The following expressions are used to find the intermediate points.

$$\frac{\Delta P_H - \Delta P_F}{m_{s_H} - m_{s_F}} = \frac{\Delta P_E - \Delta P_F}{m_{s_E} - m_{s_F}} \tag{3.1}$$

and

$$\frac{m_{f_H} - m_{f_F}}{m_{s_H} - m_{s_F}} = \frac{m_{f_E} - m_{f_F}}{m_{s_E} - m_{s_F}} \tag{3.2}$$

The data points E (m_f =0.0497 kg/s, m_s = 19.9 t/h and ΔP_t = 148.5 kPa) and F (m_f =0.051 kg/s, m_s = 16 t/h and ΔP_t = 128 kPa), when interpolated using the above expressions to m_s = 19 t/h for point H, results obtained for H are m_s = 0.05 kg/s and ΔP_t = 143.9 kPa.

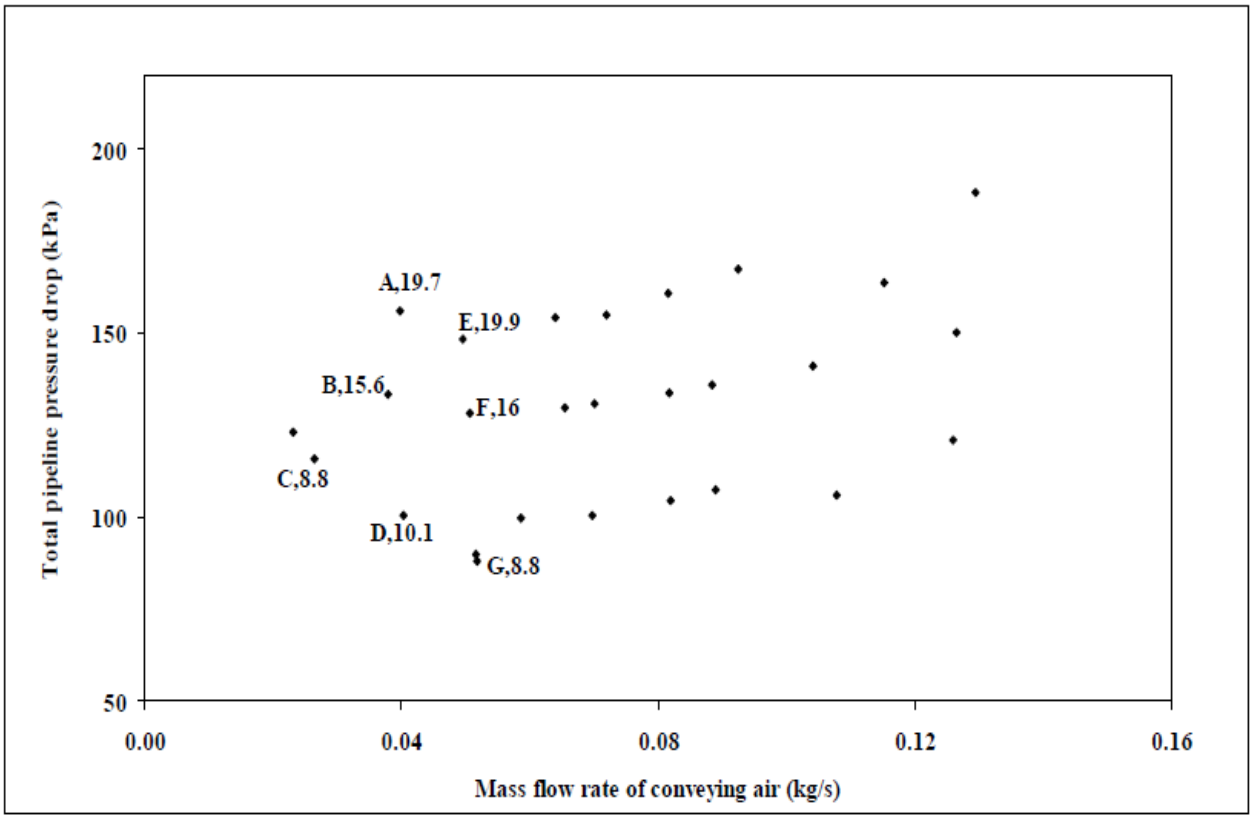

Figure 3.2: Experimental data points for total pipeline pressure loss for fly ash and 69 mm ID × 168 m pipe

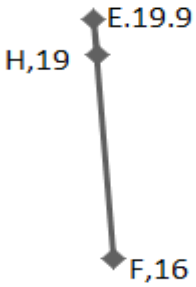

Figure 3.3: Magnifying Image of above for Interpolation

This interpolation was also done for other data points. Most of the points those are vertically oriented were used for drawing constant m_s lines and for constant velocity lines, mostly points those produce horizontal lines were interpolated. Also the points which were very far from each other are not used because it leads to increment in errors. Similar interpolation can be done for other parameters (such as V). Reasonably large numbers of intermediate points were generated for 4, 6, 8, 10 and 12 m/s of initial velocities of conveying as shown in Figure 3.4, so that the trend lines could be drawn through them with sufficient confidence.

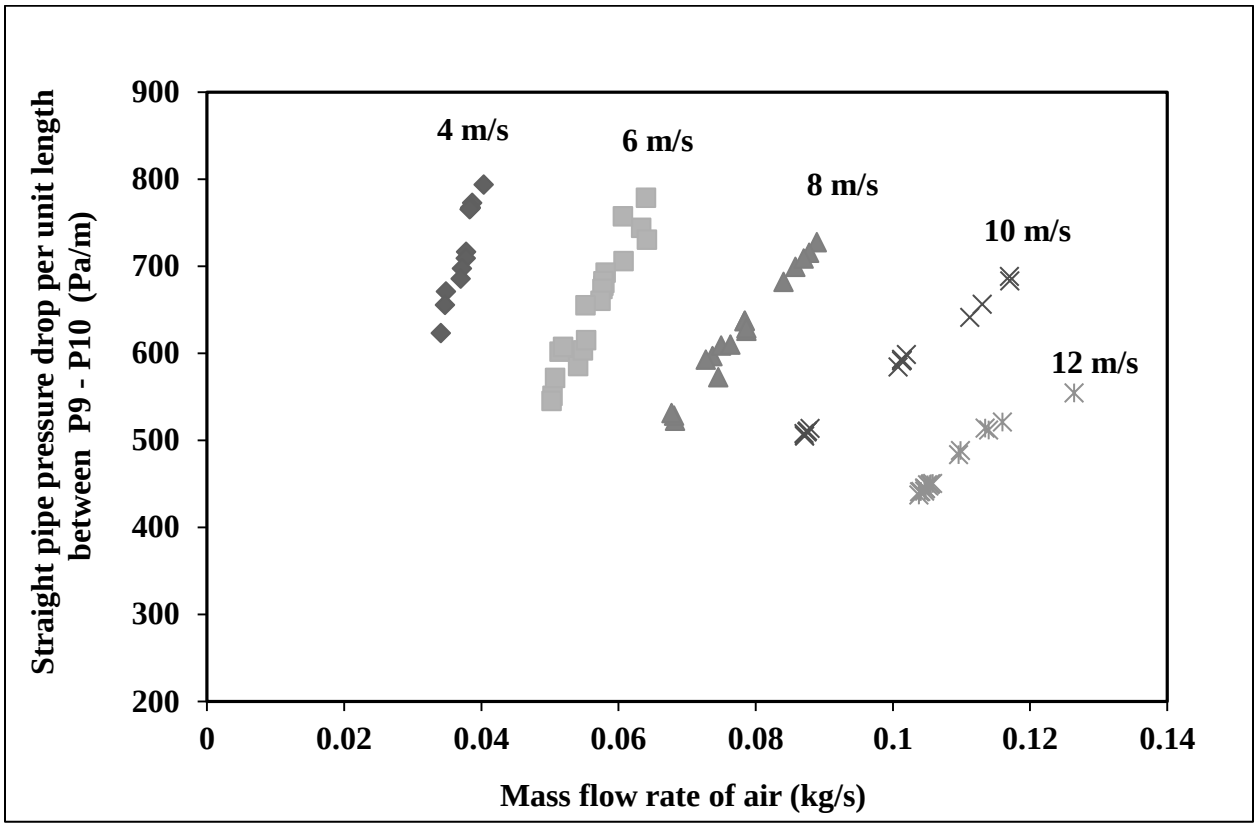

Figure 3.4: Intermediate points for pressure drop per unit length for fly ash and 69 mm ID × 168 m pipe

It was found that the intermediate points were following clear trends without more scattering of data, see Figure 3.4. Now a best approximate line was drawn for that particular property and a PCC is obtained using this method. For example, for drawing a PCC of fly ash between P9-P10 pressure tappings for 69 mm ID and 168 m long pipe, the following steps were used:

Step 1: Using the experimental data, a point graph between pipe line pressure drop per unit length and mass flow rate of air was drawn, as shown in Figure 3.5.

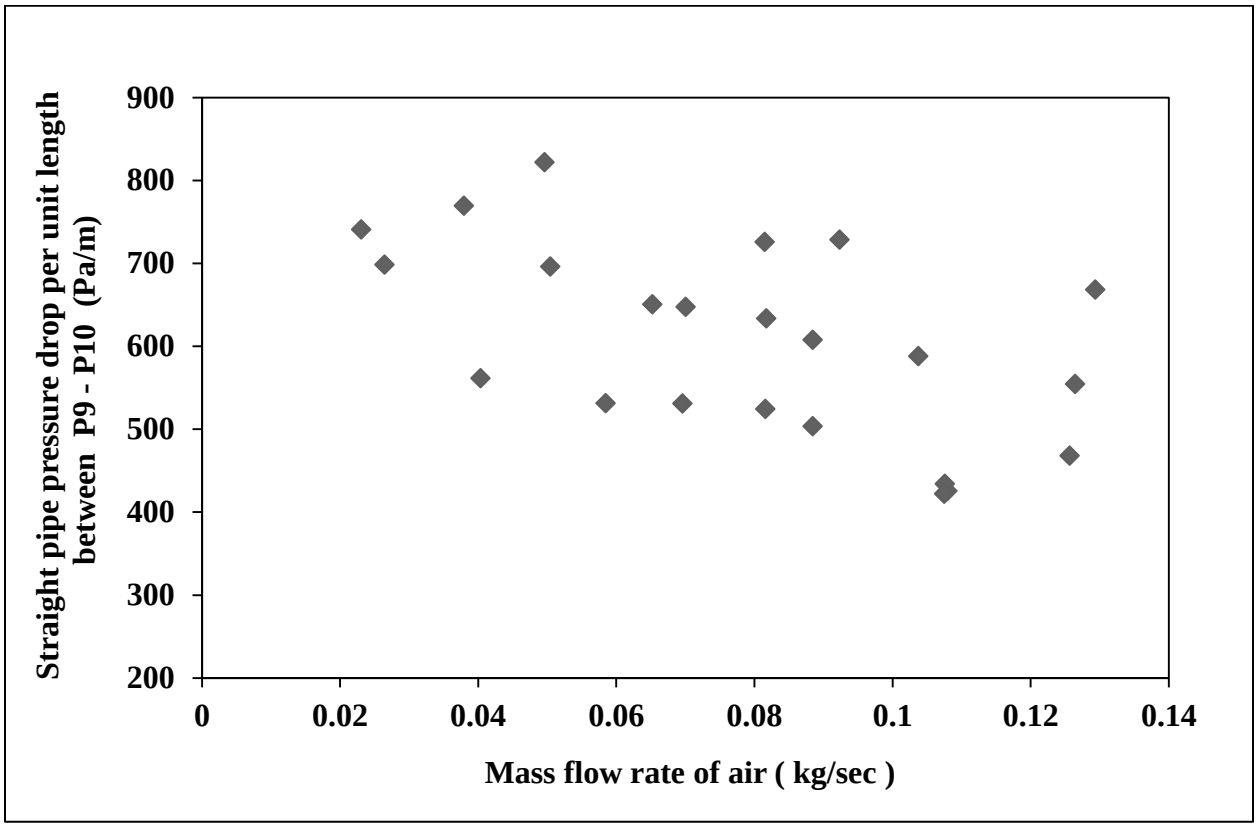

Figure 3.5: Experimental data points for straight line pressure drop per unit length (P9-P10) versus mass flow rate of air for fly ash and 69 mm ID × 168 m Pipe.

The different points in the point graph representing the different values of m_s and for obtaining the constant m_s lines, interpolation of these points was done for m_s values of 9, 14 and 19 t/h. Here most of the points, those lead to vertical lines when joined were used.

Step 2: The interpolation points obtained in the last step were then drawn as shown in the Figure 3.6. These were showing a clear trend for the constant m_s lines.

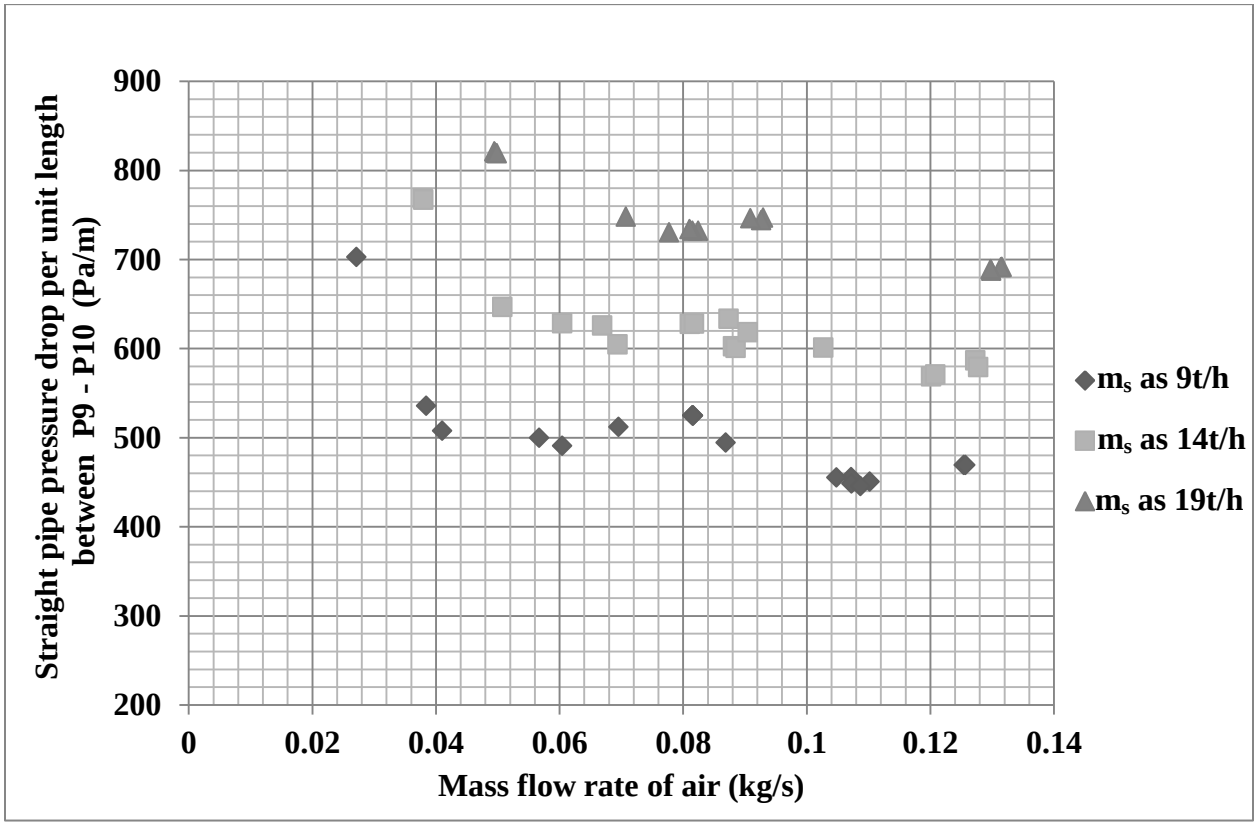

Figure 3.6: Interpolated graph of constant m_s points for straight line pressure drop per unit length (P9-P10) versus mass flow rate of air for fly ash and 69 mm ID × 168 m pipe.

Step 3: The best fit line/curve passing through the interpolated points (obtained in step 2) was drawn with the free hand. Then the exact data points were taken on these best fit lines. Using these exact points the final PCC were drawn as shown in the Figure 3.7.

3.2.2 Analysis of PCC:

The PCC is drawn using the experimental data for fly ash and 69 mm ID ×168 m long pipe. The pressure drop is used between the pressure tappings P9 and P10. The pressure drop per unit length is used in the y-axis and mass flow rate of air is taken on the x-axis as shown in Figure 3.7.

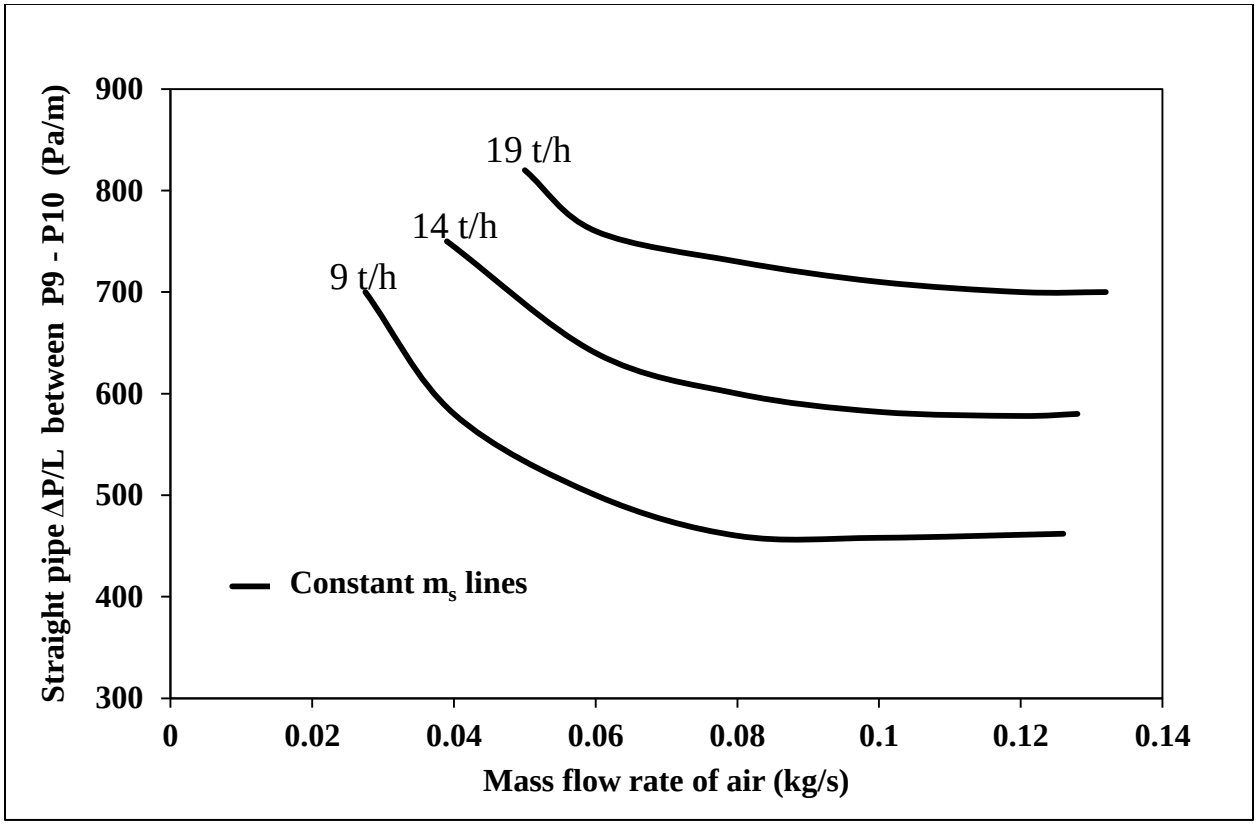

Figure 3.7: PCC for straight line pressure drop per unit length (P9-P10) versus mass flow rate of air for fly ash and 69 mm ID × 168 m pipe

The PCC shows that the trend of pressure drop per unit length first decreases rather rapidly, and then the change of slope becomes low, leading towards change in trend. Same trend was also seen for the PCC drawn using the experimental data for fly ash and 69 mm ID ×168 m long pipe, here pressure drop per unit length was taken on the y-axis and the average air velocity was taken on the y-axis as shown in Figure 3.8.

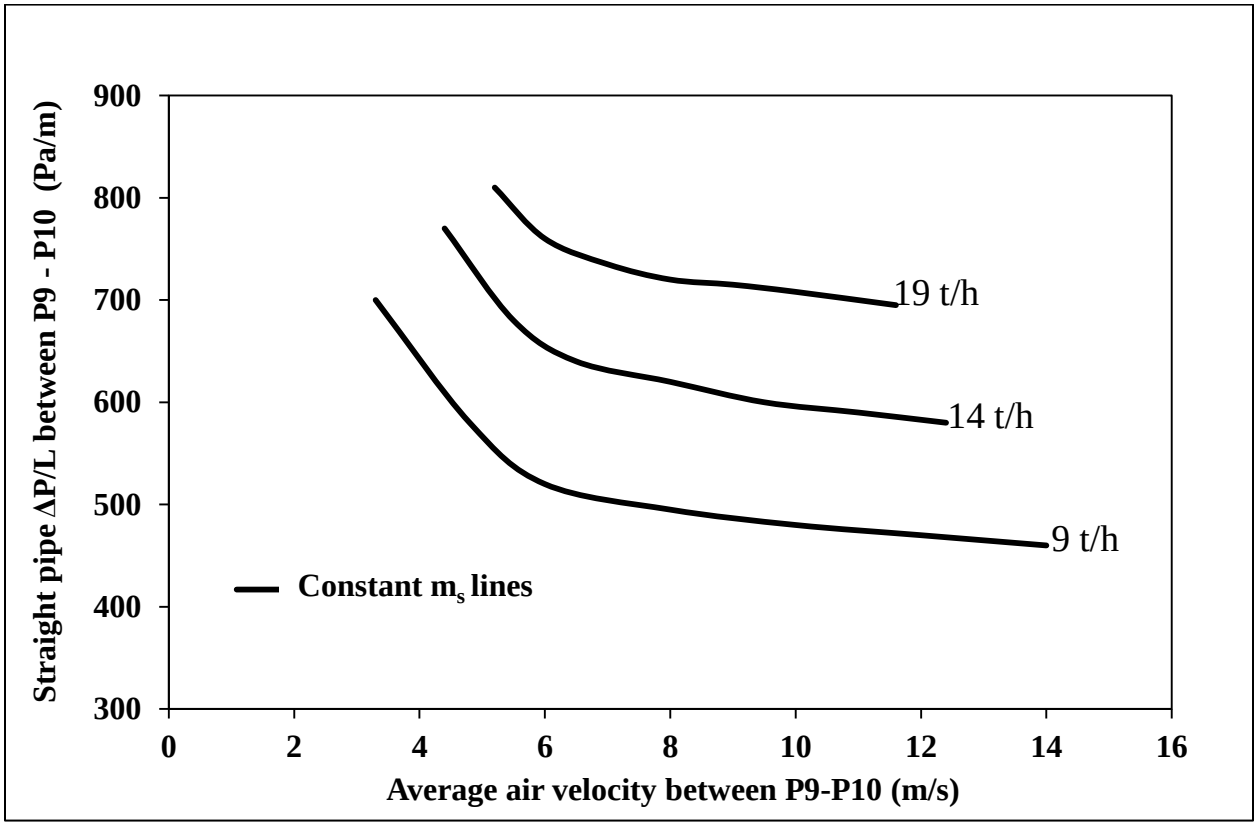

Figure 3.8: PCC for straight line pressure drop per unit length (P9-P10) versus average air velocity for fly ash and 69 mm ID × 168 m pipe

The slope was relatively same for all air velocities, constant m_s lines were not showing U-shape trend (i.e. there was continuous decrease in pressure drop with increase in air velocity) as compared to Figure 3.7.

The PCC provided in Figure 3.9 contains the constant initial air velocity (V_{fi}) lines superimposed on the m_s lines for fly ash and 69 mm ID × 168 m pipe for P9-P10 tappings. The velocity line for 4 m/s was more vertical as compared to the velocity line for 8 m/s and line was becoming more horizontal with further moving to 12m/s

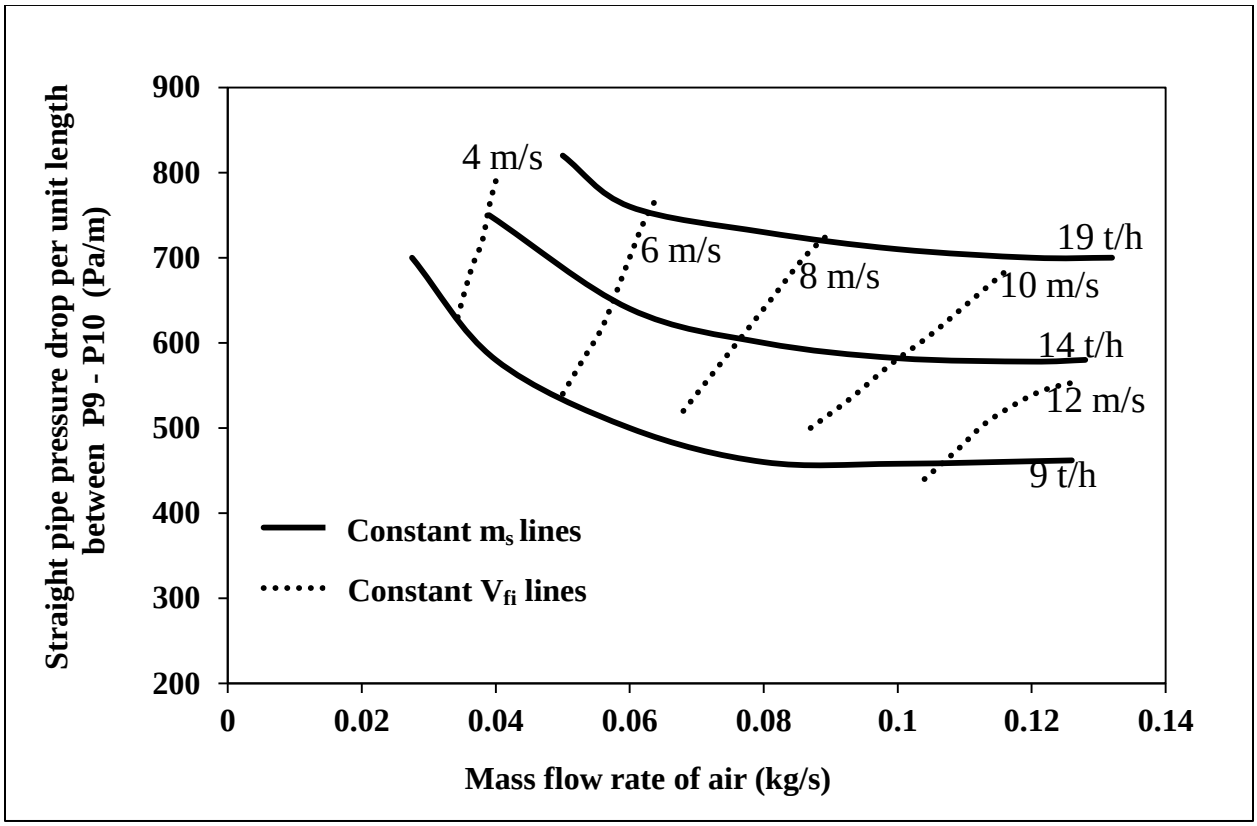

Figure 3.9: PCC for straight line pressure drop per unit length versus mass flow rate of air for fly ash and 69 mm ID × 168 m pipe for P9-P10 along with constant m_s and superimposed initial velocity lines.

In the PCC shown in the Figure 3.10, constant average air velocity (V_{fm}) lines were superimposed on m_s lines for fly ash and 69 mm ID × 168 m pipe for P9-P10 tappings.

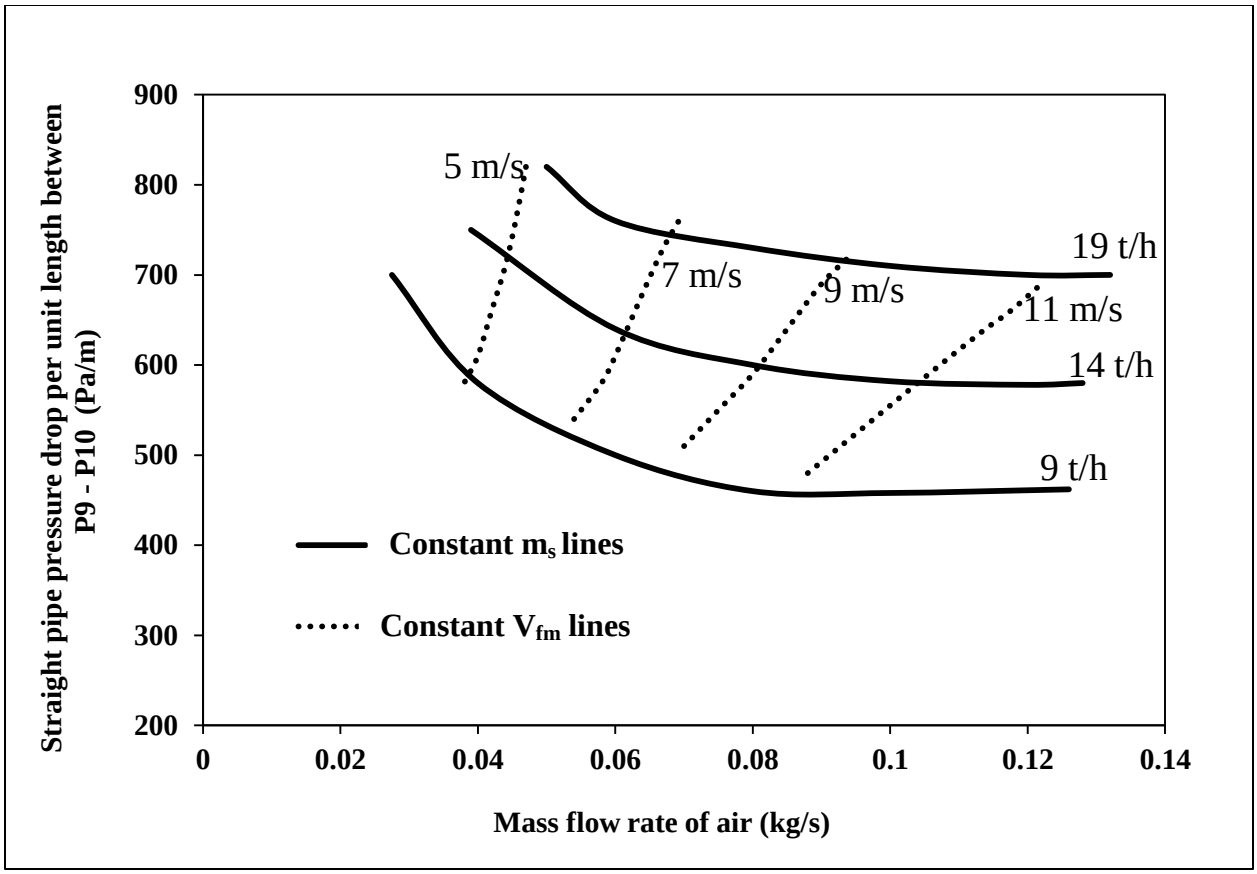

Figure 3.10: PCC for straight line pressure drop per unit length versus mass flow rate of air for fly ash and 69 mm ID × 168 m pipe for P9-P10 along with constant m_s and superimposed average velocity lines.

The velocity line for 5 m/s was seen more vertical as compared to that the velocity line for 11 m/s.

In the PCC shown in the Figure 3.11, constant initial Froude number (Fr_i) lines were superimposed on m_s lines for fly ash and 69 mm ID × 168 m pipe for P9-P10 tappings. The Froude number line for 5 was more vertical as compared to that the Froude number line for 8 and the slope was continuously decreasing with the increase in value of Froude number.

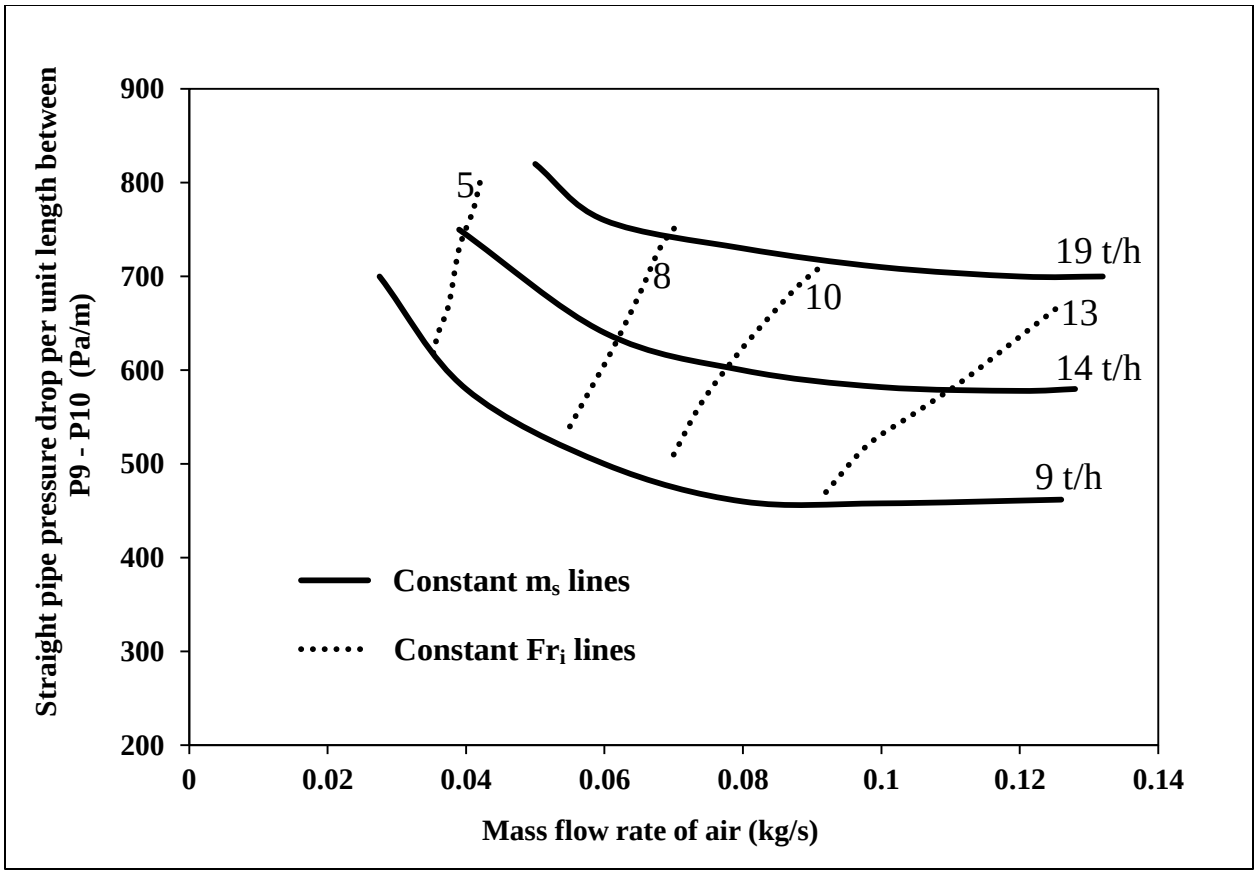

Figure 3.11: PCC for straight line pressure drop per unit length versus mass flow rate of air for fly ash and 69 mm ID × 168 m pipe for P9-P10 with constant m_s and superimposed initial Froude number lines.

In the PCC shown in the Figure 3.12, constant mean Froude number (Fr_m) lines were superimposed on m_s lines for fly ash and 69 mm ID × 168 m pipe for P9-P10 tappings. The Froude number line for 6 was more vertical as compared to that of the Froude number line for 8 and the slope was continuously decreasing with the increase in value of Froude number.

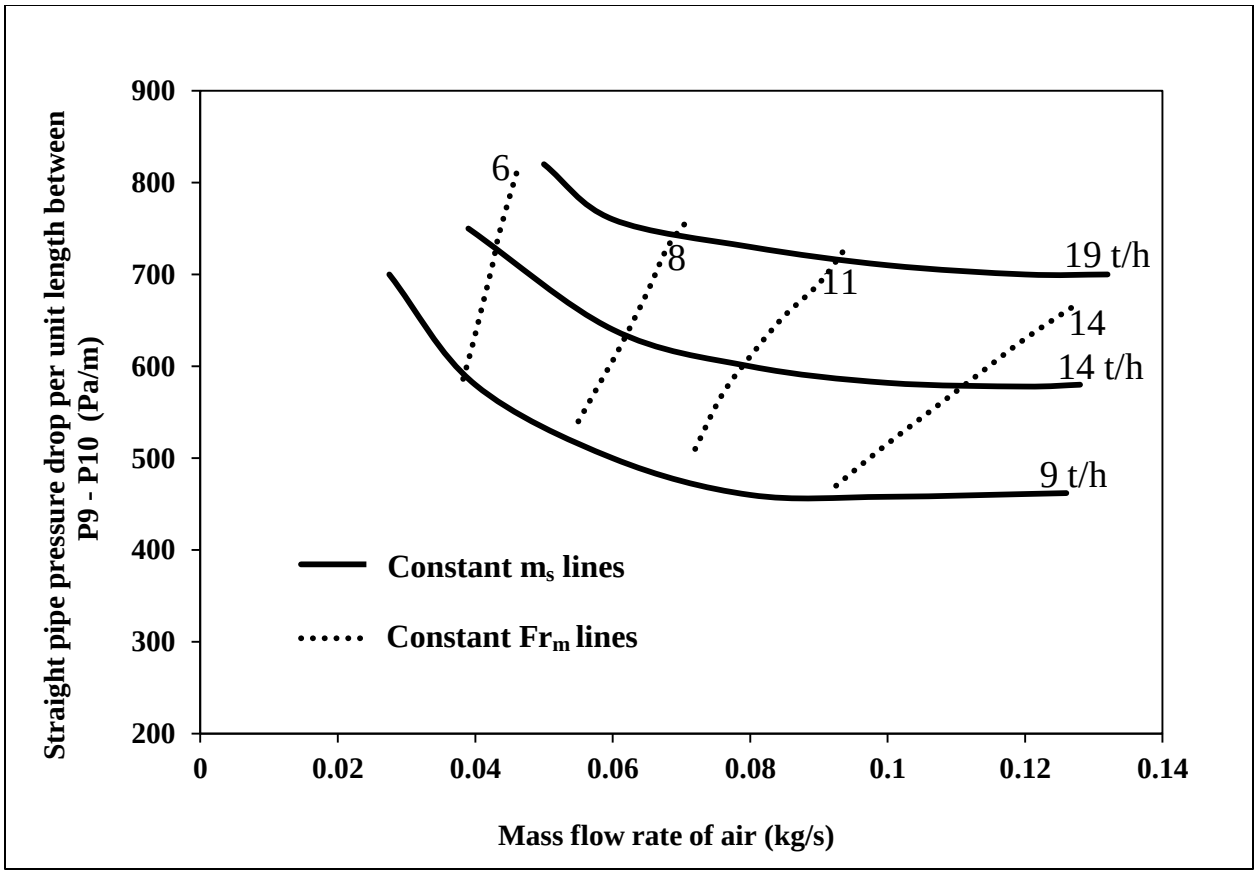

Figure 3.12: PCC for straight line pressure drop per unit length versus mass flow rate of air for fly ash and 69 mm ID × 168 m pipe for P9-P10 with constant m_s and superimposed mean Froude number lines.

The PCC was drawn for the same pipe (69 mm ID × 168 m long) and fly ash, but the pressure drop was taken for the next tappings of the test rig i.e. for P11 and P12 as shown in Figure 3.13. PCC was drawn against average mass flow rate of air on x-axis. The Froude number line for 6 was seen more vertical as compared to that of the Froude number line for 14. PCC in Figure 3.13 shown that the pressure drop in this case was continuously decreasing with the same slope and it seems to be approaching towards a straight line with zero slope i.e. approaching towards a constant pressure drop per unit length line.

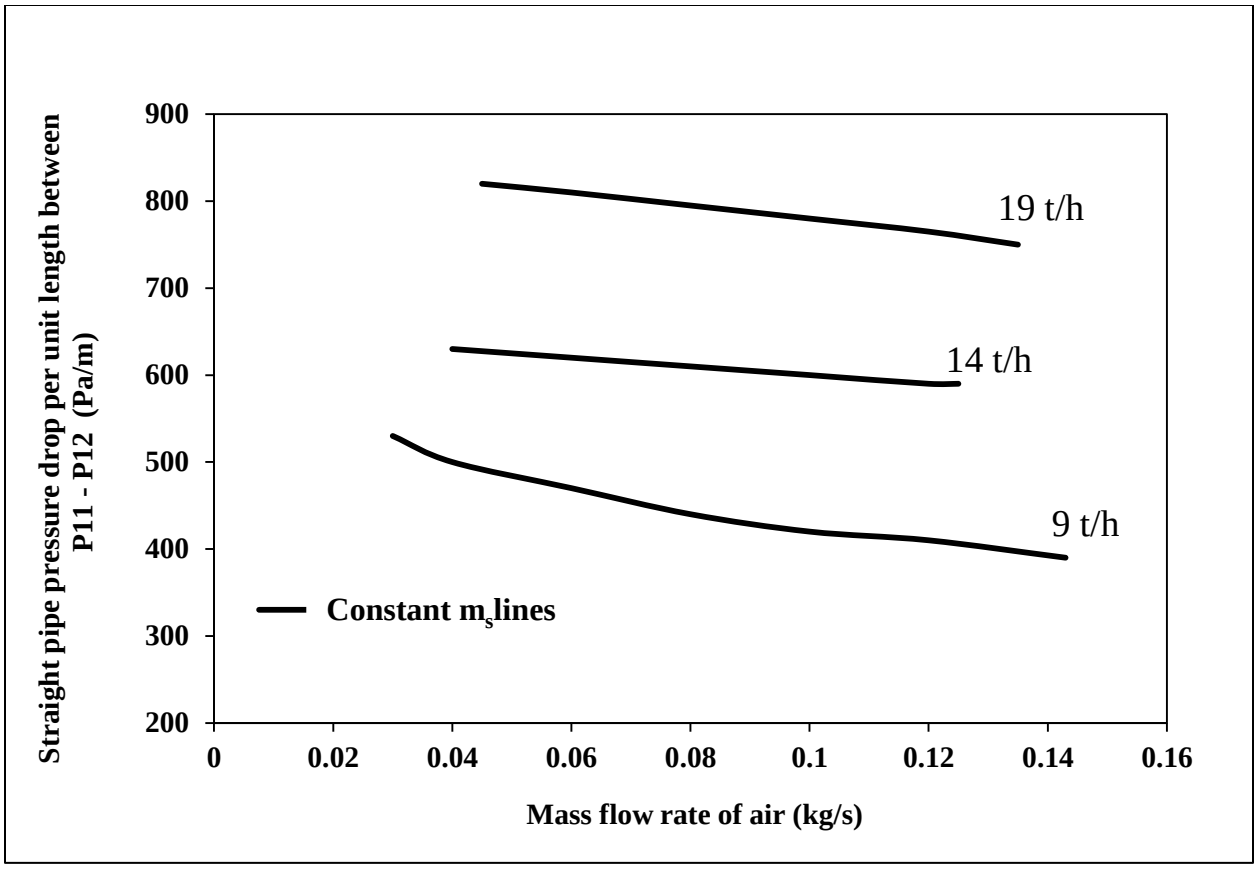

Figure 3.13: PCC for straight line pressure drop per unit length (P11-P12) versus mass flow rate of air for fly ash and 69 mm ID × 168 m pipe.

Here another PCC was drawn against average air velocity on x-axis as shown in Figure 3.14. PCC in Figure 3.14 shown that the pressure drop in this case was continuously decreasing with the same slope and it seems to be approaching towards a straight line with zero slope i.e. approaching towards a constant pressure drop per unit length line it was not following change in trend as shown for P9-P10 PCC (Figure 3.7). The similar trend was seen for all mass flow rate of solid lines.

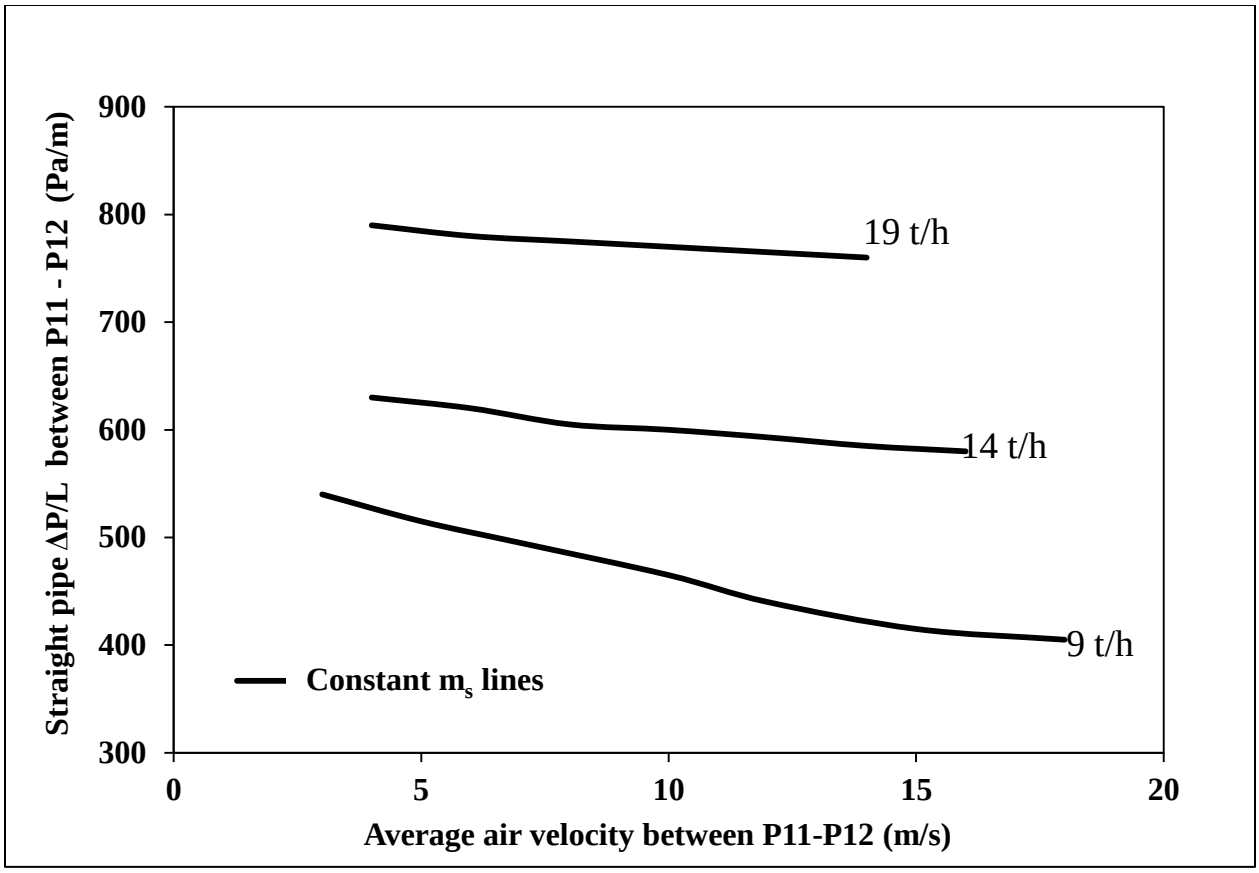

Figure 3.14: PCC for straight line pressure drop per unit length (P11-P12) versus average air velocity for fly ash and 69 mm ID × 168 m pipe.

In the PCC shown in the Figure 3.15, constant initial air velocity (V_{fi}) lines were superimposed on m_s lines for fly ash and 69 mm ID × 168 m pipe for P11-P12 tappings. The velocity line for 5 m/s was more vertical as compared to that the velocity line for 13 m/s which was similar to the trend shown in case of initial tappings (i.e for P9-P10). Mass flow rate of solid lines were not showing the U-shape trend in case of P11-P12 tapping points.

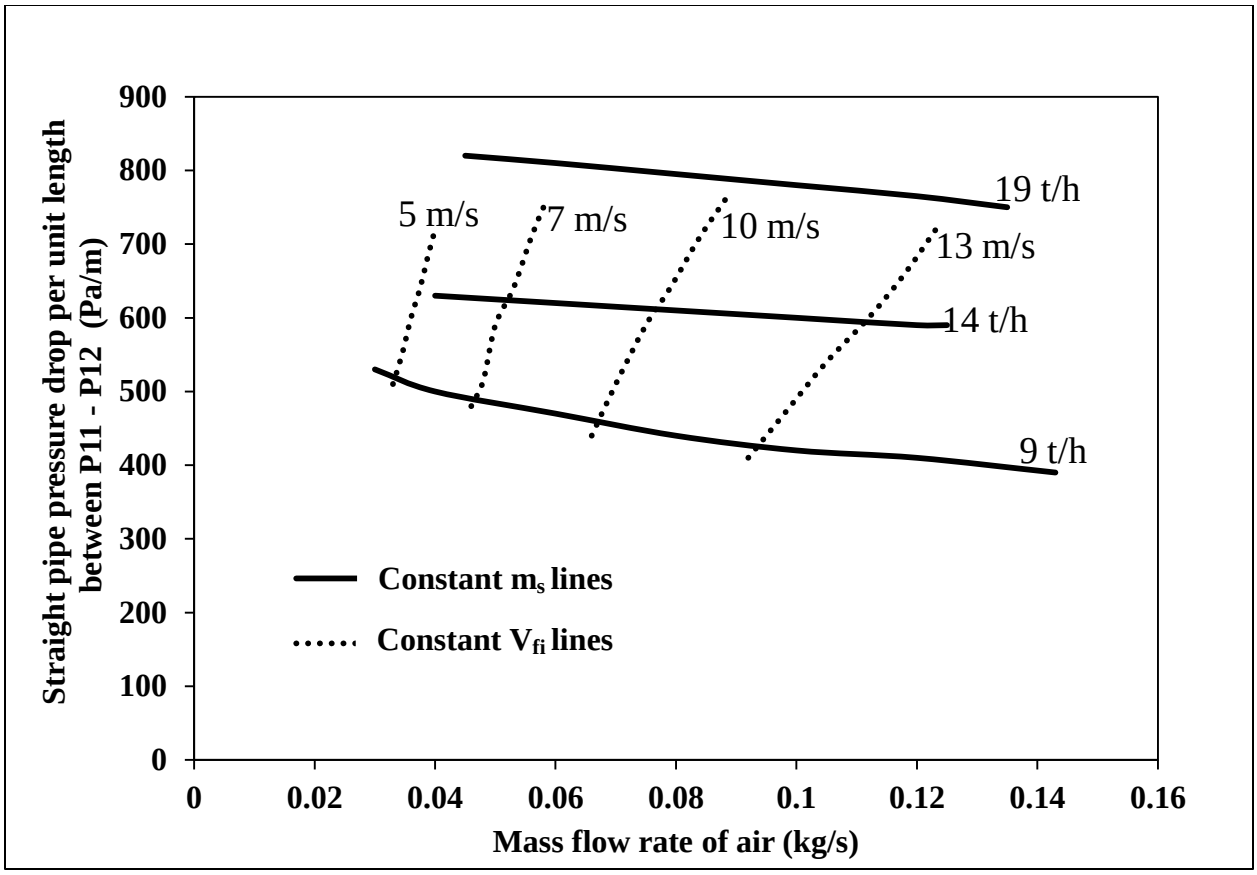

Figure 3.15: PCC for straight line pressure drop per unit length versus mass flow rate of air for fly ash and 69 mm ID × 168 m pipe for P11-P12 along with constant m_s and superimposed initial velocity lines.

In the PCC shown in the Figure 3.16, constant average air velocity (V_{fm}) lines were superimposed on m_s lines for fly ash and 69 mm ID × 168 m pipe for P11-P12 tappings. The velocity line for 5 m/s was more vertical as compared to that the velocity line for 14 m/s which was similar to the trend shown in case of initial tappings (i.e for P9-P10). Mass flow rate of solid lines were not showing the U-shape trend in case of P11-P12 tapping points.

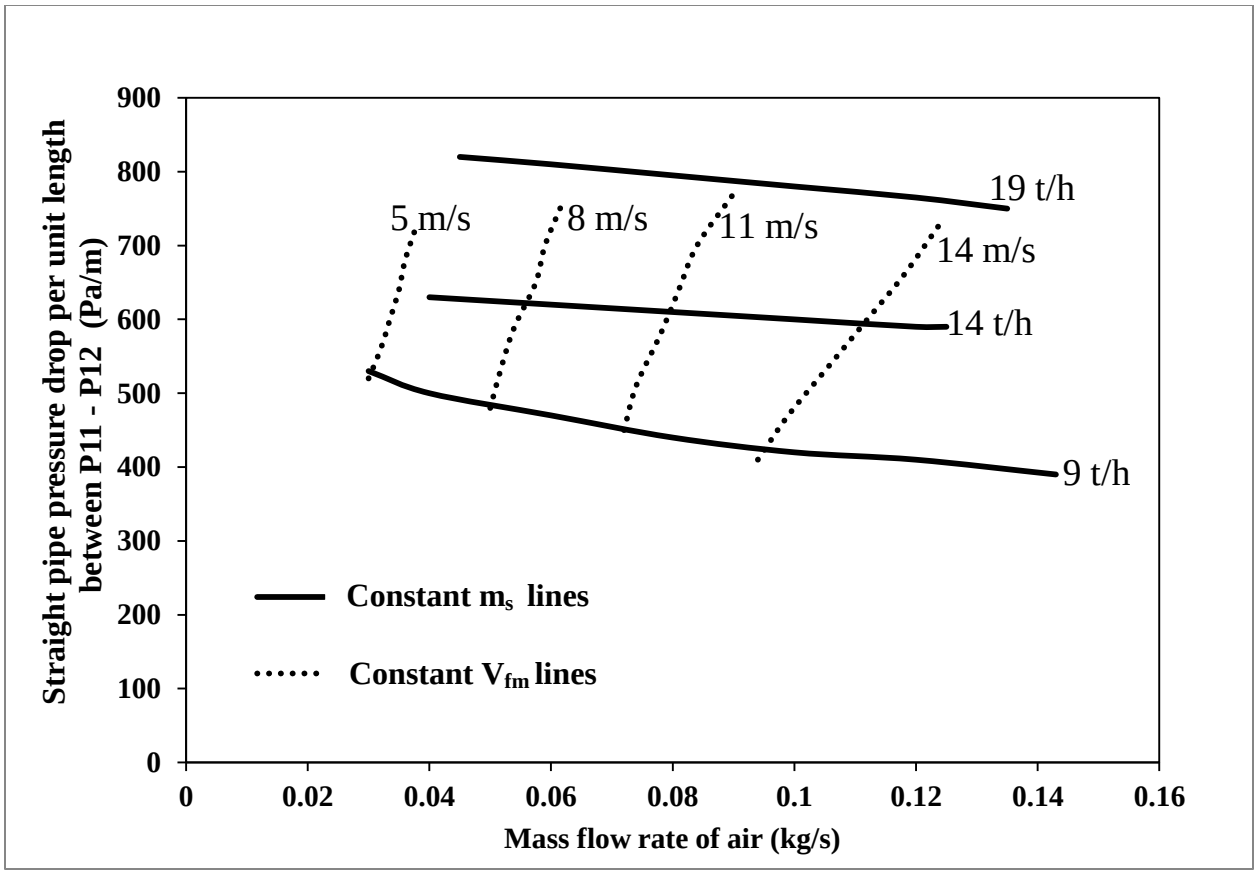

Figure 3.16: PCC for straight line pressure drop per unit length versus mass flow rate of air for fly ash and 69 mm ID × 168 m pipe for P11-P12 along with constant m_s and superimposed average velocity lines.

In the PCC shown in the Figure 3.17, constant initial Froude number (Fr_i) lines were superimposed on m_s lines for fly ash and 69 mm ID × 168 m pipe for P11-P12 tappings. The Froude number line for 7 was more vertical as compared to that of the Froude number line for 14 which was similar to the trend shown in case of initial tappings (i.e for P9-P10). Mass flow rate of solid lines were not showing the U-shape trend in case of P11-P12 tapping points.

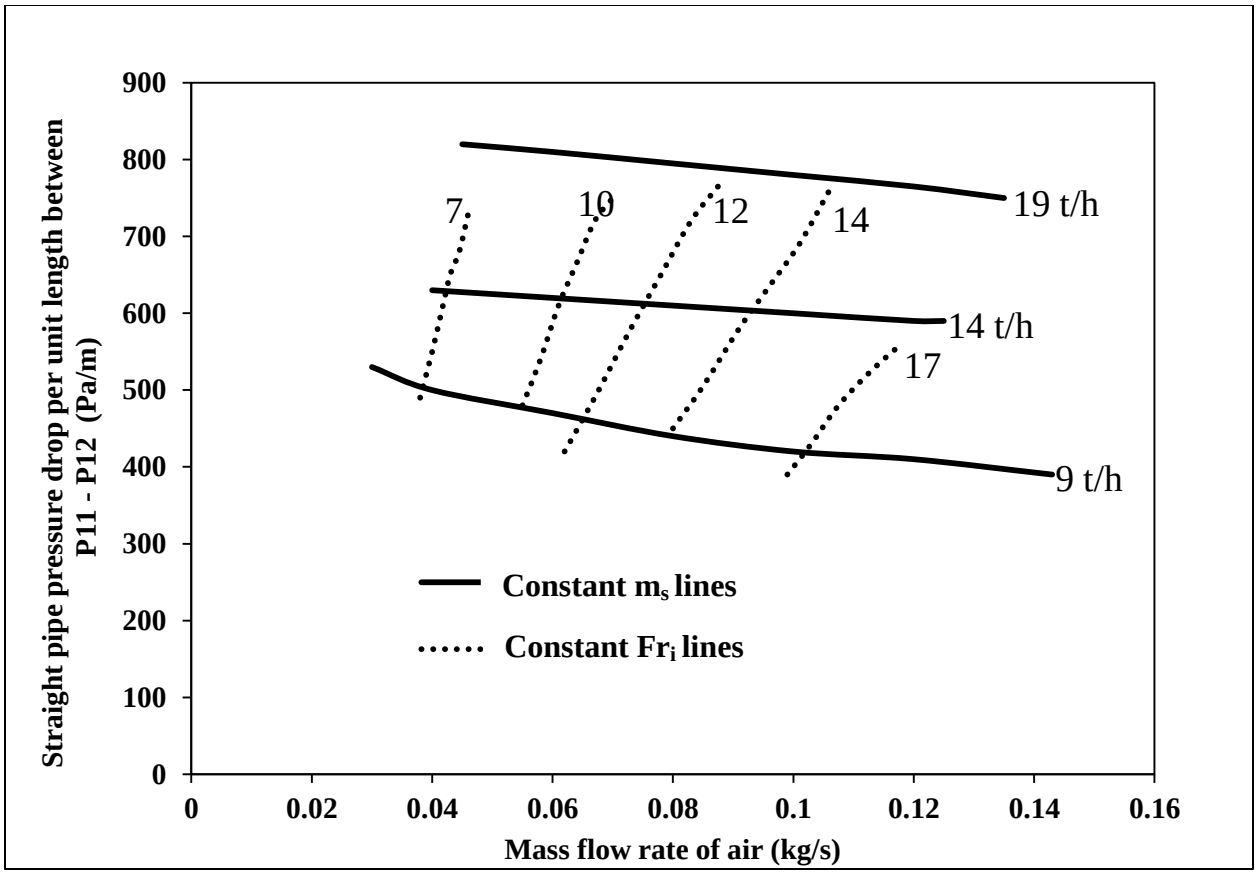

Figure 3.17: PCC for straight line pressure drop per unit length versus mass flow rate of air for fly ash and 69 mm ID × 168 m pipe for P11-P12 with constant m_s and initial Froude number lines.

In the PCC shown in the Figure 3.18, constant mean Froude number (Fr_m) lines were superimposed on m_s lines for fly ash and 69 mm ID × 168 m pipe for P11-P12 tappings. The Froude number line for 6 was more vertical as compared to that of the Froude number line for 14 which was similar to the trend shown in case of initial tappings (i.e for P9-P10). Mass flow rate of solid lines were not showing the U-shape trend in case of P11-P12 tapping points.

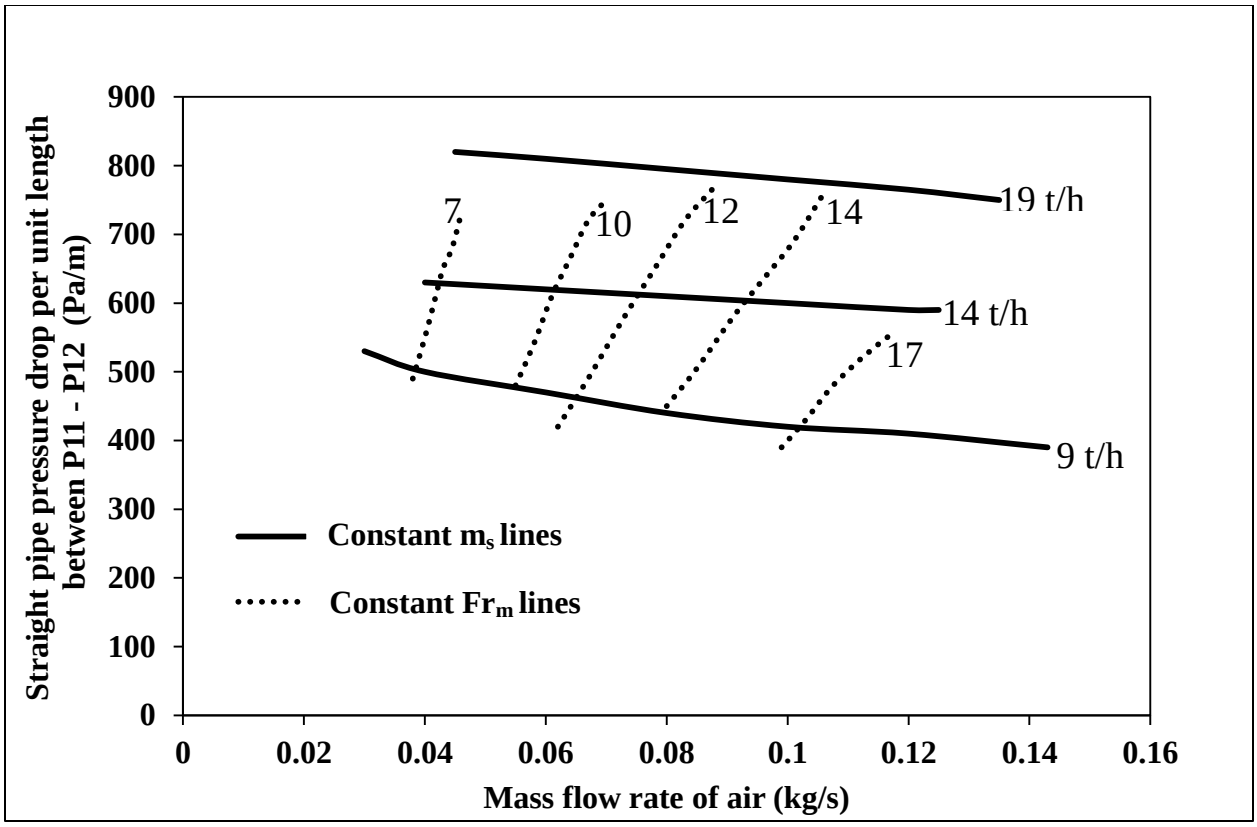

Figure 3.18: PCC for straight line pressure drop per unit length versus mass flow rate of air for fly ash and 69 mm ID × 168 m pipe for P11-P12 with constant m_s and superimposed mean Froude number lines.

All $\Delta P/L$ verses m_f PCC discussed above shows that when moving for the higher value of mass flow rate of air, the change in velocity (both initial and mean) becomes more prominent and hence same for Froude number Fr (both initial and mean).

Similar work was done for other pipe lines and the similar results were obtained. The comparison graphs for other pipe lines are discussed below.

3.2.3 Comparison of PCC:

Fly Ash

Using steady state straight-pipe pressure drop data for a range of solids and air flow rates through P9-P10 and P11-P12 tapping points for the 69 mm I.D. × 168 m long pipe , the following straight-pipe PCC have been obtained (Figure 3.19). PCC for individual tapping points P9-P10 and P11-P12 have been superimposed on the same plot for the purpose of comparing the characteristics with respect to tapping point locations (i.e. along the flow direction or pipe length). Constant mean Froude number and superficial air velocity lines for individual PCC are also shown.

Figure 3.19 shows that between 0.04 to 0.08 kg/s of airflow, the pressure gradient (and slopes of PCC) are greater for P9-P10 data than those for the P11-P12 data. The solid flow lines for initial tappings (P9-P10) show a change in trends in solids flow lines (e.g. corresponding to $Fr_m = 7$ line for the 19 t/h curve). However, the same solid flow lines for final tappings (P11-P12) show no change in trend (compared to that shown by P9-P10 PCC) for the same range of air flow rates (0.04 to 0.08 kg/s). From 0.08 to 0.12 kg/s, both sets of PCC have continued on with almost the same trend (gradual pressure decrease) and similar pressure drop values. It must also be appreciated that no clear Pressure Minimum Curve (PMC) was observed in either set of PCC, indicating a gradual change in flow characteristics (with respect to air flow). In contrast, distinct pressure minimum lines are observed for granular products, (Marcus et al., 1990). Using steady state straight-pipe pressure drop data through P9-P10 and P11-P12 tapping points for the 105 mm I.D. × 168 m long pipe, the following straight-pipe PCC have been obtained (Figure 3.20).

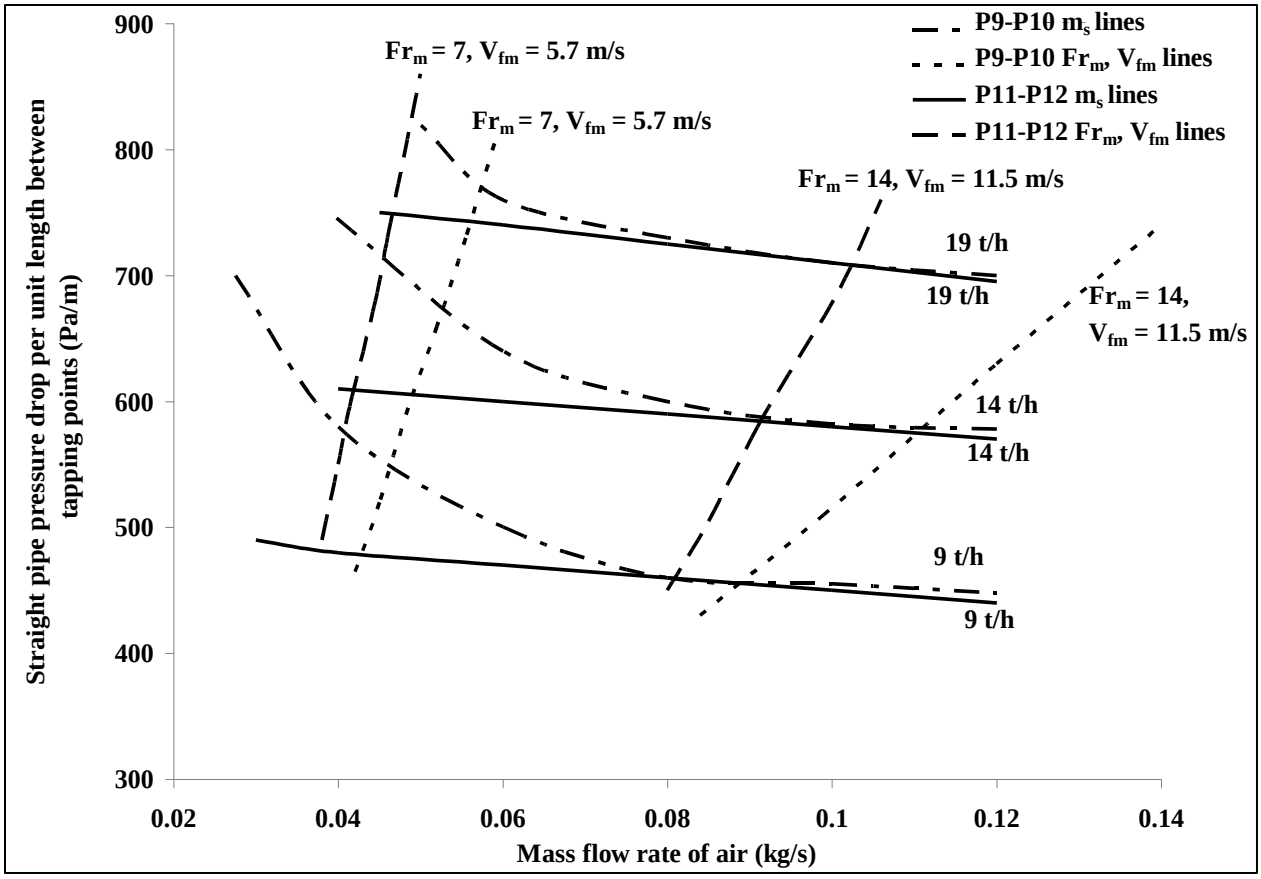

Figure 3.19: Comparison of PCC for straight-pipe pressure (P9-P10 versus P11-P12), fly ash, 69 mm I.D. × 168 m long pipe

Figure 3.20 shows that between 0.06 and 0.11 kg/s of airflow, both the P9-P10 than P11-P12 PCC show a substantial change in trend. From a significantly decreasing pressure gradient for air flows $Fr_m \leq 7$, the PCC have become almost horizontal thereafter (for both P9-P10 and P11-P12 data sets). P9-P10 PCC have provided consistently higher values of pressure gradient than those for the P11-P12 PCC. No clear Pressure Minimum Curve (PMC) was observed in either set of PCC. Using steady state straight-pipe pressure drop data through P9-P10 and P11-P12 tapping

points for the 69 mm I.D. × 554 m long pipe, the following straight-pipe PCC have been obtained (Figure 3.21).

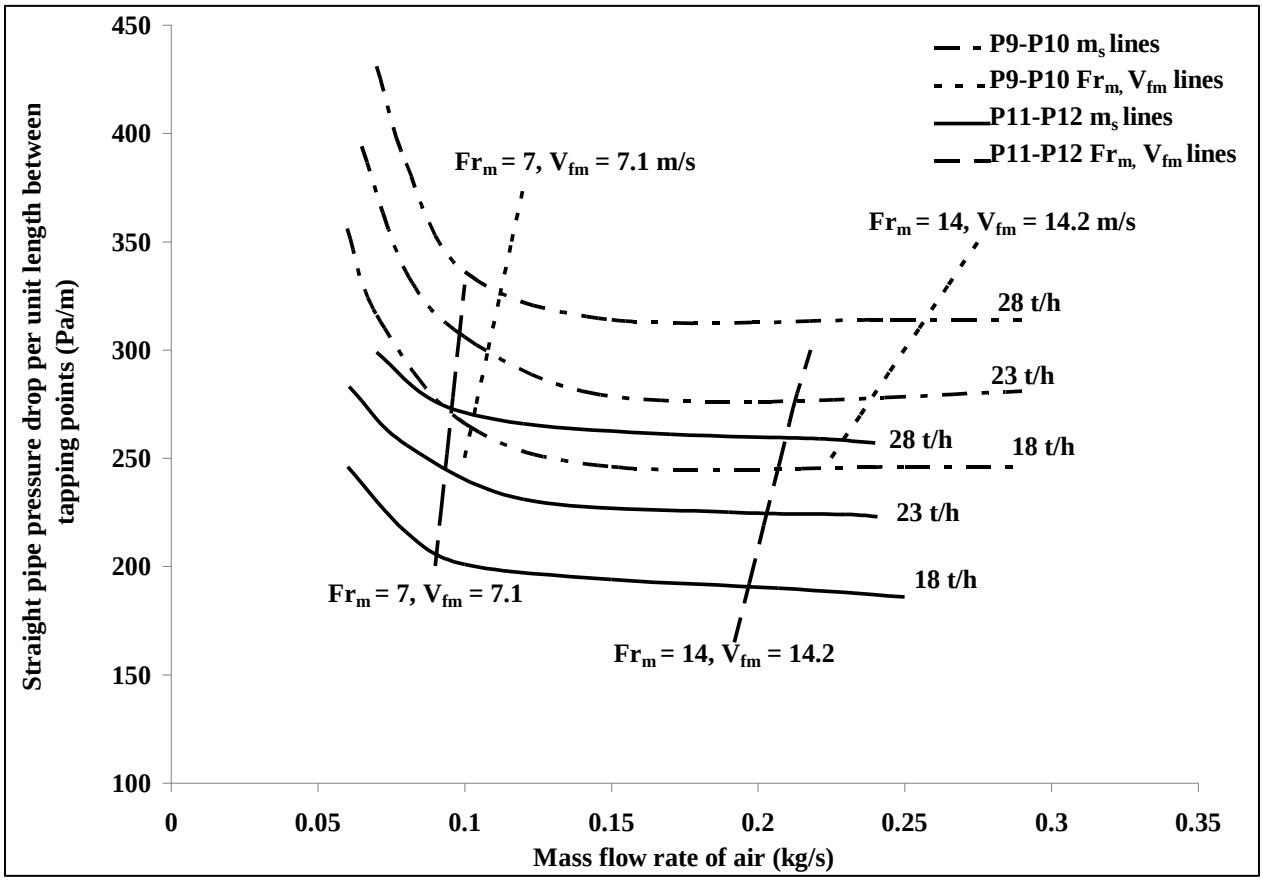

Figure 3.20: Comparison of PCC for straight-pipe pressure (P9-P10 versus P11-P12), fly ash, 105 mm I.D. × 168 m long pipe

Figure 3.21 shows none of the PCC provides a sharp change in slope. The P9-P10 PCC show a gradually decreasing slope (only minor change in slope), while the P11-P12 PCC show a slight change in trend (slight downward slope to the left of Fr_m = 13 line and slight upward slope to the right of the same line). The change in slope may be an indication of change in flow characteristics along the flow direction. However, there was no distinct Pressure Minimum

Curve (PMC) in either set of PCC, indicating that even if there were a flow transition (change in flow mechanism from dense- to dilute-phase), the change is very gradual. P9-P10 PCC has provided consistently higher values of pressure gradient than those for P11-P12 PCC.

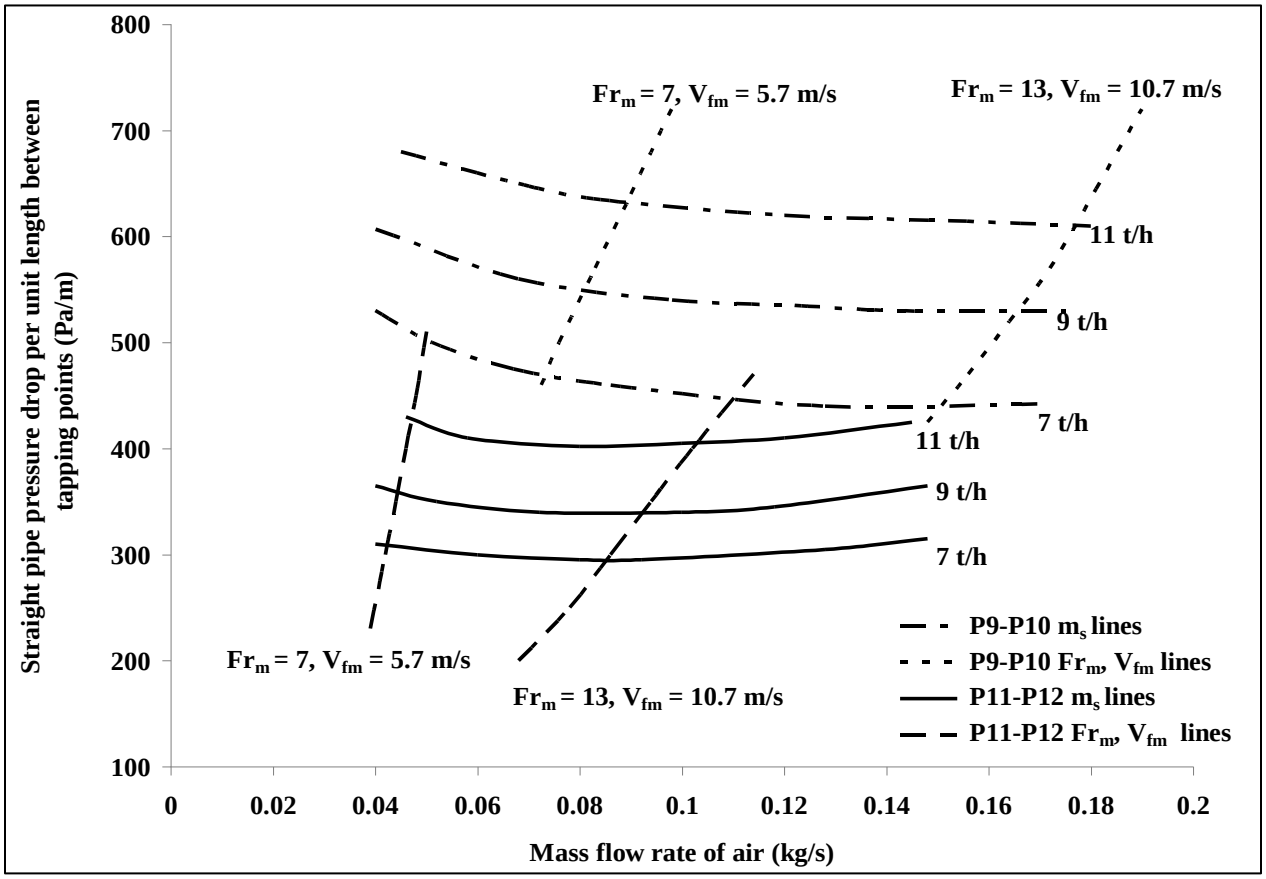

Figure 3.21: Comparison of PCC for straight-pipe pressure (P9-P10 versus P11-P12), fly ash, 69 mm I.D. × 554 m long pipe

White Powder

Using steady state straight-pipe pressure drop data for a range of solids and air flows through P9-P10 and P11^{+}-P12 tapping points for the 69 mm I.D. × 148 m long pipe, the following straight-

pipe PCC have been obtained (Figure 3.22). PCC for individual tapping points P9-P10 and P11^{+}-P12 have been superimposed on the same plot for the purpose of comparing the characteristics with respect to tapping point locations (i.e. along the flow direction or pipe length).

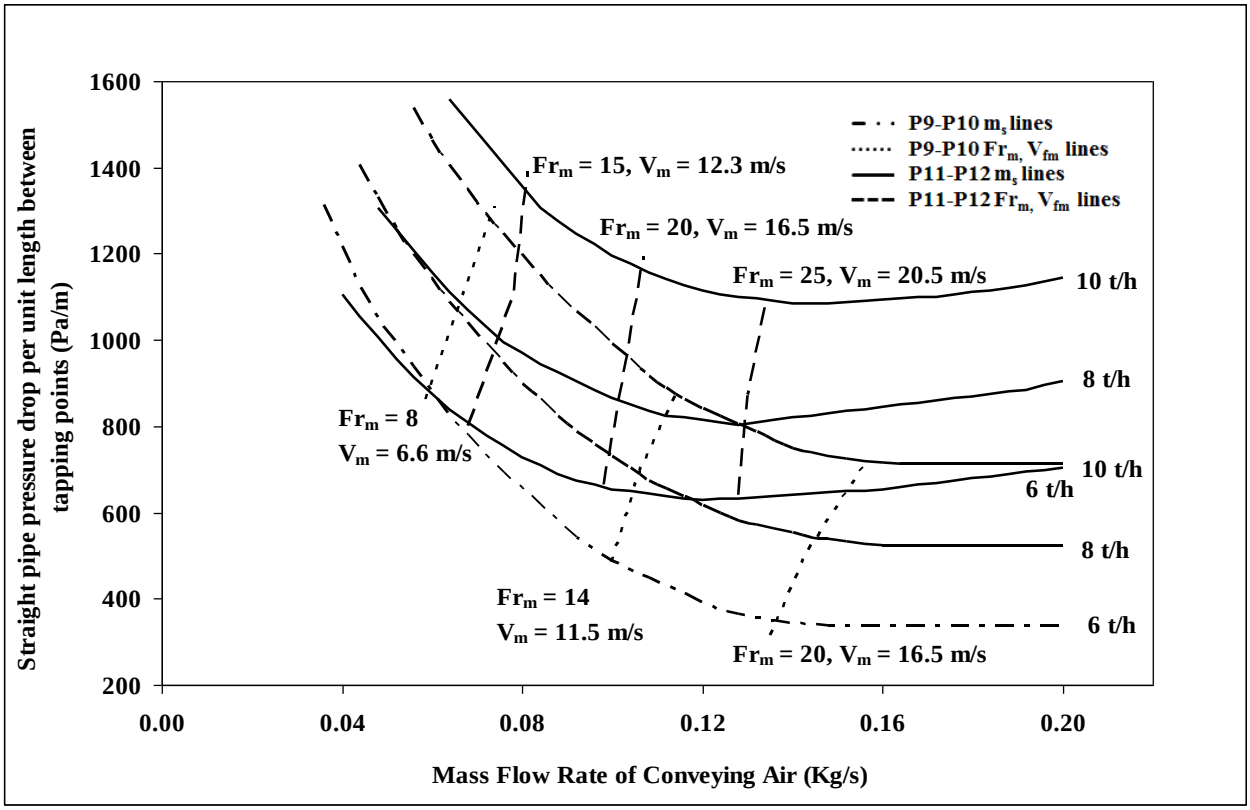

Figure 3.22: Comparison of PCC for straight-pipe pressure (P9-P10 versus P11^{+}-P12), white powder, 69 mm I.D. × 148 m long pipe

Figure 3.22 shows there is significant change in slope of the PCC with increasing air flow rates. From 0.04 to 0.12 kg/s of air flow, pressure drop decreases with increase in air flow rates. From 0.12 to 0.2 kg/s, PCC for P9-P10 become almost horizontal (i.e. no appreciable change in pressure gradient even with increasing air flow). For the same range of air flows (0.12 to 0.2

kg/s), PCC for $P11^{+}$-P12 show a noticeable upward trend (i.e. pressure drop starts to increase with increasing air flow rates). Flow visualization (through sight-glass) during the test program showed that up to an air flow rate of approximately 0.12 kg/s, the flow of powders was in non-suspension mode (dense-phase). At about 0.12-0.13 kg/s, the flow of powders became suspended (dilute-phase) and remained the same up to 0.2 kg/s. Thus, change of slope of straight-pipe PCC slope may be an indication of dense-to-dilute transition criteria. However, from the shape of PCC, it may also be appreciated that the change of in the pipeline initial tapping points (P9-P10) than the later (P11-P12) for fly ash, while the reverse happens for white powder (pressure gradients obtained from $P11^{+}$-P12 are greater than those obtained from P9-P10 for white powder). This indicates the flow complexity and modelling challenges for dense-phase pneumatic conveying of different powders as powders can behave quite differently and unexpectedly under actual flow conditions. This also emphasizes the requirement of pilot-plant testing and scaling up the test information to industrial situation, rather than making assumptions regarding product behaviour that can lead to drastically wrong predictions (especially when scaled-up).

3.3 Evaluation of existing models for PMC:

Dense to dilute-phase transition criteria is generally represented by the location of pressure minimum curve (PMC) in the straight-pipe PCC (Marcus et al, 1990). A list of models for prediction of pressure minimum curve (i.e. the dense to dilute-phase transition criteria) is

provided in the following. Because of the relatively distinct location of pressure minima for coarser particles compared to fine powders (the change in flow mechanism from dense to dilute-phase is gradual for fine powders, i.e. no distinct location of PMC for fine powders), majority of the previous efforts to model PMC were limited to only coarser particles. These models have been evaluated in the following to investigate into their predictive capability for fine powders. The lower boundary of dilute-phase flow of coarser particles (i.e. at the initiation of saltation of particles) is represented by the PMC (Marcus et al, 1990, Yi et al., 1998).

3.3.1Existing models

Rose and Duckworth (1969) investigated the minimum conveying velocity within a pipe line of 32 mm diameter by conveying mustard seed, glass bead, lead bead and steel bead and developed the following correlation for minimum conveying velocity for dilute phase (which corresponds to the PMC, Marcus et al, 1990):

$$V_{\min} = 2.33 G_s^{0.286} D^{0.5} d^{-0.857} \rho_p^{-1} \rho^{0.714} U_t^{1.43} \tag{3.3}$$

Matsumoto (1974) (reported in Ratnayake, 2005) investigated the minimum conveying velocity with pipelines for 29 mm and 49 mm in diameter using glass bead, copper bead and polystyrene as the test materials and provided the following model for minimum velocity for dilute-phase:

$$V_{\min} = 3.4\sqrt{gD}\left(\frac{\rho}{\rho_p}\right)^{0.294}\left(\frac{U_t}{\sqrt{gd}}\right)^{1.02} m*^{0.277} \tag{3.4}$$

Rizk (1976) provided the following model (equation 3.5) for pressure minimum curve by conveying Sryropor and Polystrol through pipelines having 50 to 400 mm diameters.

$$m^* = \frac{1}{10^{\delta}} Fr_{\min} \chi \tag{3.5}$$

Where,

$$\delta = 1.44d + 1.96 \tag{3.6}$$

$$\chi = 1.11d + 2.50 \tag{3.7}$$

Weber (1981) provided correlation for minimum conveying velocity as provided in equation 3.8 and 3.9. Weber (1981), however, did not clearly indicate whether the models are applicable for both fine and coarse particles.

For $U_t \le 3m/s$ $$Fr_i = [7 + \frac{8}{3} U_t] m^{*0.25} \left(\frac{d}{D}\right)^{0.1} \tag{3.8}$$

For $U_t \ge 3m/s$ $$Fr_i = 15 m^{*0.25} \left(\frac{d}{D}\right)^{0.1} \tag{3.9}$$

Schade (1987) investigateded minimum conveying velocity for a number of diameters (50 to 150 mm) and test materials (such as granule, sand, styropor, rubber, and polystyrol) and provided the following correlation:

$$V_{\min} = 2.8 G_s^{0.1} D^{0.428} d^{-0.023} \rho_p^{0.306} \rho^{-0.405} \quad (3.10)$$

Cabrejos and Klinzing (1994) investigated minimum conveying velocity by conveying alumina, glass beads and for polyester polymers through a pipeline of 50 mm diameter. Their model to indicate PMC was:

$$\frac{V_{\min}}{\sqrt{gd}} = \frac{U_t}{\sqrt{gd}} + 0.00224 \left(\frac{\rho_p}{\rho} \right)^{1.25} \left(m^* \right)^{0.5} \quad (3.11)$$

Kalman et al. (2005) presented a pickup velocity model (equations 10 to 12) using a modified Reynolds number (Re_p*) and Archimedes number term by conveying glass, zirconium, alumina, iron, salt sand, talk and ammonium oxide.

For Ar > 16.5 $$\mathrm{Re}_p^* = 5 Ar^{\frac{3}{7}} \quad (3.12)$$

For 0.45 < Ar < 16.5 $$\mathrm{Re}_p^* = 16.7 \quad (3.13)$$

For Ar < 4.5 $$\mathrm{Re}_p^* = 21.8 Ar^{\frac{1}{3}} \quad (3.14)$$

3.3.2 Validation of existing models:

The existing models have been evaluated on the straight-pipe PCC of fly ash and white powder for the following pipe sections (PCC in which the solids lines of the straight-pipe pressure drops exhibited change in trends; i.e. 'U'-shaped curve):

- P11-P12 tappings of 69 mm I.D. × 554 m long pipe for fly ash;
- P11+-P12 tappings of 69 mm I.D. × 148 m long pipe for white powder

For evaluation of some models it is required to draw the constant density lines which are drawn using the technique discussed under *Method used for plotting the PCC's:* 3.3.1 (Interpolation Technique) and these constant density lines are also shown in the Figures 3.23 and 3.24.

Figure 3.23 shows that Kalman et al. (2005), Cabrejos and Klinzing (1994) and Matsumoto (1974) models significantly under-predicts PMC (i.e. the predicted PMC are located at very low air flow rates that are below the range of conveying conditions). In fact, the predictions using Matsumoto (1974) model are drastically low (almost coinciding with the y-axis). Weber (1981) provided good predictions (i.e. the predicted PMC are very close to the range of experimental pressure minimum points). Schade (1987) provided considerable over-predictions (i.e. the predicted PMC are located to the right of the experimental pressure minimum points).

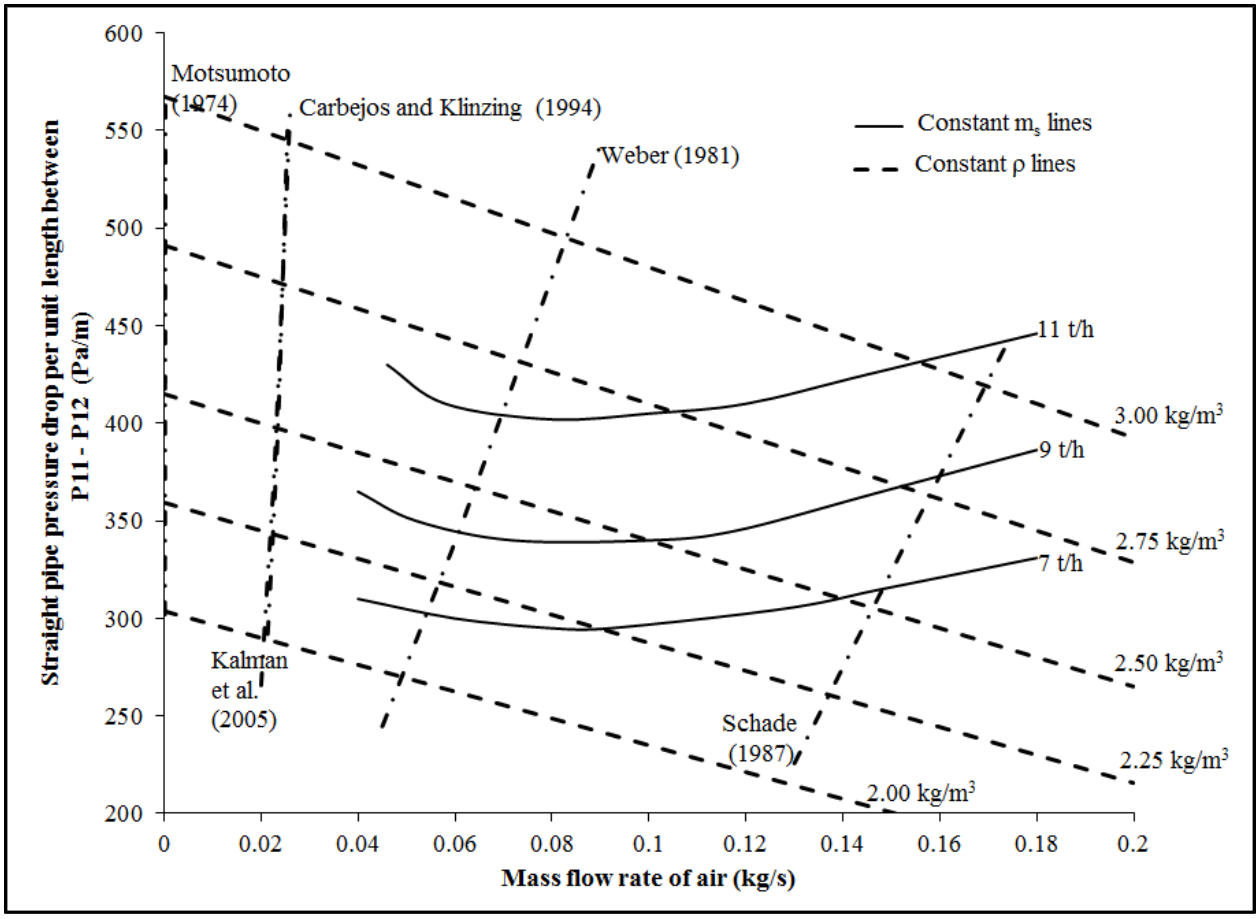

Figure 3.23: Evaluation of models for PMC on straight-pipe PCC, fly ash, P11-P12, 69 mm I.D. × 554 m long pipe

Figure 3.24 shows that Kalman et al. (2005), Cabrejos and Klinzing (1994) and Matsumoto (1974) models significantly under-predicts PMC. Schade (1987) again provides considerable over-predictions, whereas, predictions with Weber (1981) model, though provides some over-predictions, but are closer to the experimental points compared to that obtained by Schade (1987). Predictions using Rose and Duckworth (1969) and Rizk (1976) were found to be out of domain of the plot (large deviation for experimental plots), hence the same have not been shown in Figures 3.23 and 3.24.

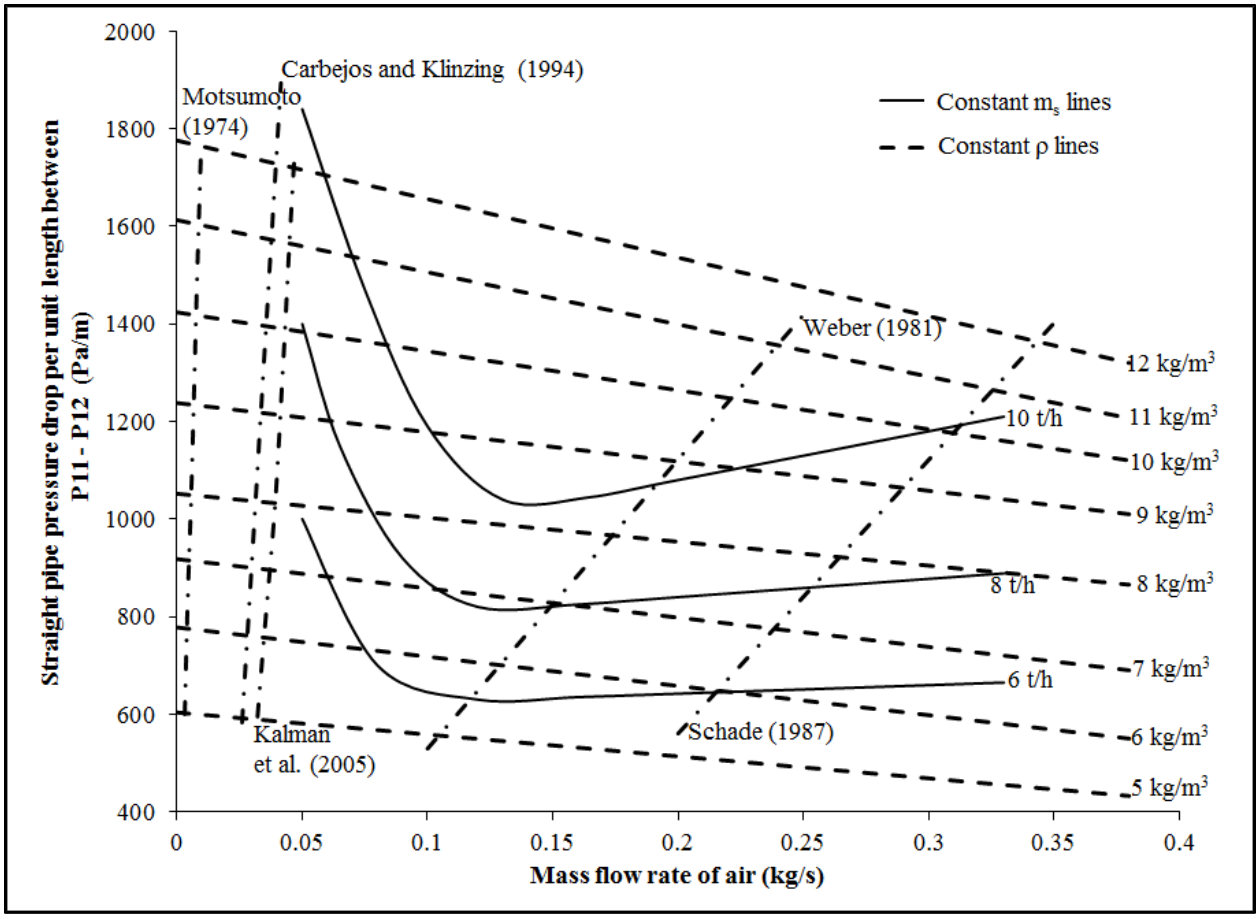

Figure 3.24: Evaluation of models for PMC on straight-pipe PCC, white powder, P11+-P12, 69 mm I.D. × 148 m long pipe

Based on the results presented in this chapter, it can be concluded that even for the same product, straight-pipe PCC can be different depending on pipeline diameter or length and location of pressure tapping points on the same pipeline. This indicates that the flow mechanism changes along the flow direction. Straight-pipe PCC obtained from initial tapping points in the pipeline (P9-P10) have generally shown steeper PCC than those obtained further along the pipeline (P11-P12). There was no distinct PMC in any of the straight pipe PCC, indicating that even if there were a flow transition (change in flow mechanism from dense- to dilute-phase), the change was

very gradual. The nature of the "U"-shape and location of the PMC for the total pipeline PCC are significantly influenced by the pipeline layout (e.g. location and number of bends) and not entirely by the dense- to dilute-phase transition of flow mechanism. The different models for PMC proposed by previous researchers (Rose and Duckworth, 1969; Matsumoto, 1974; Rizk, 1976; Weber, 1981; Schade, 1987; Cabrejos and Klinzing, 1994; Kalman et al., 2005) discussed above were not providing significantly accurate results. Weber (1981) provided good prediction but not giving the accurate results. To account for the change in flow characteristics along the flow direction (such as dense- to dilute-phase) future research may be carried out by employing different models for different regimes (as the flow phenomena of dense- and dilute-phase are very different: non-suspension to suspension flow mode).

CHAPTER 4: Modelling Dense- to Dilute-Phase Transition Criteria

Previous investigations (Chapter 3) to examine the scale-up accuracy and stability of the different "existing" models for Pressure Minimum Curve (Rose and Duckworth, 1969; Matsumoto, 1974; Rizk, 1976; Weber, 1981; Schade, 1987; Cabrejos and Klinzing, 1994; Kalman et al., 2005) by plotting the predicted pressure minimum curve on to the experimental straight pipe pneumatic conveying characteristics (PCC) for fly ash and "white powder" have shown that the models generally can provide significant inaccuracy. Therefore, an effort has been made to develop a pressure minimum model which will predict the PMC with significant accuracy under scale up conditions. The design parameters are chosen in such a way that the effect of every parameter came into play directly or indirectly. Particle diameter (d) must affect pressure minimum point as with the change in particle size the flow behavior changes. Dynamic viscosity (μ) is the resistance to the flow so it must affect the pressure minimum point. The effective density of fluidised dense phase inside the pipe is difference between densities of particle and that of air ($\rho_p - \rho$) hence it will also affect the pressure minimum point. Keeping above points into mind, the velocity at pressure minimum point (V_{pmc}) taken to be a function of diameter of the particle (d), dynamic viscosity (μ), acceleration due to gravity (g), difference between density of particle and that of air ($\rho_p - \rho$) and density of air (ρ). The expression obtained is as follows.

$$V_{pmc} = f(\rho, d, g, \mu, \rho_p - \rho) \tag{4.1}$$

The above expression can also be written as:

$$f'(V_{pmc}, \rho, d, g, \mu, \rho_p - \rho) = 0 \tag{4.2}$$

4.1 Development of model using Buckingham π theorem

BUCKINGHAM π THEOREM as described by Cengel et al. (2003) is used for development of the model. The variables taken in our problem are having following dimensions.

μ	$[ML^{-1}T^{-1}]$
$(\rho_p - \rho)$	$[ML^{-3}]$
V_{pmc}	$[LT^{-1}]$
d	[L]
g	$[LT^{-2}]$
ρ	$[ML^{-3}]$

As per the three primary dimensions the repeating variables selected are:

- Density (ρ)
- Particle diameter (d)
- Dynamic fluid viscosity (μ)

Primary variables left over are:

- Acceleration due to gravity (g)
- Velocity at pressure minimum point (V_{pmc})
- Difference of density of particle and that of air ($\rho_p - \rho$)

The numbers of π terms are n-m, which comes out to be three and derived as follows:

First π term:

$\pi_1 = \rho^{a_1} d^{b_1} \mu^{c_1} g$

$[M^0L^0T^0] = [ML^{-3}]^{a_1} [L]^{b_1} [M L^{-1}T^{-1}]^{c_1} [LT^{-2}]$

Solving for the values of a_1, b_1 and c_1 it was found that:-

$a_1 = 2$

$b_1 = 3$

$c_1 = -2$

Therefore

$$\pi_1 = \frac{\rho^2 d^3 g}{\mu^2} \quad (4.3)$$

Second π term:

$\pi_2 = \rho^{a_2} d^{b_2} \mu^{c_2} V_{pmc}$

$[M^0L^0T^0] = [ML^{-3}]^{a_2} [L]^{b_2} [M L^{-1}T^{-1}]^{c_2} [LT^{-1}]$

Solving for the values of a_2, b_2, c_2 it was found that:-

$a_2 = 1$

$b_2 = 1$

$c_2 = -1$

Therefore

$$\pi_2 = \frac{\rho d V_{pmc}}{\mu} = Re \quad (4.4)$$

Third π term:

$\pi_5 = \rho^{a_3} d^{b_3} \mu^{c_3} (\rho_p - \rho)$

$[M^0L^0T^0] = [ML^{-3}]^{a_3}\,[L]^{b_3}\;\;[M\,L^{-1}T^{-1}]^{c_3}\;\;[ML^{-3}]$

Solving for the values of $a_3,\ b_3,\ c_3$ it was found that:-

$a_3 = -1$

$b_3 = 0$

$c_3 = 0$

Therefore

$$\pi_3 = \frac{(\rho_p - \rho)}{\rho} \tag{4.5}$$

From the above three π terms 1st and 3rd π terms (equation 4.3 and 4.5) are combined to form a new π term as employed by Cengel et al. (2003).

$$\pi_3\pi_1 = \frac{\rho^2 d^3 g}{\mu^2}\frac{(\rho_p - \rho)}{\rho} = \frac{\rho(\rho_p - \rho)d^3 g}{\mu^2} = \mathrm{Ar} \tag{4.6}$$

After getting both the π terms/dimensionless number (Re and Ar) the terms are modelled as:

$$\mathrm{Re} = \mathrm{KAr}^x \tag{4.7}$$

Where K and x are constants, for obtaining the values of k and x, regression is done using the pressure minimum curve obtained from experimental data of fly ash (69mm ID and 554m long pipe, P11-P12 tappings) and white powder (69mm ID and 148m long pipe, $P11^+$-P12 tappings), which were showing U-shape trends. The final model (with constant k and x values) obtained from the fly ash data is shown in equation 4.8:

$$Re = 8.027Ar^{1.001} \qquad [R^2 = 0.999] \qquad (4.8)$$

Experimental values of Re at pressure minimum curve (calculated from test data) were compared with predicted values (using equation 4.8), as shown in Figure 4.1.

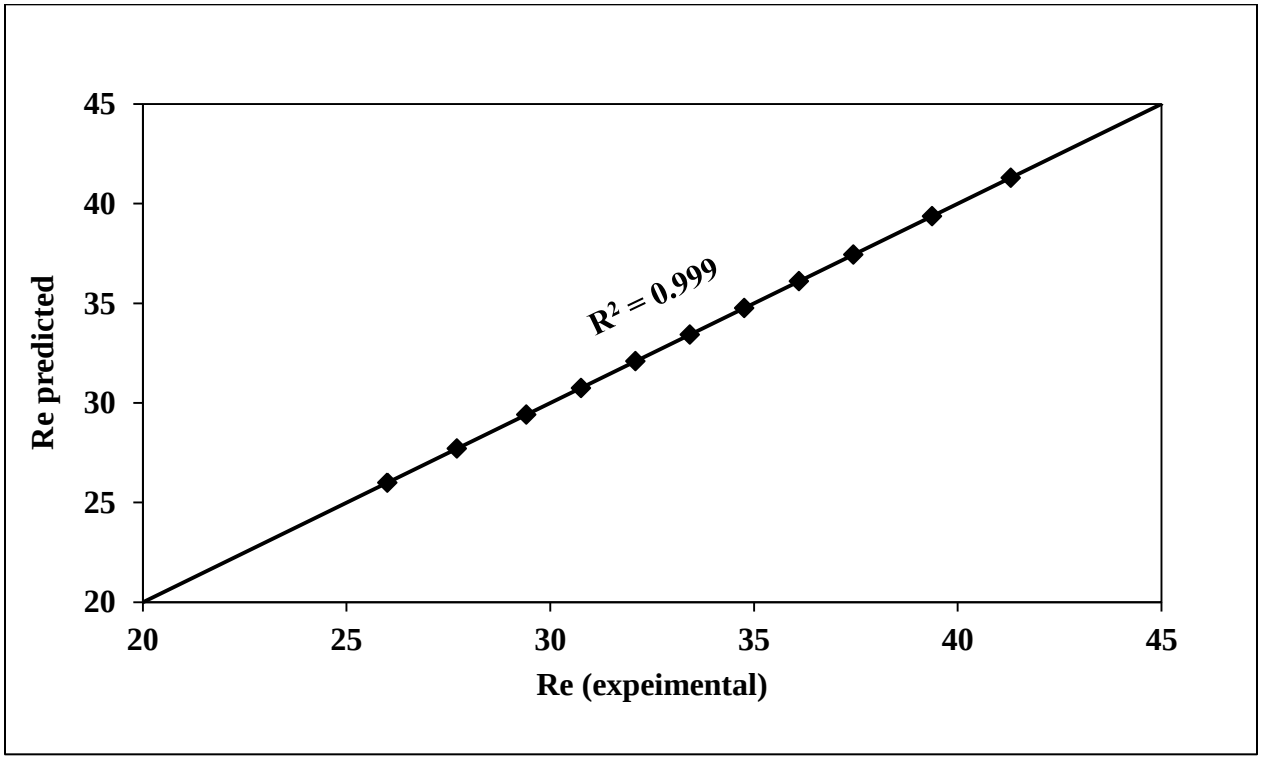

Figure 4.1: Reynolds number at pressure minimum curve - predicted versus experimental for fly ash for model: $Re = 8.027Ar^{1.001}$

The high value of R^2 for the model suggests that the agreement between the experimental and predicted values of Re was very good (i.e. the correlation shows an "excellent fit"). The model (with constant k and x values) obtained from the white powder (69mm ID and 148m long pipe, $P11^+$-P12 tappings) data is shown in equation 4.9:

$$Re = 1.694Ar^{1.004} \qquad [R^2 = 0.999] \qquad (4.9)$$

Experimental values of Re at pressure minimum curve (calculated from test data) were compared with predicted values (using equation 4.9), as shown in Figure 4.2.

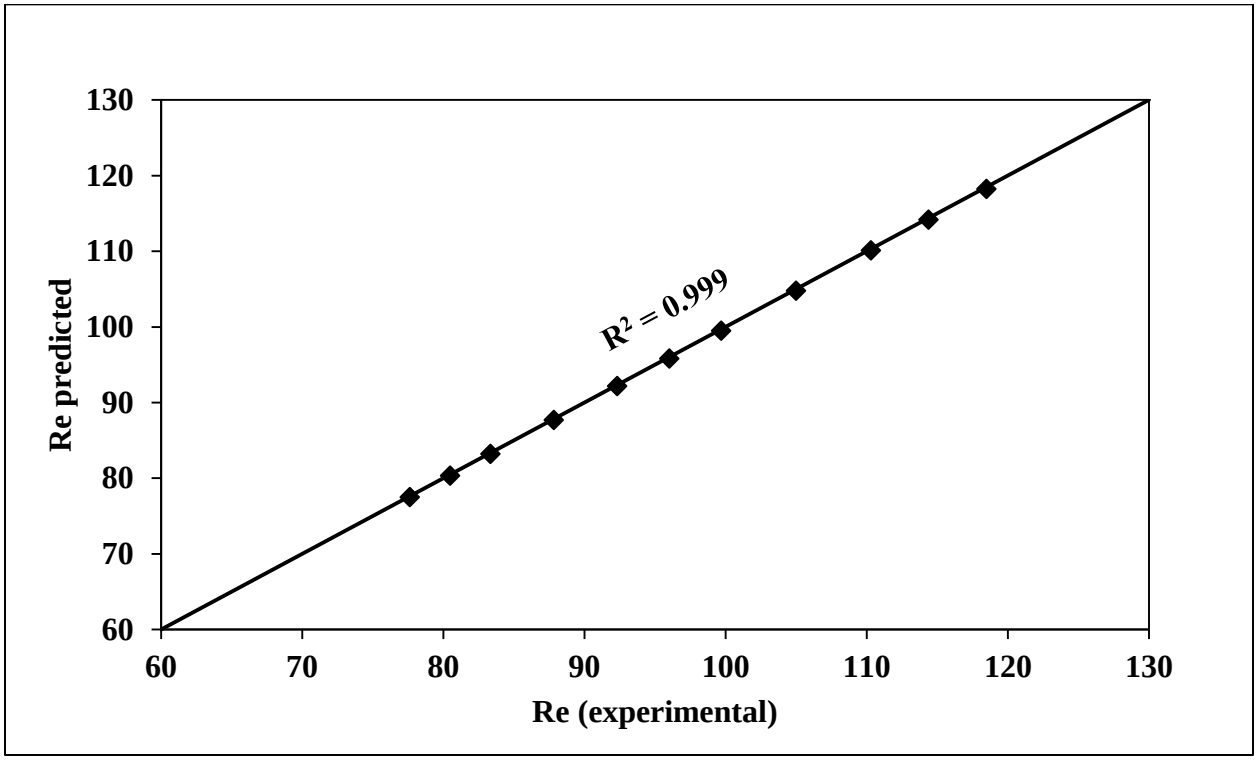

Figure 4.2: Reynolds number at pressure minimum curve - predicted versus experimental for fly ash for model: $Re = 1.694Ar^{1.004}$

The high value of R^2 (similar to the fly ash model) for the model suggests that the agreement between the experimental and predicted values of Re was very good (i.e. the correlation shows an "excellent fit"). Hence these models are chosen to predict the Pressure Minimum Curve (PMC) under scale up conditions.

4.2 Evaluation of the model

The models obtained above (i.e. in equation 4.8 and 4.9) are evaluated for fly ash (69mm ID and 554m long pipe, P11-P12 tappings) and white powder (69mm ID and 148m long pipe, $P11^{+}$-P12 tappings) and compared with the existing models discussed in the previous chapter (Figure 3.23 and 3.24) by superimposing on the same PCC. The results obtained are shown in the Figure 4.3 and 4.4.

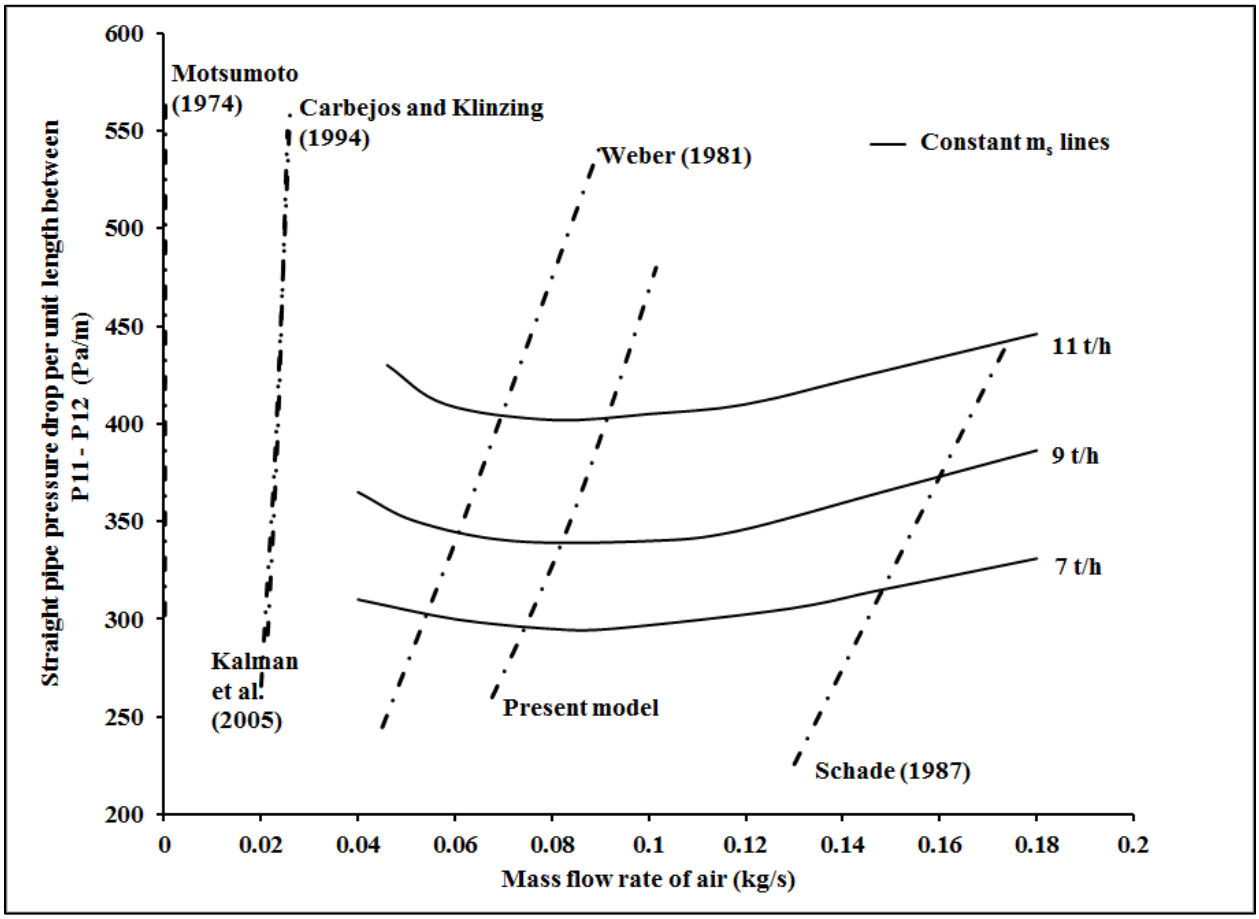

Figure 4.3: Evaluation of new model and existing models for PMC on straight-pipe PCC, fly ash, P11-P12, 69 mm I.D. × 554 m long pipe

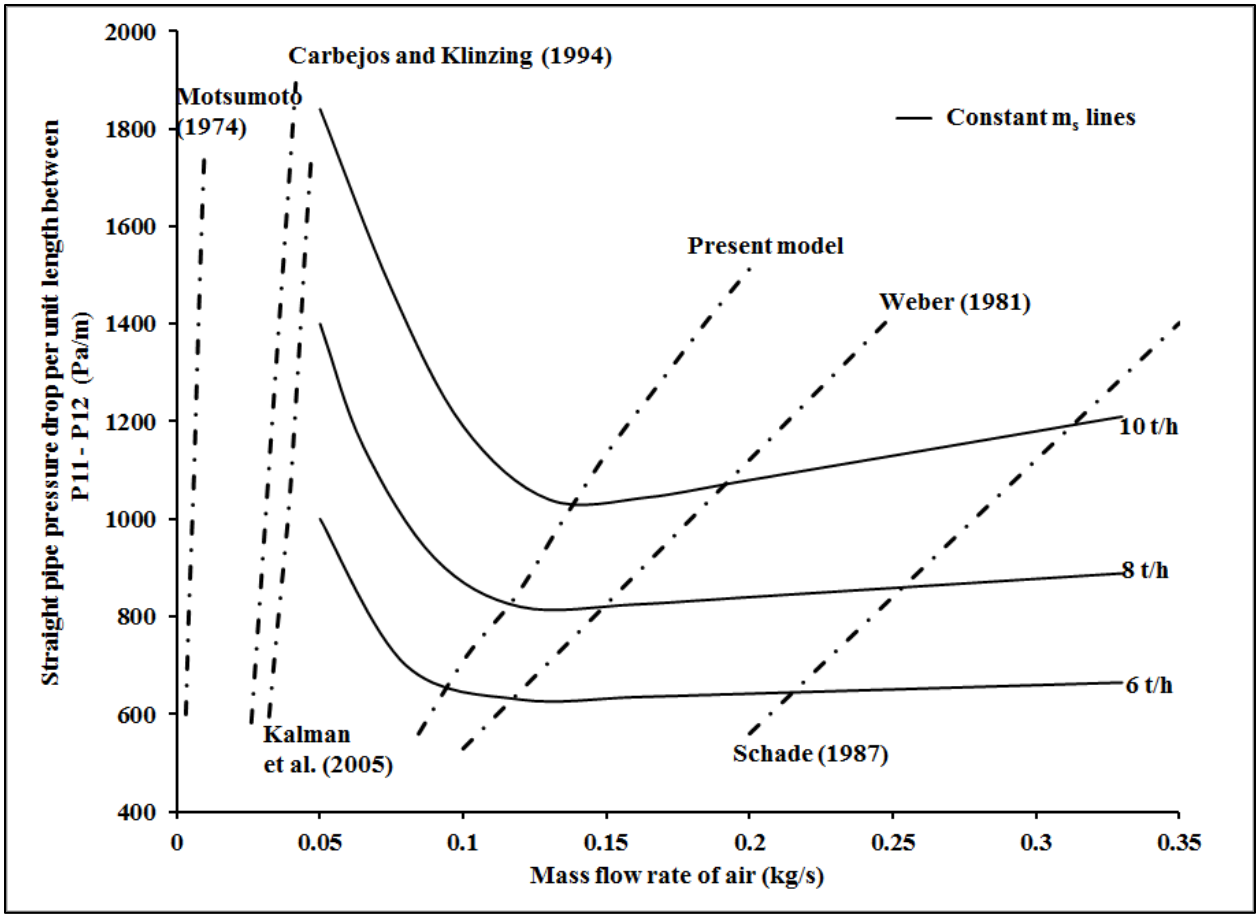

Figure 4.4: Evaluation of new model and existing models for PMC on straight-pipe PCC, white powder, $P11^{+}$-P12, 69 mm I.D. × 148 m long pipe

The PMC obtained from the fly ash and white powder models (equation 4.8 and 4.9) are coming very closer to the experimental pressure minimum points. It is clear from the Figure 4.3 and Figure 4.4 that the predictions of present models are much more accurate as compared to other existing models. As the present models (equation 4.8 and 4.9) is obtained by doing regression from fly ash (69mm ID and 554m long pipe, P11-P12 tappings) and white powder (69mm ID and 148m long pipe, $P11^{+}$-P12 tappings) data, so the predictions of present models as in the Figures 4.3 and 4.4 are nothing but just testing the back calculations.

Therefore it is difficult to rely upon both the models on the basis of above prediction. Hence for better reliability of both the models, the predictions of the models were tested for scale up conditions and the results are discussed in the following. The prediction of fly ash model (equation 4.8) is tested for fly ash (69mm ID and 554m long pipe, P9-P10 tappings), and the result is shown in the Figure 4.5.

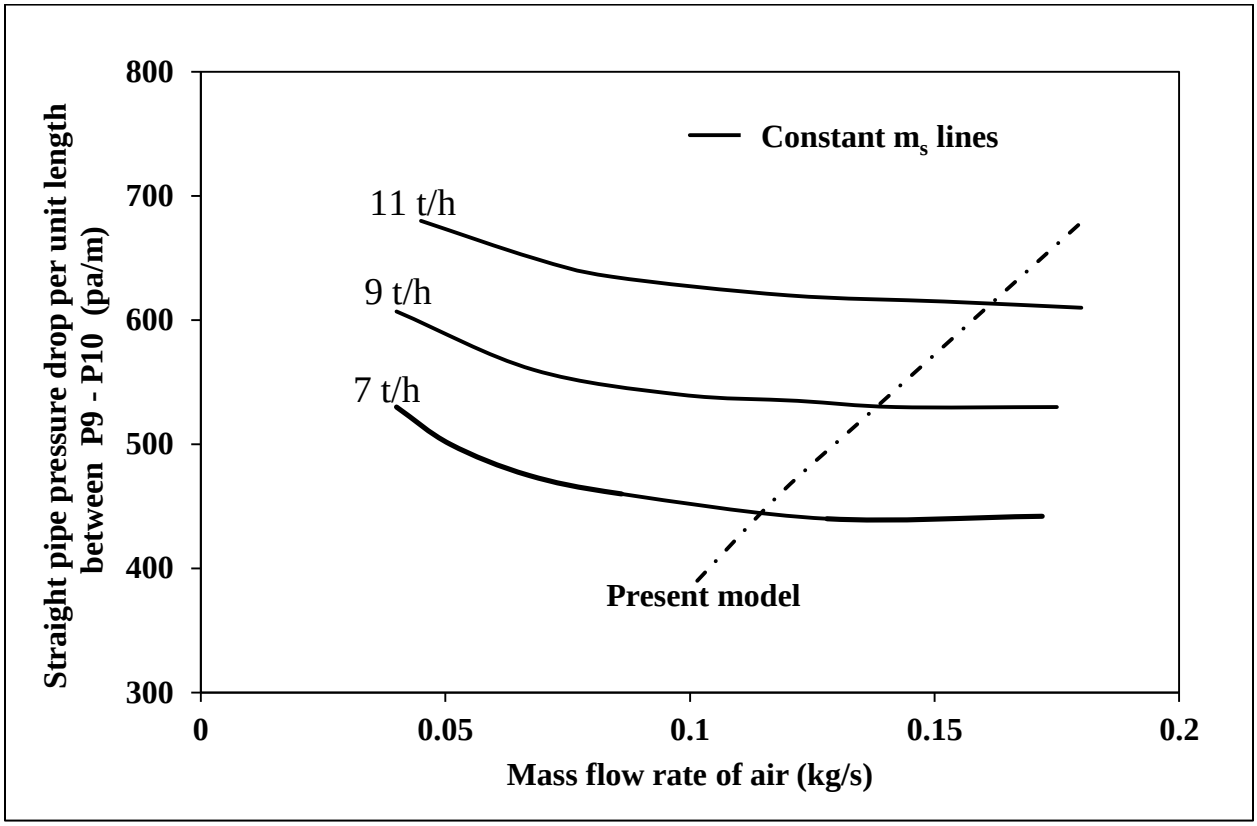

Figure 4.5: Evaluation of new model for PMC on straight-pipe PCC, fly ash, P9-P10, 69 mm I.D. × 554 m long pipe

The fly ash model (equation 4.8) is predicted for the fly ash pipe-line having same diameter and length (i.e. for 69 mm I.D. × 554 m long pipe), but for the different tapping points (i.e. for P9-P10) and the pressure minimum curve obtained from the model is shown in the Figure 4.5. The

model predicted plot suggests that the dense to dilute transition occurs at m_f ranges from 0.12 to 0.16 kg/s, which seems to be a good prediction. The prediction of fly ash model (equation 4.8) is tested for fly ash (105 mm ID and 168 m long pipe, P9-P10 and P11-P12 tappings). The results are shown in the Figures 4.6 and 4.7.

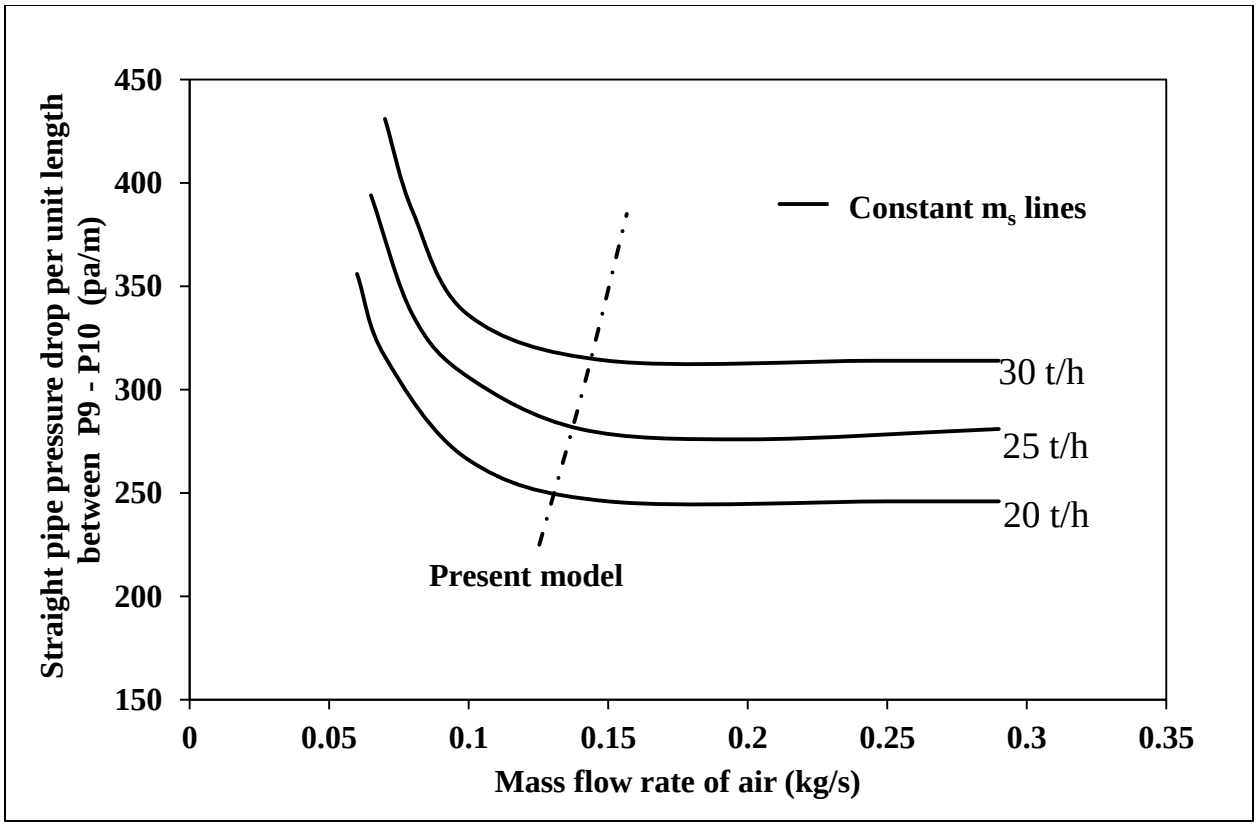

Figure 4.6: Evaluation of new model for PMC on straight-pipe PCC, fly ash, P9-P10, 105 mm I.D. × 168 m long pipe

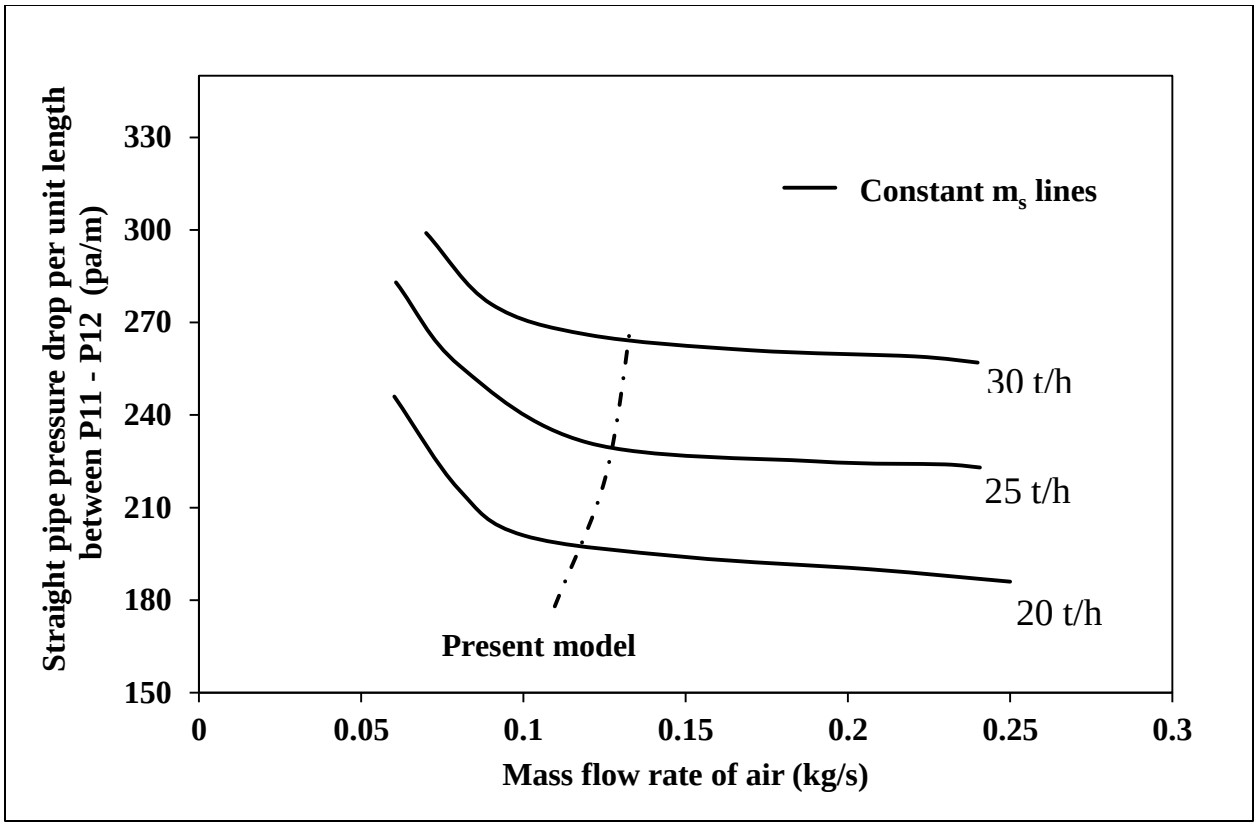

Figure 4.7: Evaluation of new model for PMC on straight-pipe PCC, fly ash, P11-P12, 105 mm I.D. × 168 m long pipe

The fly ash model (equation 4.8) is predicted for the fly ash pipe line having different internal diameter (ID) but for same length (i.e. for 105 mm I.D. × 168 m long pipe, P9-P10 and P11-P12 tappings) and the pressure minimum curves obtained from the model are shown in the Figures 4.6 and 4.7. The model line suggests that the dense to dilute-phase transition for both the cases occurs at m_f ranges from 0.1 to 0.15 kg/s, which seems to be a good prediction under the diameter scale up condition.

The prediction of "white powder" model (equation 4.9) is tested for white powder (69 mm ID and 148 m long pipe, P9-P10 tappings), and the result is shown in the Figure 4.8.

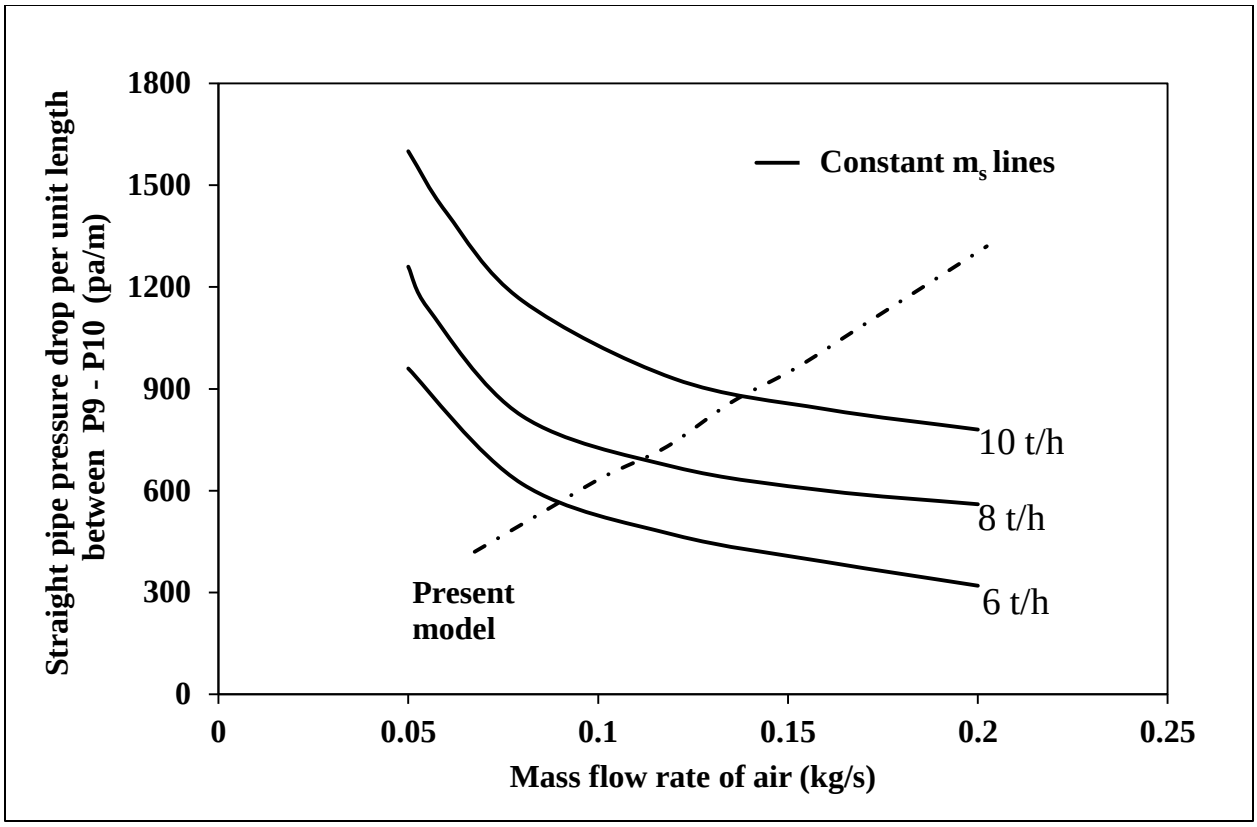

Figure 4.8: Evaluation of new model for PMC on straight-pipe PCC, white powder, P9-P10, 69 mm I.D. × 148 m long pipe

The white powder model (equation 4.9) is predicted for the white powder pipe-line having same diameter and overall length (i.e. for 69 mm I.D. × 148 m long pipe) but for the different tapping points (i.e. for P9-P10) and the pressure minimum curve obtained from the model is shown in the Figure 4.8. The PMC line obtained from the model indicate change in slope to some extent.

Based on the new model and its predictions presented in this chapter, the new model is representing the Pressure Minimum Curve (PMC) (i.e. showing change in flow mechanism from dense- to dilute-phase) in case of fly ash (69mm ID and 554m long pipe) and white powder (69mm ID and 148m long pipe). The new model predictions are much better than the predictions

shown by the models proposed by other researchers, but only limited validation of the model was done here due to lack of data. Further research has to be conducted, to understand the change in flow characteristics along the flow direction (dense- to dilute-phase) and to validate the model experimentally.

CHAPTER 5: Modelling Straight Pipe Pressure Drop for Fluidised Dense Phase

Pressure drop for solid and gas flow through a straight pipe is as (barth et al. 1958):

$$\Delta p = \frac{(\lambda_f + m^* \lambda_s) L \rho V^2}{2D} \tag{5.1}$$

Pressure minimum criteria:

$$\frac{d\Delta p}{dV} = 0 \tag{5.2}$$

$$\frac{d}{dV}\left\{\frac{(\lambda_f + m^* \lambda_s) L \rho V^2}{2D}\right\} = 0 \tag{5.3}$$

To determine the above equation 5.3, model for λ_s must be known beforehand. The existing dense-phase model for λ_s in the form $k(m)^a(Fr)^b$ are empirical and generally inaccurate under scale-up conditions of pipe length and diameter (Mallick 2010). Marcus et al. (1990) and Wypych et al. (1990) have provided a dilute-phase model (WEBER A4 model) which is reported to work well for dilute phase (Wypych et al. 1990). This model is as given below:

$$\lambda_s = \lambda_s{}^* \frac{C}{V} + \frac{2\beta}{Fr^2 C/V} \tag{5.4}$$

In this model $\lambda_s{}^*$ is an empirical factor that includes particle to wall impact and particle to air friction factor. The value of $\lambda_s{}^*$ are available in Marcus et al. (1990) and Wypych et al. (1990). In the case of dense-phase, one additional factor must be taken into consideration: particle to particle collision (due to close proximity of the particle for the highly concentrated

nature of flow). An attempt had been made in the following to include the particle –particle impact effect using energy-based modelling approach.

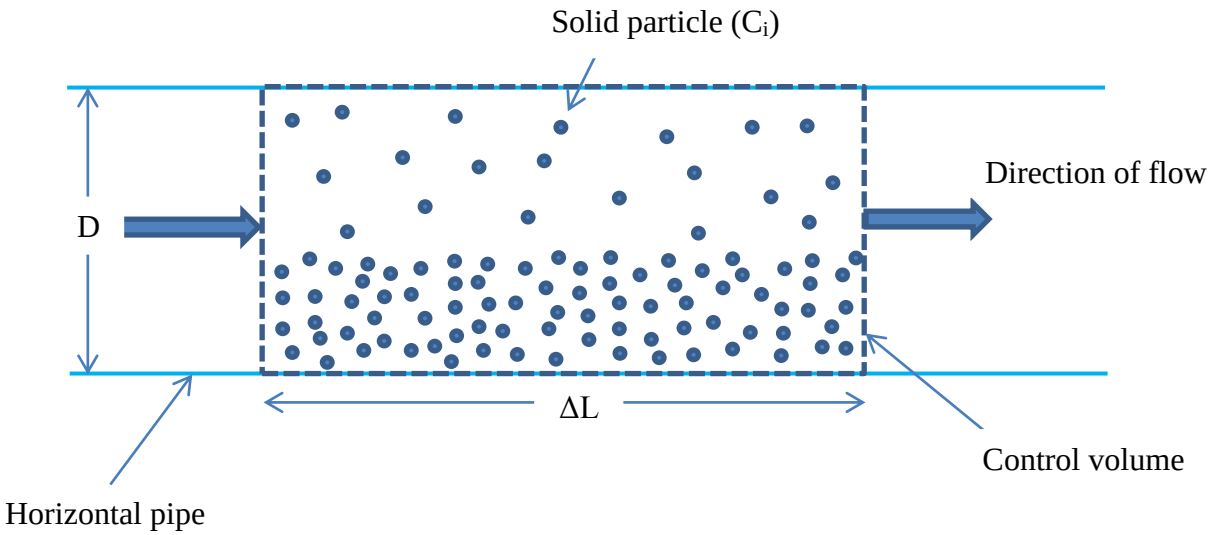

Figure 5.1: Dense phase flow of fine powders in a control volume

E_L = Energy loss (K.E.) due to particle impact against other particles (i.e. assuming non-elastic particle-particle collision) and further re-acceleration of the decelerated/stopped to particle velocity (= C) within a control volume.

ΔM_p = Total mass of particles in a control volume [kg].

N = Total number of particles in a control volume.

m_p = mass of each particle [kg].

ρ_p = Particle density [kg/m^3].

ε = voidage.

Assumption:

There are total (n+1) subgroups within 'N' number of particles which have got decelerated to different velocities (for each group); starting from 0 to C:

$$\underbrace{\{0, 0+\Delta C, 0+2\Delta C, 0+3\Delta C \ldots\ldots 0+n\Delta C\}}_{\text{Total (n+1) terms}}$$

As

$n\Delta C = C$ This in turn gives $n = \frac{C}{\Delta C}$

Therefore,

Number of particles in each of the (n+1) groups = $\frac{N}{n+1}$

5.1 Energy-based modelling:

E_1 = Energy required to import K.E. to particle which have gone to C = 0.

E_2 = Energy required to import K.E. to particle which have gone to C = 0+ΔC.

Similarly for

E_{n+1} = Energy required to import K.E. to particle which have gone to C = 0+nΔC.

As we have energy required is equal to K.E required.

So

$$E_1 = \frac{1}{2}\left\{m_p \frac{N}{n+1}\right\}\{C^2 - 0^2\}$$

$$E_2 = \frac{1}{2}\left\{m_p \frac{N}{n+1}\right\}\{C^2 - \Delta C^2\}$$

$$E_3 = \frac{1}{2}\left\{m_p \frac{N}{n+1}\right\}\{C^2 - 2\Delta C^2\}$$

Similarly for

$$E_{n+1} = \frac{1}{2}\left\{m_p \frac{N}{n+1}\right\}\{C^2 - n\Delta C^2\}$$

$E_L = E_1 + E_2 + E_3 + \ldots\ldots\ldots\ldots\ldots\ldots\ldots\ldots\ldots\ldots\ldots\ldots\ldots\ldots\ldots\ldots + E_{n+1}$

$$E_L = \left\{\frac{1}{2} m_p \frac{N}{n+1}\right\} C^2\{(1^2 + 1^2 \ldots\ldots\ldots\ldots (n+1)\text{terms})$$

$$- (\Delta C/C)^2(1^2 + 2^2 \ldots\ldots\ldots n \text{ terms})\}$$

$$E_L = \left\{\frac{1}{2} m_p \frac{N}{n+1}\right\} C^2\{(n+1) - (\Delta C/C)^2(n(n+1)(2n+1)/6)\}$$

Substituting $\frac{\Delta C}{c} = \frac{1}{n}$

$$E_L = \left\{\frac{1}{2} m_p \frac{N}{n+1}\right\} C^2\{(n+1) - (1/n)^2(n(n+1)(2n+1)/6)\}$$

$$E_L = \left\{\frac{1}{2} m_p \frac{N}{n+1}\right\} C^2(n+1)\left\{1 - \frac{2n+1}{6n}\right\}$$

$$E_L = \left\{\frac{m_p N}{2}\right\} C^2\left\{\frac{6n - 2n - 1}{6n}\right\}$$

$$E_L = \left\{\frac{m_p N}{2}\right\} C^2\left\{\frac{6n - 2n - 1}{6n}\right\}$$

$$E_L = \left\{\frac{m_p N}{2}\right\} C^2\left\{\frac{4n - 1}{6n}\right\}$$

$$E_L = \left\{\frac{m_p N}{2}\right\} C^2\left\{\frac{2}{3} - \frac{1}{6n}\right\}$$

As n tends to infinity (∞) then 1/6n tends to zero.

So

$$E_L = \left\{\frac{m_p N}{2}\right\} C^2 \left\{\frac{2}{3}\right\}$$

Since $m_p N = \Delta M_p$

$$E_L = \frac{\Delta M_p C^2}{3}$$

$$\text{Therefore kinitic energy loss per unit specific volume} = \frac{\frac{\Delta M_p C^2}{3}}{\frac{\Delta M_p}{\rho^*}}$$

Where, $\rho^* = \rho_p(1-\varepsilon)$

$$\text{Kinitic energy loss per unit specific volume} = \frac{C^2 \rho^*}{3} = C(C\rho^*/3)$$

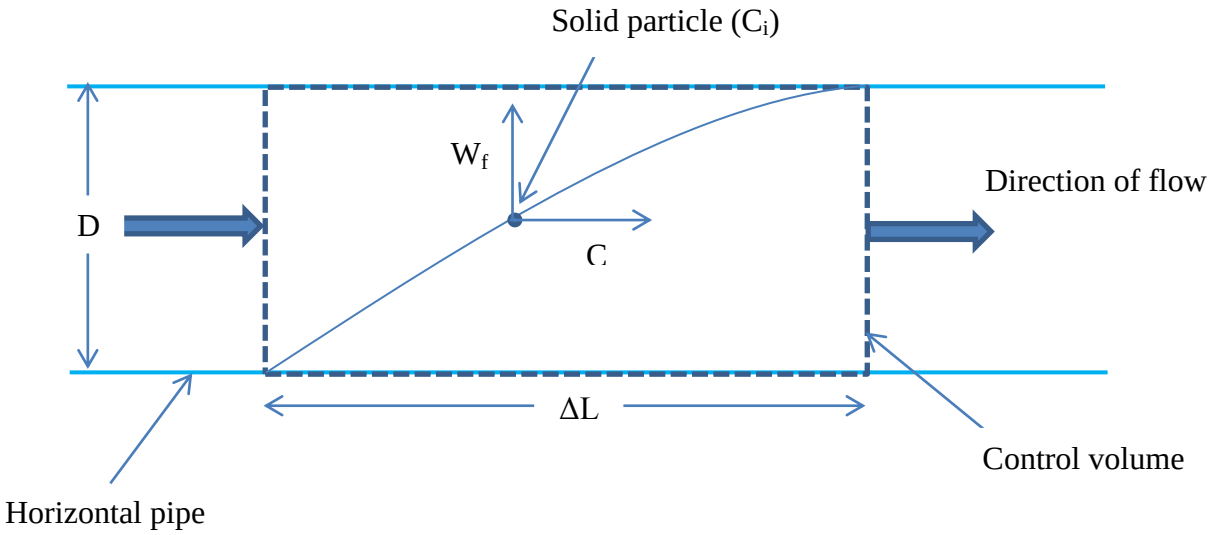

Figure 5.2: Schematic diagram showing single particle movement

As per the Figure 5.2, a single particle motion time (t) is calculated as:

$$t = \frac{\Delta L}{C} = \frac{D}{W_f} \qquad \text{and} \qquad C = \frac{\Delta L W_f}{D}$$

Kinitic energy loss per unit specific volume $= \left\{\frac{\Delta L W_f}{D}\right\}\left\{\frac{C\rho^*}{3}\right\}$

From chapter 6 – Marcus et. al. (Book: Pneumatic conveying of solids)

$$\lambda_s m^* \frac{\rho V^2}{2}\frac{\Delta L}{D} = \lambda_s{}^* \rho^* C^2 \frac{\Delta L}{D} + \rho^* g \Delta L \frac{W_f}{V} \tag{5.5}$$

Adding the kinetic energy loss per unit specific volume in the above expression (5.5)

$$\lambda_s m^* \frac{\rho V^2}{2}\frac{\Delta L}{D} = \lambda_s{}^* \rho^* C^2 \frac{\Delta L}{D} + \rho^* g \Delta L \frac{W_f}{V} + \frac{\Delta L W_f}{D}\frac{C\rho^*}{3} \tag{5.6}$$

As

$$m^* = \frac{\rho^* C}{\rho V}$$ Ref: page 226-Morcus et. al.]

Substituting in equation (5.6),

$$\lambda_s \frac{\rho^* C}{\rho V}\frac{\rho V^2}{2}\frac{\Delta L}{D} = \lambda_s{}^* \rho^* C^2 \frac{\Delta L}{D} + \rho^* g \Delta L \frac{W_f}{V} + \frac{\Delta L W_f}{D}\frac{C\rho^*}{3} \tag{5.7}$$

$$\lambda_s \frac{CV}{2D} = \lambda_s{}^* \frac{C^2}{D} + g\frac{W_f}{V} + \frac{CW_f}{3D}$$

$$\lambda_s = \lambda_s{}^* \frac{C^2}{D}\frac{2D}{CV} + g\frac{W_f}{V}\frac{2D}{CV} + \frac{CW_f}{3D}\frac{2D}{CV}$$

$$\lambda_s = \lambda_s{}^* \frac{C}{V} + \frac{2W_f/_V}{Fr^2 C/_V} + \frac{W_f}{3V}$$

As we have $\beta = \frac{W_f}{V}$

By putting the value of β

$$\lambda_s = \lambda_s^{*} \frac{C}{V} + \frac{2\beta}{Fr^2 C/V} + \frac{\beta}{3} \tag{5.8}$$

The solid friction factor is modified by including the particle and particle collision and expression obtained is as per the equation 5.8. The value of λ_s^{*} is obtained from the experimental data point for fly ash (69mm ID and 168m long pipe line, P11-P12 tappings). The experimental data point is chosen in the very dilute region (where C/V ratio is assumed to be 0.99). The terminal velocity (W_f) was obtained for fly ash and ESP dust with the help of plot provided in Wypych (2006), which comes out to be 0.06 m/s and 0.005 m/s respectively. Then with the help of equation 5.1 and experimental data the value of λ_s^{*} was obtained. The final expressions obtained in the case of fly ash are shown in equation 5.9 and 5.10.

Fly ash

As per original WEBER A4 model:

$$\lambda_s = 0.00437 \frac{C}{V} + \frac{2\beta}{Fr^2 C/V} \tag{5.9}$$

New model (including particle and particle collision):

$$\lambda_s = 0.0032 \frac{C}{V} + \frac{2\beta}{Fr^2 C/V} + \frac{\beta}{3} \tag{5.10}$$

Here C/V is the ratio of particle velocity to the superficial velocity of fluid. It can be calculated using the expressions given in equation 5.11 and 5.12 proposed by Wypych et al. (1990).

$$\frac{C}{V} = \frac{1}{1+V_{\infty}\left(\frac{\lambda_S^*}{2gD}\right)^{0.5}} \tag{5.11}$$

Here V_{∞} can be obtained from following expression

$$V_{\infty} = \left[\frac{4gd(\rho_p-\rho)}{3C_{d\rho}}\right]^{0.5}\left[1-\left(\frac{d}{D}\right)^2\right] \tag{5.12}$$

ESP dust

Similar procedure was followed using the experimental data point for ESP dust (69 mm ID and 554 m long pipe line, P9-P10 tappings data). The expressions obtained are listed in the equation 5.13 and 5.14:

As per original WEBER A4 model:

$$\lambda_s = 0.014\frac{C}{V} + \frac{2\beta}{Fr^2 C/V} \tag{5.13}$$

New model (including particle and particle collision):

$$\lambda_s = 0.013\frac{C}{V} + \frac{2\beta}{Fr^2 C/V} + \frac{\beta}{3} \tag{5.14}$$

5.2 Evaluation of pressure drop model

The models listed above were evaluated for total pipe line pressure drop to evaluate accuracy of new model. For calculation of total pipe-line pressure drop an iterative programme was used. The programme was originally used by Mallick (2010). The program consists of following features:

- Programme starts from the end of pipe-line where pressure was equal to atmosphere pressure (i.e. 100 kPa).
- Pipe-line was divided into small sections, individual pressure change was calculated for each section, using the pressure drop model for straight pipe, the losses due to initial acceleration and bend were also considered by using the models proposed by Chambers and Marcus (1986).
- For each part iterations were performed by assuming pressure at the end of each section, for performing iterations solver in excel was used. The programme was written and edited using excel VBA (visual basic editor), which perform iteration up to a significant accuracy with the help macros.
- The programme written and used by Mallick (2010) was modified by changing the expression for calculating pressure drop, the sample of the modified programme for 69 mm ID and 168 m long pipe line is provided in Appendix A.

The fly ash new model (equation 5.10) and original Weber A4 model (equation 5.9) are evaluated for fly ash (69 mm ID and 168 m long pipe line, 69 mm ID and 554 m long pipe line and 105 mm ID and 168 m long pipe line). The original Weber A4 model was evaluated

so that we can compare the results of original weber A4 model with our new derived model. The results obtained for pressure drop are plotted on the PCC and are compared with the experimental pressure drop lines. The resultant PCC's are shown in the Figure 5.3, 5.4 and 5.5.

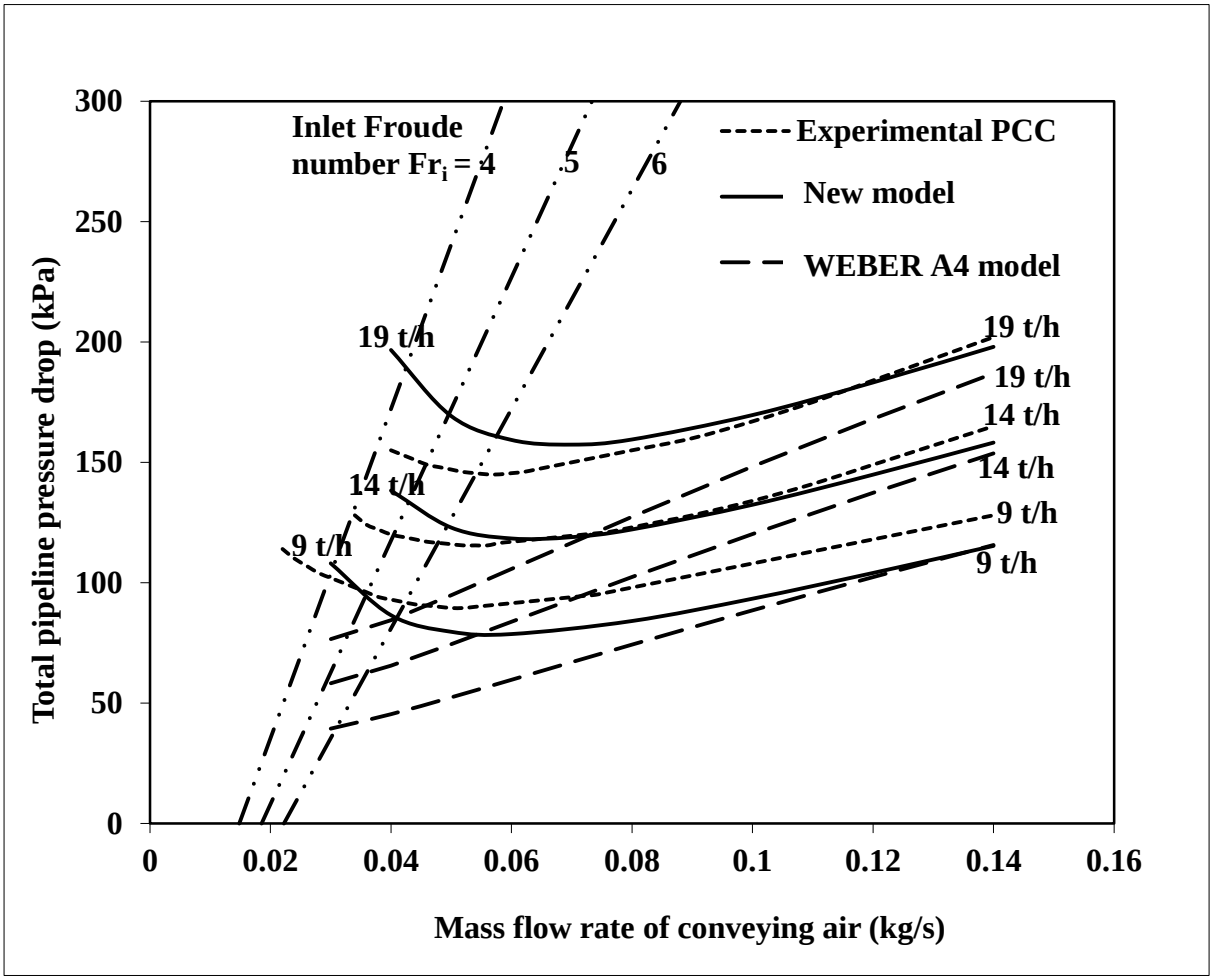

Figure 5.3: Experimental Versus Predicted PCC for Fly ash and 69 mm I.D. × 168 m Pipe using Equations (5.9) and (5.10)

The result is shown in Figure 5.3. It is clear from the Figure 5.3 that the new model (equation 5.10) gives better prediction than that of original WEBER A4 model (equation 5.9). The new model is giving good predictions in case of high mass flow rate of air (m_f) values (i.e. in case of dilute-phase region) and giving over prediction in case of low m_f values (i.e. in case of dense-phase region). It is also inferred from the Figure 5.3 that the new model is better in

case of high mass flow rate of solid (m_s) values (i.e. is better predicting in case of m_s = 19 t/h as compared to that of m_s = 9 t/h). The new model gives 'U'-shape trend (i.e. slop is changing from dense to dilute) and on the other side original Weber A4 model provides straight down predictions (no 'U'-shape).

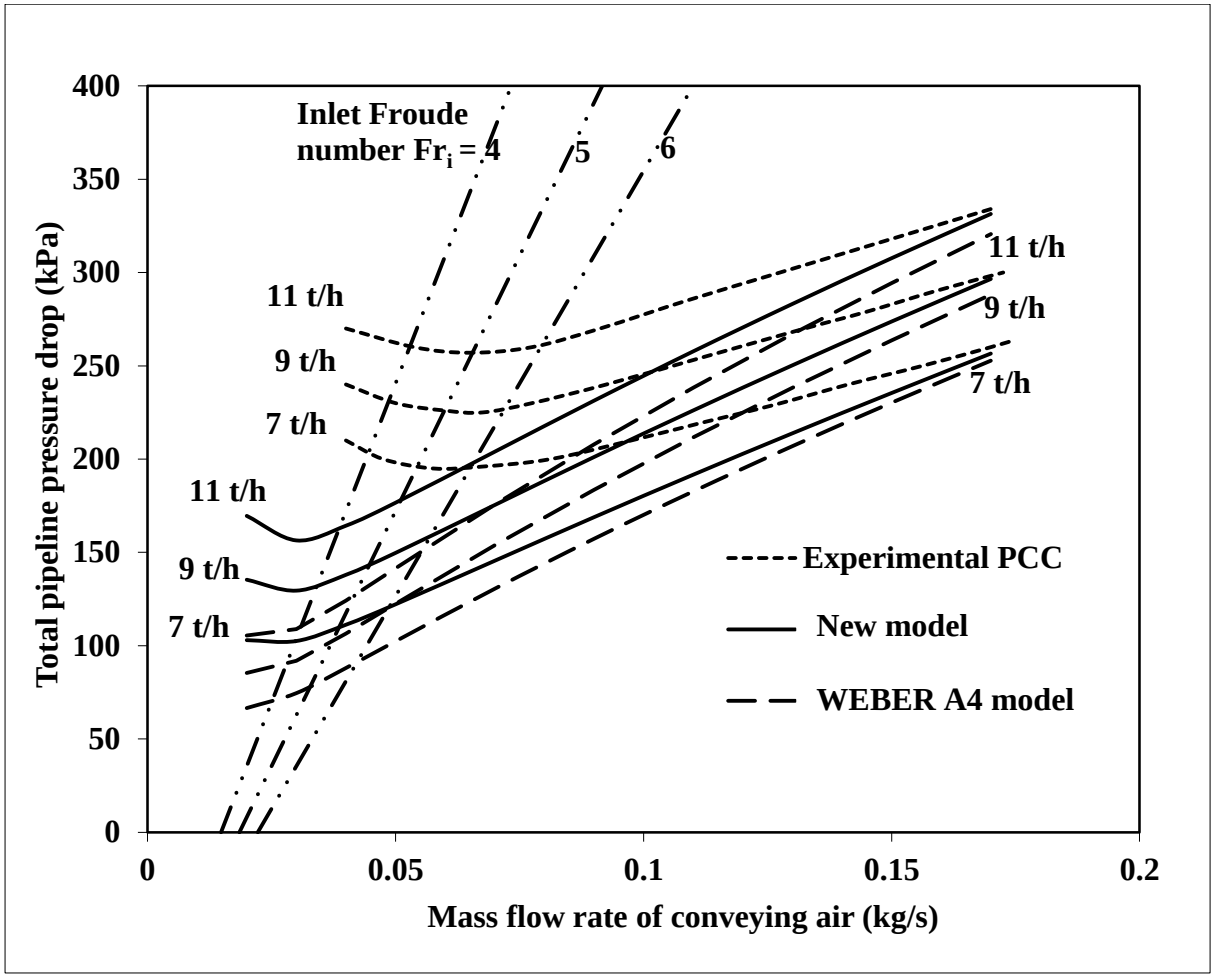

Figure 5.4: Experimental Versus Predicted PCC for Fly ash and 69 mm I.D. × 554 m Pipe using Equations (5.9) and (5.10)

The new model (equation 5.10) predictions are drawn on to the experimental PCC for fly ash and 69 mm ID and 554 m long pipe and the result are shown in Figure 5.4. It is clear from the Figure 5.4 that the new model gives better prediction than that of original WEBER A4 model (equation 5.9). The model exhibits under-prediction as compared to that of the experimental

curve. The under prediction is more in case of dense region as compared to that of the values obtained in case of dilute region, but the new model predicts values much closer to that of the experimental values.

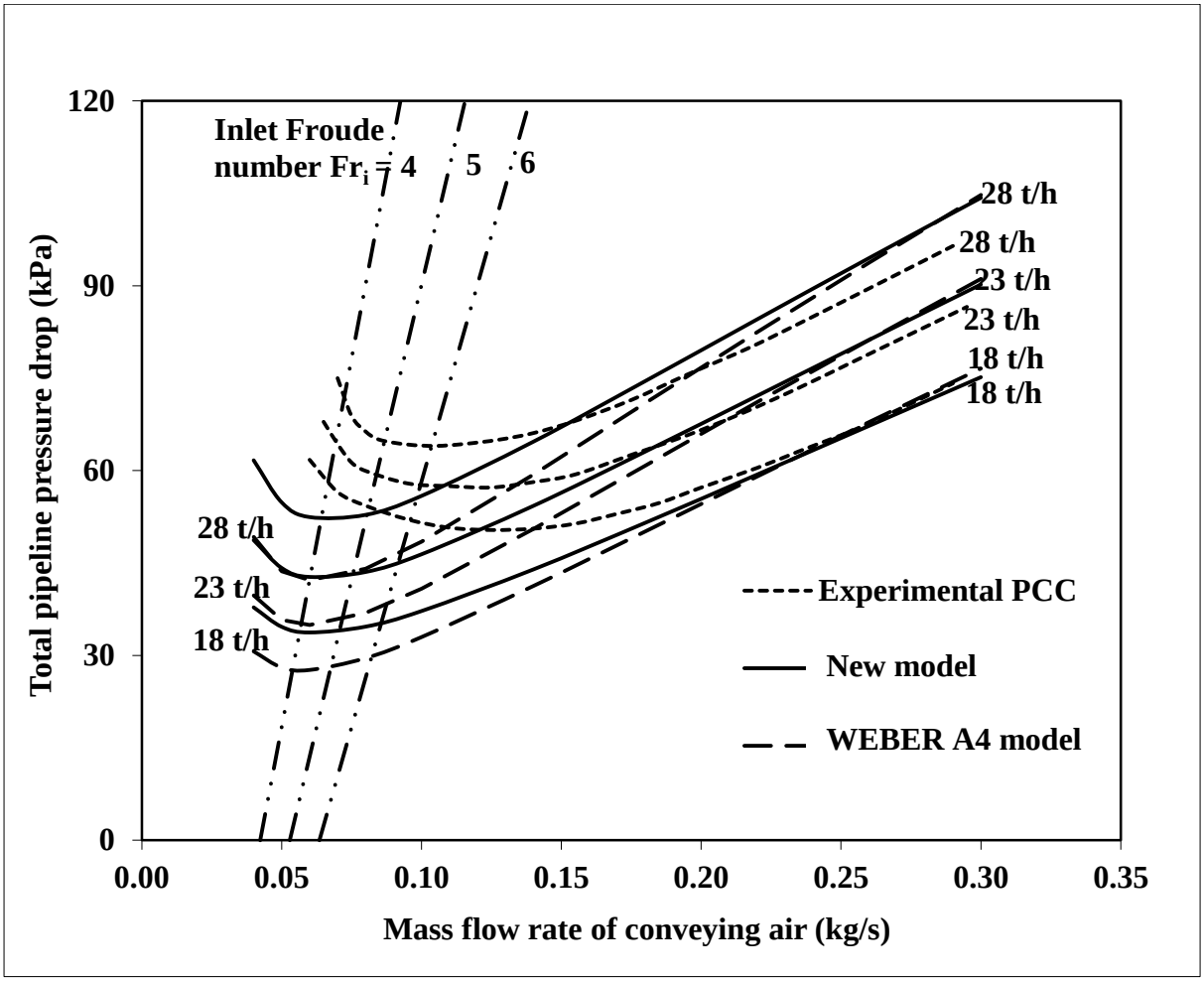

Figure 5.5: Experimental Versus Predicted PCC for Fly ash and 105 mm I.D. × 168 m Pipe using Equations (5.9) and (5.10)

The new model (equation 5.10) predictions are drawn on to the experimental PCC for fly ash and 105 mm ID and 168 m long pipe and the result is shown in Figure 5.5. It is clear from the Figure 5.5 that the new model gives better prediction than that of original WEBER A4 model

(equation 5.9). The model exhibits under prediction in dense phase and some over prediction in dilute-phase. The predictions in case of m_s = 18 t/h are bit accurate in case of dilute phase.

The models for ESP dust (equation 5.13 and 5.14) were evaluated by predicting total pipe-line pressure drop in pipe-lines (69mm ID and 168m long, 69mm ID and 554m long and 105mm ID and 168m long). The results obtained for pressure drop are plotted on the PCC and are compared with the experimental pressure drop values. The resultant PCC are shown in the Figure 5.6, 5.7 and 5.8.

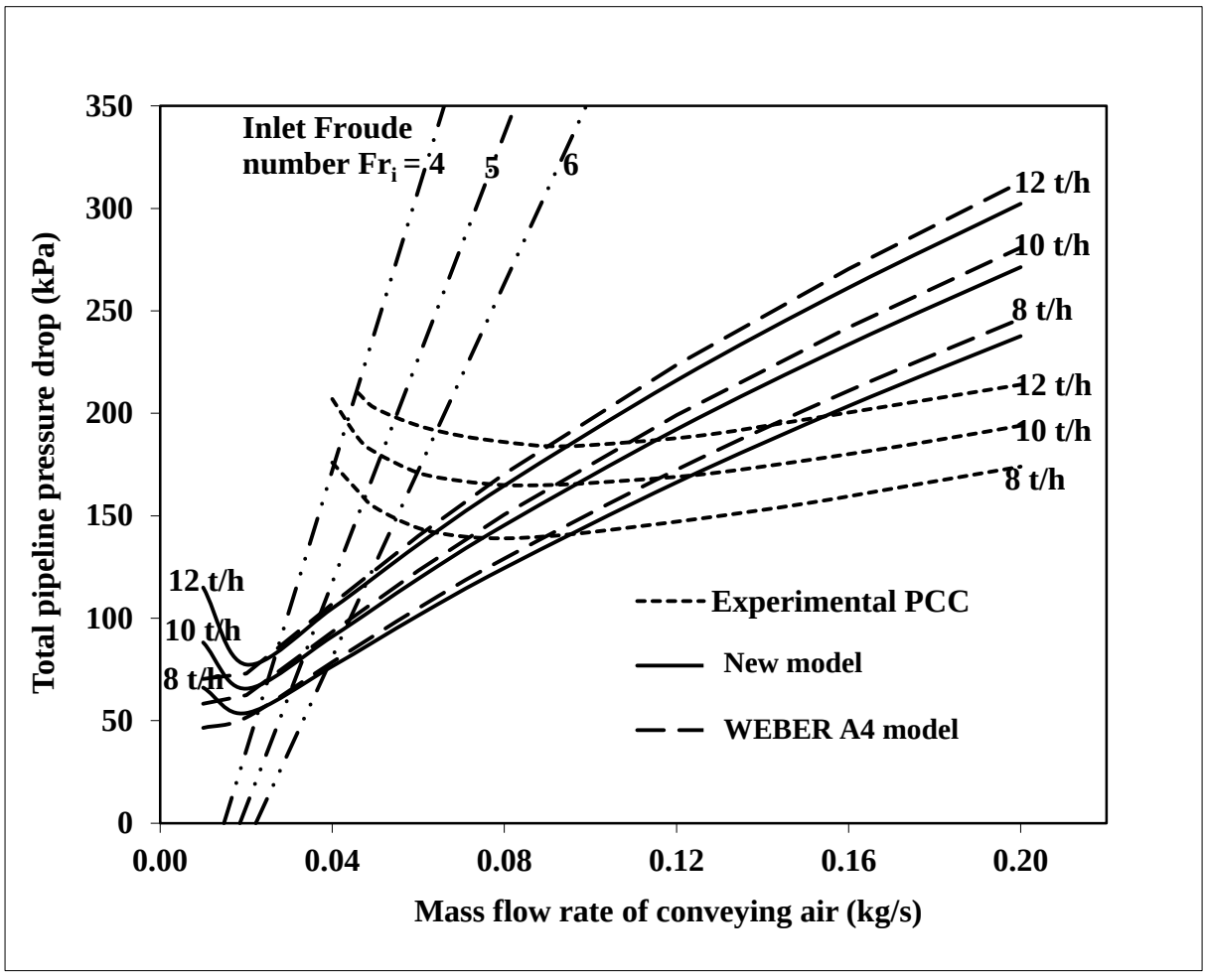

Figure 5.6: Experimental Versus Predicted PCC for ESP dust and 69 mm I.D. × 168 m Pipe using Equations (5.13) and (5.14)

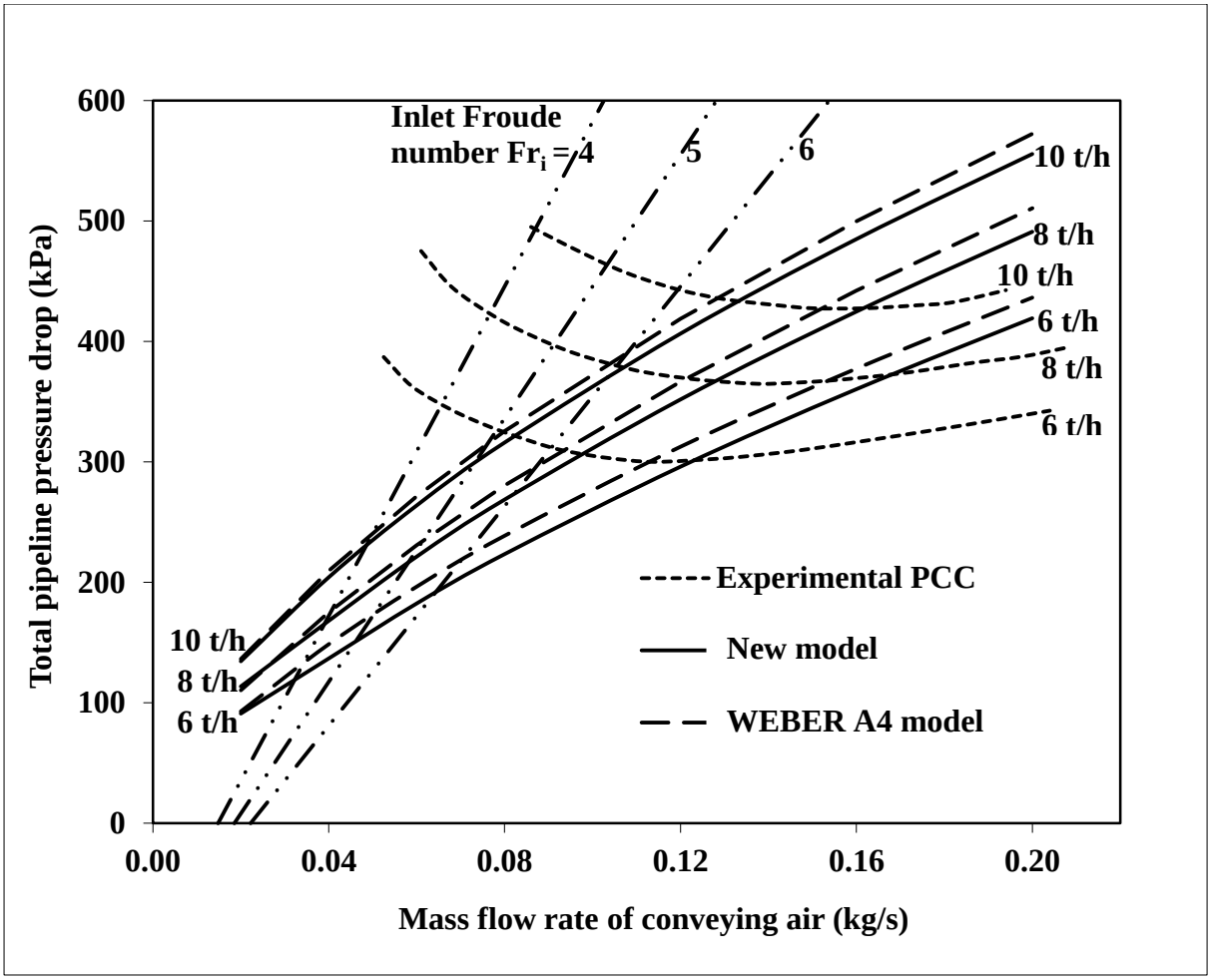

Figure 5.7: Experimental Versus Predicted PCC for ESP dust and 69 mm I.D. × 554 m Pipe using Equations (5.13) and (5.14)

Figure 5.6 shows that the constant mass flow rate line obtained are providing significant over-prediction in dilute phase (i.e. at high m_f air flows) and giving gross under-predictions in dense phase (i.e. at low m_f values). The predictions obtained are of overall poor quality. There is no such 'U'-shape trend exhibited by new model, only at small m_f values 'U'-shape trend is seen. Similar predictions are seen in case of Figure 5.7 where prediction of the ESP dust models (equation 5.13 and 5.14) for, 69 mm ID × 554m long pipe line are shown. A surprising result is seen in the Figure 5.7 the pressure drop is continuously decreasing with

the decrease in m_f values, which was not apparent for the other predictions (i.e. in Figures 5.3 to 5.6). It is due to very low values of terminal velocity values (0.005 m/s) for ESP dust. The new model (equation 5.14) predictions are drawn on to the experimental PCC for ESP dust and 105mm ID and 168m long pipe and the results are shown in Figure 5.8.

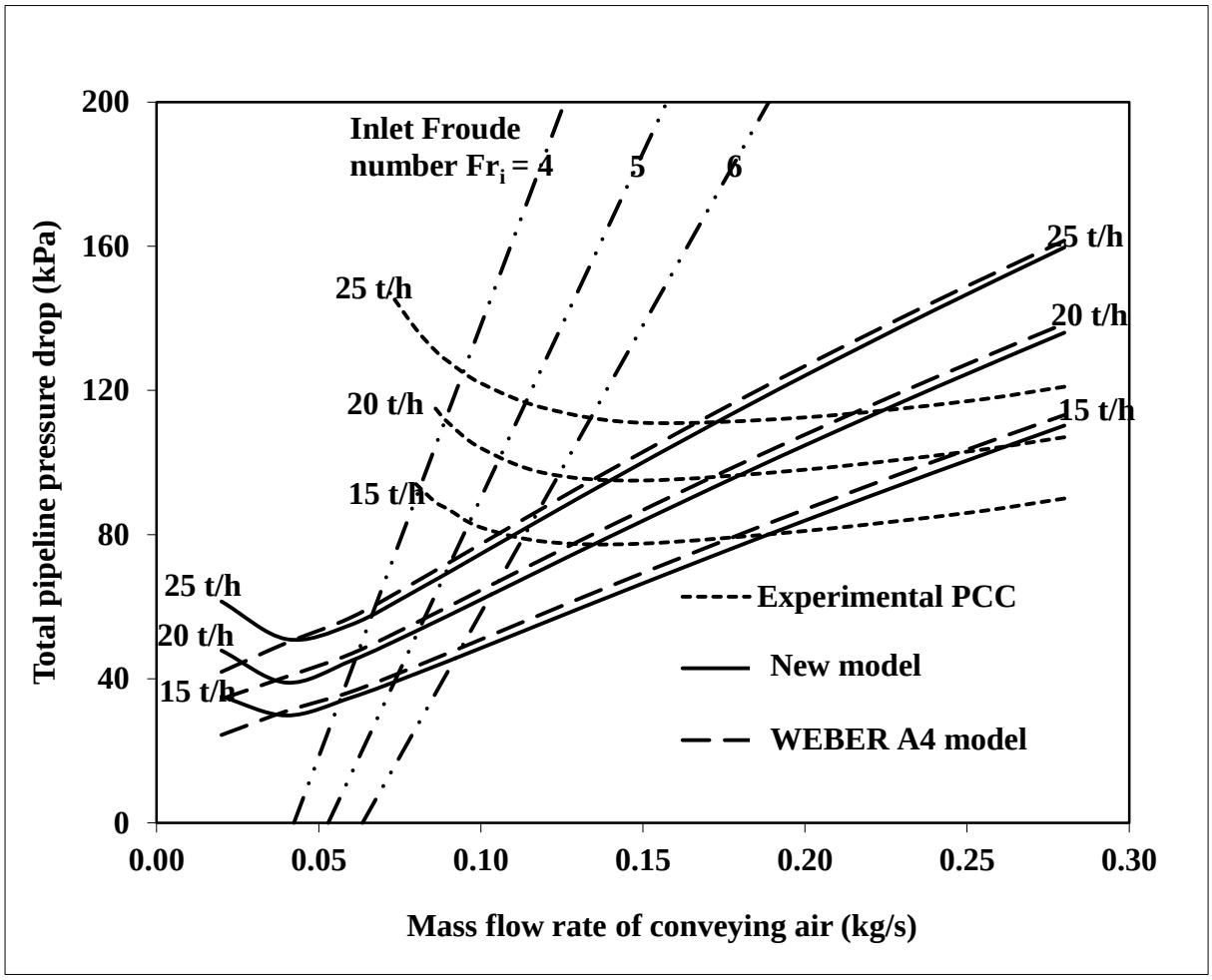

Figure 5.8: Experimental Versus Predicted PCC for ESP dust and 105 mm I.D. × 168 m Pipe using Equations (5.13) and (5.14).

Figure 5.8 shows that the constant mass flow rate of solid lines obtained are providing significant over-prediction in dilute phase (i.e. at high m_f air flows) and giving gross under-

predictions in dense phase (i.e. at low m_f values). The pressure drop is continuously decreasing with the decrease in m_f values; a very small increase in pressure drop is seen at very low m_f values.

5.3 Packed bed modelling

From the above evaluation of the new models it is seen that the model gives better prediction than that of the orignal WEBER A4 model, but the predictions are generally not accurate when compared to experimental data. The results are good in case of fly ash where value of terminal settling velocity is 0.06 m/s, which in turn gives good contribution to β/3 term in the new model, but in case of ESP dust the value of terminal velocity is 0.005 m/s, which in turn provides insignificant contribution to of β/3 term. Hence the results are not so good in case of ESP dust. So, to obtain good predictions from the model, more advancement in pressure drop model was required. An attempt for that was made as given in the following:

In pneumatic conveying the particles, are flowing with the fluid in the same direction (as shown in the Figure 5.9). The particle shown are flowing along with the fluid with velocity C m/s and the velocity of fluid is V m/s. The velocity of fluid must be more than that of the velocity of particles as shown in the Figure 5.9. Solid particles produce hindrance to the flowing fluid.

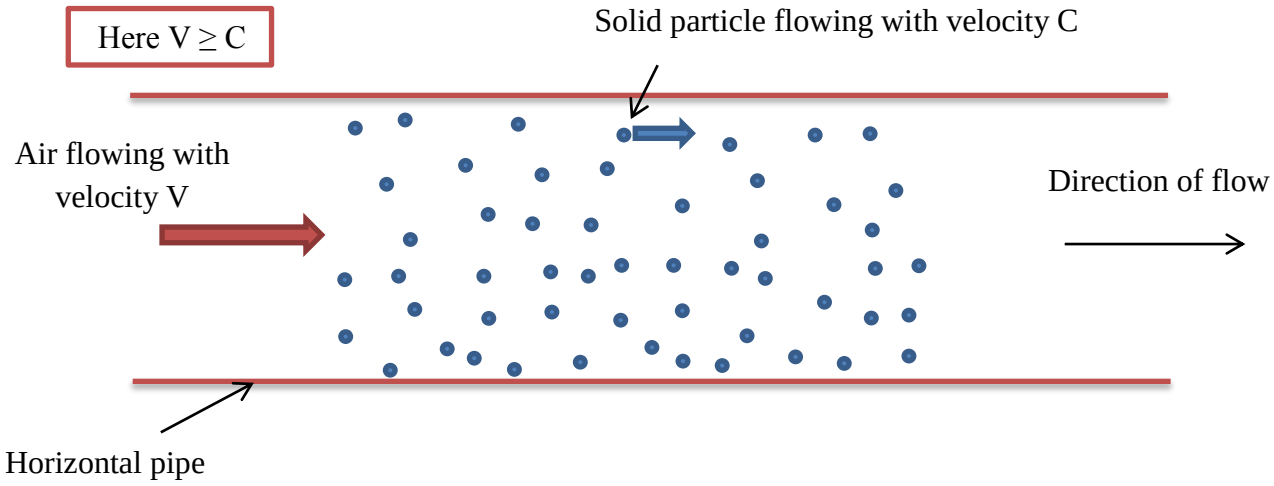

Figure 5.9: Pneumatic conveying (assuming particle are flowing with fluid)

Now for considering the effect of hindrance of the particles relative method is used. The particles are assumed to be at rest and the fluid is flowing through the passage between them as shown in the Figure 5.10. The relative velocity of the fluid with respect to particle is (V-C). So the fluid is considered as if it is flowing through the solid particles with velocity V-C m/s and solid particle are at rest.

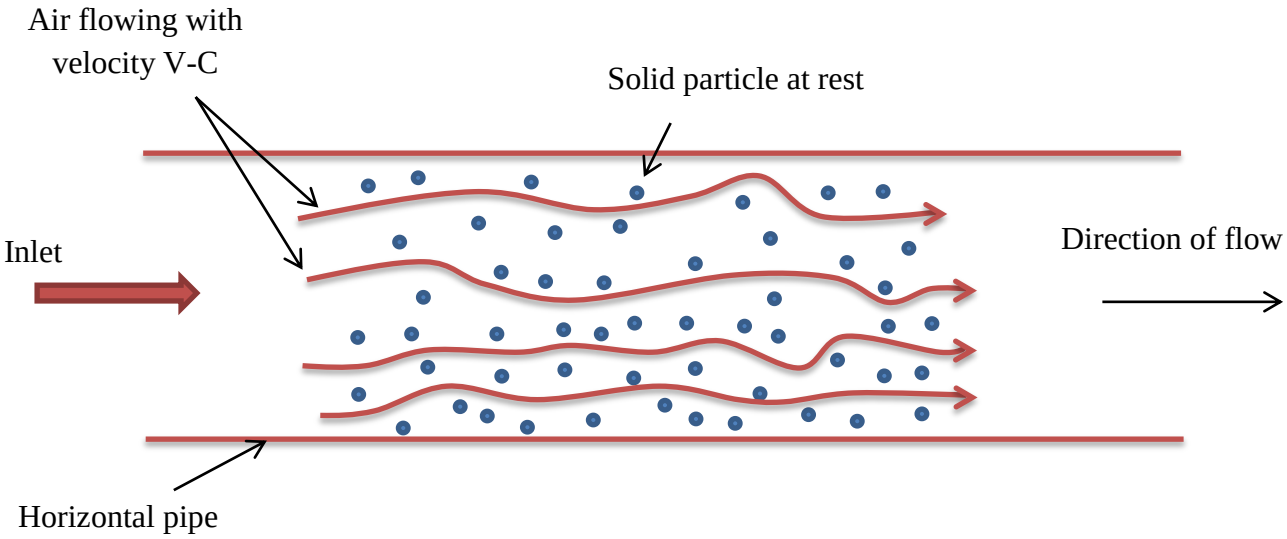

Figure 5.10: Pneumatic conveying (assuming particles are at rest)

As described in the Figure 5.10 the model must be modified with the hindered pressure drop. Geankoplis and Christie (2003) derived the expression for the similar packed bed flow pressure drop. The expression named as Ergun equation, provided in equation 5.15.

$$\Delta p = \frac{150\mu V \Delta L}{{D_p}^2}\frac{(1-\varepsilon)^2}{\varepsilon^3} + \frac{1.75\rho V^2 \Delta L}{D_p}\frac{(1-\varepsilon)}{\varepsilon^3} \tag{5.15}$$

The final expression proposed in the Ergun equation is used for obtaining the pressure drop loss due to the hindrance of the particles. So by adding the pressure drop calculated from the new model to the pressure drop calculated from the Ergun's equation (for a packed bed having fluid velocity as relative velocity i.e. V-C), pressure drop can be calculated. Hence the new expression obtained by the adding the equations 5.1 and equation A.17 (after replacing V by V-C) is provided in the equation 5.16.

$$\Delta p = \frac{150\mu (V-C) \Delta L}{{D_p}^2}\frac{(1-\varepsilon)^2}{\varepsilon^3} + \frac{1.75\rho (V-C)^2 \Delta L}{D_p}\frac{(1-\varepsilon)}{\varepsilon^3} + \frac{(\lambda_f + m^* \lambda_s) L \rho V^2}{2D} \tag{5.16}$$

Where

$$\lambda_s = {\lambda_s}^* \frac{C}{V} + \frac{2\beta}{Fr^2 {C}/{V}} \tag{5.17}$$

The above expression for pressure drop is evaluated for fly ash and 69 mm ID and 168 m long pipe line. The value of λ_s^* is calculated as 0.00131 for a very dilute-phase experimental

data point with the help of equations 5.13 and 5.14. Then by using the total pipe-line pressure drop macro programing, the pressure drop is calculated with the help of equations 5.16 and 5.17. The prediction obtained exhibits gross amount of pressure drop (e.g. for m_s equal to 9 t/h and m_f equal to .02 kg/s the pressure drop is coming out to be 16995 kPa), which shows that the above model (equation 5.13 and 5.14) is inaccurate.

CHAPTER 6: Conclusions and Future Scope of Work

6.1 Conclusions

Based on the results presented in this thesis, it can be concluded that even for the same product, straight-pipe PCC can be different depending on pipeline diameter or length and location of pressure tapping points on the same pipeline. This indicates that the flow mechanism changes along the flow direction. Straight-pipe PCC obtained from initial tapping points in the pipeline have generally shown steeper PCC than those obtained further along the pipeline. There was no distinct PMC in any of the straight pipe PCC, indicating that even if there were a flow transition (change in flow mechanism from dense- to dilute-phase), the change was very gradual. The nature of the "U"-shape and location of the PMC for the total pipeline PCC are significantly influenced by the pipeline layout (e.g. location and number of bends) and not entirely by the dense- to dilute-phase transition of flow mechanism.

The different models for PMC proposed by previous researchers were not providing accurate results. A proposed new model and its predictions were presented, it can be concluded that, the new model is representing the Pressure Minimum Curve (PMC) (i.e. showing change in flow mechanism from dense- to dilute-phase) in case of fly ash (69mm ID and 554m long pipe) and white powder (69mm ID and 148m long pipe). The model predictions are much better than the predictions shown by the models proposed by other researchers, but only limited validation of the model was done here due to lack of data. Further research has to be conducted, to understand the change in flow characteristics along the flow direction (dense- to dilute-phase) and to validate the model experimentally.

The pressure drop model developed by considering the particle and particle collision (new model) has provided better prediction for fly ash than that of the original WEBER A4 model. The model did not perform well in case of ESP dust due to very small value of terminal

velocity. The new model for fly ash and ESP dust exhibits 'U'-shape trend, which was very similar to the trend shown by experimental data line. The model proposed by considering the Ergun equation (packed bed model) predicts a huge over prediction. Further research should be required to predict the dense-phase pressure drop model.

6.1 Future Scope of work

The following areas of investigation still require further attention:

a) Understanding the change in flow characteristics along the flow direction (dense- to dilute-phase), future research may be carried out to experimentally validate the proposed model for scale up considerations and by employing different models for different regimes (as the flow phenomena of dense- and dilute-phase are very different: non-suspension to suspension flow mode).

b) To understand the change in flow mechanisms, experimental data are to be generated for different fine powders and pipe layouts, to validate the model proposed in this thesis. A new empirical relation must be obtained using that data which will explain the change in flow mechanism.

c) Further work must be done to predict a pressure drop model which will work significantly well for both dense- and dilute-phase, empirical approach will be used for the modelling. The effect of particle hindrance and settling will be considered further during the modelling. The flow of single solid particle in FDP is to be studied, both experimentally and empirically.

LIST OF PUBLICATIONS

Referred Journals (Under Review)

Bansal, A., Mallick S.S. and Wypych P.W. Investigating Straight Pipe Pneumatic conveying characteristics for fluidized dense phase pneumatic conveying. *Particulate Science and Technology.*

Conferences papers (Published/Accepted)

Setia, G., **Bansal, A.** and Mallick, S.S. Investigating Straight-Pipe Pneumatic Conveying Characteristics and Minimum Transport Boundaries for Fluidized Dense-Phase Pneumatic Conveying of Fine Powders. *CHoPS 2012 conference, 10 to 13 September 2012, Friedrichshafen, Germany (Accepted for oral presentaion).*

Bansal, A., Setia G. and Mallick, S.S. Investigating pneumatic conveying characteristics and minimum transport velocity for fluidised dense-phase transport of fine powders. *TACEE-2012, 23 to 24 march, 2012, BITS Pilani.*

LIST OF SYMBOLS AND ABBREVIATIONS

Ar	Archimedes number
B	Bend loss factor
C	Particle velocity in suspension [m/s]
D	Internal diameter of pipe [m]
d	Particle diameter [m]
d_{50}	Median particle diameter [μm]
f_{g-s}	Gas-solid friction factor
$\mathrm{Fr} = \frac{V}{\sqrt{gD}}$	Froude number of flow
$\mathrm{Fr}_i = \frac{V_i}{\sqrt{gD}}$	Froude number at pipe inlet
$\mathrm{Fr}_m = \frac{V_m}{\sqrt{gD}}$	Mean Froude number related to the section of pipe
Fr_{bo}	Froude number of flow at bend outlet
Gs	Product mass flow rate per unit area, $Gs = m_s/A[kg/sm^2]$
g	Acceleration due to gravity [m/s^2]
L	Length of pipe or test section [m]
m_f	Mass flow rate of air [kg/s]
m_p	Mass of each particle [kg]
m_s	Mass flow rate of solids [kg/s]

$m^* = m_s / m_f$	Solids loading ratio
$\overline{m^*}$	Average solid-gas loading ratio
ΔM_p	Total mass of particles in a control volume
N	Total number of particles in a control volume
ΔP	Pressure drop through a straight horizontal pipe [Pa]
ΔP_g	Pressure drop due to flowing gas only
ΔP_s	Pressure drop due to presence of solids
R	Radius of pipe [m]
$Re = \rho VD/\mu$	Reynolds number of gas
Re_p	Particle Reynolds number
V	Superficial air/gas velocity [m/s]
V_f	Volume of air in a control volume [m/s]
V_s	Volume of solids in a control volume [m/s]
V_∞	Free settling velocity of particle [m/s]
W_f, U_t	Settling velocity of the particle [m/s]
ρ	Density [kg/m^3]
$\rho_{sus} = \frac{Mass\ of\ solids + Mass\ of\ gas}{Volume\ of\ solids + Volume\ of\ gas}$	Suspension density [kg/m^3]
ρ_m	Mean air density for a pipeline section [kg/m^3]
ρ_p	Particle density [kg/m^3]

ρ_s	Particle density [kg/m^3]
ρ_{bo}, ρ_o	Density of air bend outlet [kg/m^3]
$\beta = W_f/V$	Velocity ratio related to particle fall velocity in a cloud
ε	Voidage
λ_{bs}	Solids friction factor through bends
λ_f	Air/gas only friction factor
λ_{fb}	Air only friction factor in bend
λ_s	Solids friction factor through straight pipe
λ_s^*	Impact and friction factor
C/V	ratio at minimum transport condition
μ	Dynamic viscosity for single fluid (e.g. air) [Pas]
τ_{w-sf}	Shear stress due to friction between wall and solid-gas mixture.

Subscripts

e	exit
f	Fluid (air)
h	Horizontal
i	inlet condition

m	Mean value for the section/interval of pipe, based on average air density
min	Minimum
p	particle
s	Solids
v	Vertical (equation 8.9)

Abbreviations

ESP	Electro Static Precipitator
I.D.	Internal Diameter of pipe
PCC	Pneumatic Conveying Characteristics
PMC	Pressure Minimum Curve

References

Ashenden, S.J., Pittman A.N. and Bradley, M.S.A. 1995. An economic assessment of air assisted gravity conveying as an alternative to pneumatic conveying. 5th Int. Conf. on Bulk Materials Storage, Handling and Transportation, Newcastle, Australia.

Barth, W. 1963. deposition transport and re-raise of fine particles in an airstream, CIT (35): 209-214

Bi, H.T., Grace, J.R. 1995. Flow regime diagrams for gas-solid fluidization and upward transport, Journal of Multiphase Flow (21): 1229–1236.

Cai L., Xaioping C., Pan X., Changsui X., 2011, Effect of moisture content on conveying characteristics of pulverized coal for pressurized entrained flow gasification, Experimental Thermal and Fluid Science, 35(6): 1143-1150.

Cabrejos, F.J. and G.E. Klinzing: Minimum Conveying Velocity in Horizontal Transport and the pickup and saltation mechanisms of solid particles ; bulk solid handling Vol 14 (1994) No. 3: 349-353.

Cengel, Yunus A. Heat and Mass Transfer: A Practical Approach, 3rd Edition (Boston: McGraw Hill, 2003).

Datta B. K., and Ratnayaka C. 2005. A possible scaling –up technique for dense phase pneumatic conveying, Particlulate Science and Technology, Vol. 23: 201-204

Datta, Biplab K., Ratnayaka, C., Saasen, Arild and Bastesen, Yngve 2003. A new design approach for pneumatic conveying, Annual transactions of the Nordic Rheology Society, Vol. 11: 57-62

Jones, M.G. and Williams, K.C. 2003. Solids friction factors for fluidized dense phase conveying. Particulate Science and Technology. (21): 45-56.

Kalman H., A. Satern, D. Meir and E. Rabinovich 2005. Pickup (critical) velocities of particles, Powder Technology, Vol. 160: 103-113.

Keys, S. and Chambers, A.J. 1993. Scaling pneumatic conveying characteristics for pipeline pressure drop. In the proceedings of National Conference on Bulk Materials Handling, Preprints, Capricorn International Resort, Yeppoon, Queensland, 22-25 September: 205-213.

Klintworth, J. and Marcus, R.D. 1985. A review of low-velocity pneumatic conveying systems, Bulk Solids Handling, Vol. 5, No. 4: 747-753.

Klinzing G.E., Myler C.A., Zaltash A. and Dhodapkar S. 1989. A simplified correlation for solid friction factor in horizontal conveying system based on Yang's unified theory, Powder Technology, Vol. 58: 187-193

Leung, M.C. 1974. Phase transition and phonon-drag conductivity. Chemical Engineering, Volume 2. Pergamon press.

Mainwaring N.J. and Reed, A.R. 1987. Bulk Solids Handling, Applied Science Publishers, London, Vol. 7, No. 3: 415-425.

Marcus, R.D., Leung, L.S, Klinzing, G.E. and Rizk, F. 1990. Pneumatic conveying of solids - A theoretical and practical approach. Publ. Chapman and Hall.

Matsumoto, S., M. Hara, S. Saito and S. Maeda: Minimum Transport Velocity for horizontal pneumatic conveying: Journal of Chemical Engineering of Japan, Vol. 7 (1974) No. 6: 425-431.

Mallick, S.S. and Wypych, P.W. 2009. Minimum transport boundaries for pneumatic conveying of powders, Powder Technology (194): 181–186

Mallick, S.S. 2010. PhD Dissertation: Modelling of Fluidised Dense-Phase Pneumatic Conveying of Powders university of Wollongong.

Mills, D. 2004. An investigation of the unstable region for dense phase conveying in sliding bed flow, Granular Matter (6): 173–177

Ochi, M., 1991, Saltation velocity of the gas solid Two-Phase flow in a horizontal pipe; Proc. The first ASME-JSME Fluids Engineering Conference, FED-121: 349-353.

Pan, R. and Wypych, P.W. 1998. Dilute and dense phase pneumatic conveying of fly ash. In the proceedings of 6th International Conference on Bulk Materials Storage and Transportation, Wollongong, NSW, Australia: 183-189.

Pan, R., Mi, B. and Wypych, P.W. 1994. Pneumatic conveying characteristics of fine and granular bulk solids. KONA (Powder and Particle). (12): 77-85.

Pan, R. 1992. PhD Dissertation: Improving scale-up procedures for the design of pneumatic conveying systems University of Wollongong.

Rabinovich, E. and Kalman, H. 2010. Flow regime diagram for vertical pneumatic conveying and fluidized bed systems, Powder Technology (207): 119–133.

Rabinovich, E. and Kalman, H. 2009. Incipient motion of individual particles in horizontal particle–fluid systems: B. Theoretical analysis, Powder Technology (192): 326–338.

Rabinovich, E. and Kalman, H. 2008. Generalized master curve for threshold velocities in particle-fluid systems, Powder Technology (183): 304–313.

Rao, C. Syamala 1975. A pressure drop correlation for gas-solids flow through similarity analysis, Indian Journal of Technology, Vol. 13: 435-437

C. Ratnayake 2000, Experimental Investigation of Scaling Techniques in Pneumatic Transportation, The POSTEC Newsletter, No. 19: 12-13.

Ratnayake, C. 2005. PhD Dissertation: A Comprehensive Scaling Up Technique for Pneumatic Transport Systems, Norwegian University of Sceince and Technology (NTNU).

Rizk, F. 1982. Pneumatic transport in dilute and dense phase. Bulk Solids Handling. (2): 235-241.

Rizk, F. 1976. Pneumatic conveying at optimal operating conditions and a solution of Barth's equation $\lambda z = \Phi (\lambda z^*, \beta)$. In the proceedings of 3rd International Conference on the Pneumatic Transport of Solids in Pipes, 7-9th April: D4: 43-58.

Rizk, F. 1973. Pneumatic conveying of plastic coarse material in horizontal ducts, taking into consideration the influence of height in connection with the properties of the solid and the pipe materials, especially in the optimal operating zone. Dissertation University Karlsruhe (TH).

Rose, H.E. and R.A. Duckworth: Transport of solid particles in liquid and gasses; The Engineer, Vol. 227 (1969) No. 5903: 392-396.

Schaberg, F. and Mehring, B. F. 1987. Dense phase conveying: large outputs/long distances, Proc Pneumatech (4): 281–299

Schade, B. 1987: Zum ubergang Sprung-strahnenforderung bieder Horizontalen Pneumatischen Feststoffordrung; Dissertation, University of Karlsruhe.

Schroter, K. 1965. pneumatic conveying in particular the diffuse phase transport, Aufber Techn. Nr.6.

Schuchart, P. 1968. Widerstansgesetze beim pneumatischen Transport in Rohrkrummern, Symposium series no. 27 (The Institution of Chemical Engineers): 65 – 72.

Shigemoto, N., Hayashi, H. and Miyaura K. 1993. Selective formation of Na-X zeolite from coal fly ash by fusion with sodium hydroxide prior to hydrothermal reaction, Journal of Materials Science (28): 4781-4786.

Stegmaier, W. 1978. Zur berechnung der horinentalen pneumatischen forderung feinkorniger feststoffe - for the calculation of horizontal pneumatic conveying of fine grained solids. Fordern and Heben. (28): 363-366.

Weber, M. 1981. Principles of hydraulic and pneumatic conveying on pipes. Bulk Solids Handling. 1 (1): 57-63.

Williams, K.C. and Jones, M.G. 2006. Solid friction power law variations and their influence on pressure losses in fluidised dense phase pneumatic conveying. In 320 the proceedings of The Fifth World Congress on Particle Technology. April 23-26, Florida, USA.

Williams, K.C. and Jones, M.G. 2004. Numerical model velocity profile of fluidised dense phase pneumatic conveying. In the proceedings of 8th International Conference on Bulk Materials Storage and Transportation, Wollongong, NSW, Australia, 5-8 July: 354-358.

Wypych, P. W. 1989. PhD Dissertation: Pneumatic conveying of bulk solids, University of Wollongong.

Wypych, P.W. and Arnold, P.C. 1989. Plug-phase pneumatic transportation of bulk solids and the importance of blow tank air injection, Powder Handling and Processing, Vol. 1, No. 3: 271-275.

Wypych, P.W. and Hauser, G. 1990. Design considerations for low-velocity conveying systems & pipelines. Pneumatech 4, Glasgow, Scotland.

Wypych, P.W., Kennedy, O.C. and Arnold, P.C. 1990. The future potential of pneumatically conveying coal through pipelines. Bulk Solids Handling. 10(4): 421-427

Wypych, P.W and Yi, J. 2003. Minimum transport boundary for horizontal dense phase pneumatic conveying of granular materials. Powder Technology. (129):111-121.

Wypych, P.W., Hastie, D. B. and Yi, J. 2005. Prediction of optimal operating conditions for dense-phase pneumatic conveying systems. Final research report for the International Fine Particle Research Institute, Inc, USA.

Wypych P.W. 2006. Course notes written on pneumatic conveying of bulk solids and dust control, University of Wollongong.

Yi, J., Wypych, P.W. and Pan, R. 1998. Minimum conveying velocity in dilute-phase pneumatic conveying. Powder Handling and Processing. 10 (3): 255-261.

Zegler, Frank; Bernard Kutter (2010-09-02). "Evolving to a Depot-Based Space Transportation Architecture". AIAA SPACE 2010 Conference & Exposition. AIAA. Retrieved 2011-01-25. "It consumes waste hydrogen and oxygen to produce power, generate settling and attitude control thrust."

Appendix A

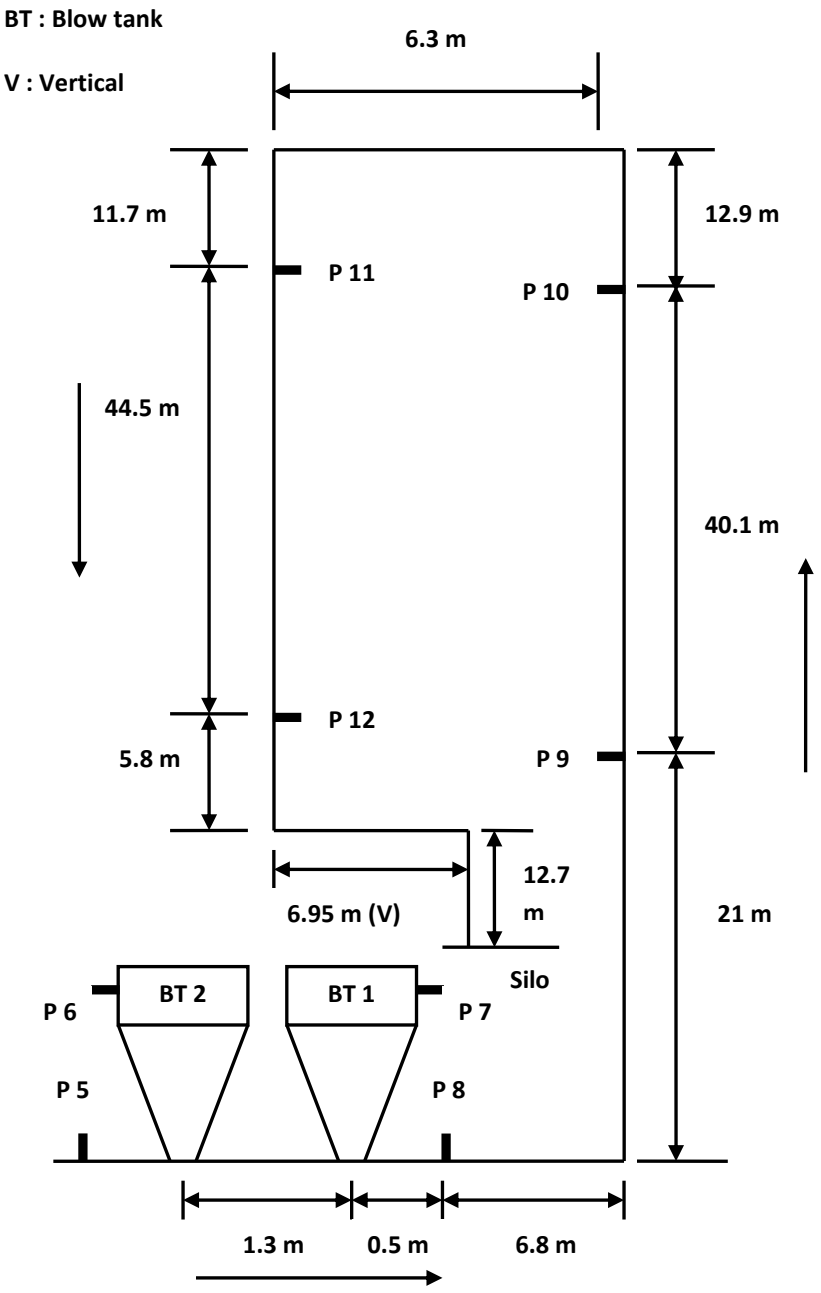

Figure A1: Layout of the 105 mm I.D. × 168 m long test rig for fly ash

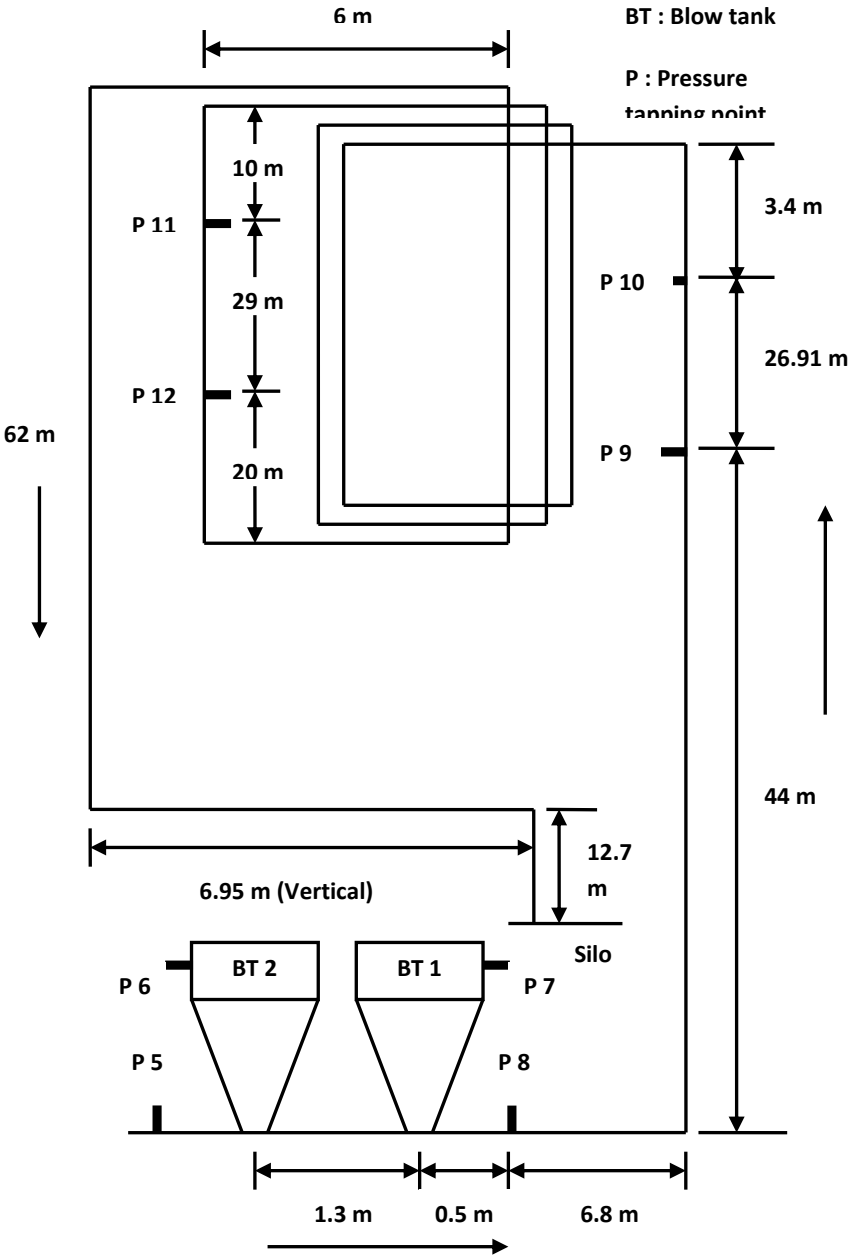

Figure A2: Layout of the 69 mm I.D. × 554 m long test rig for fly ash

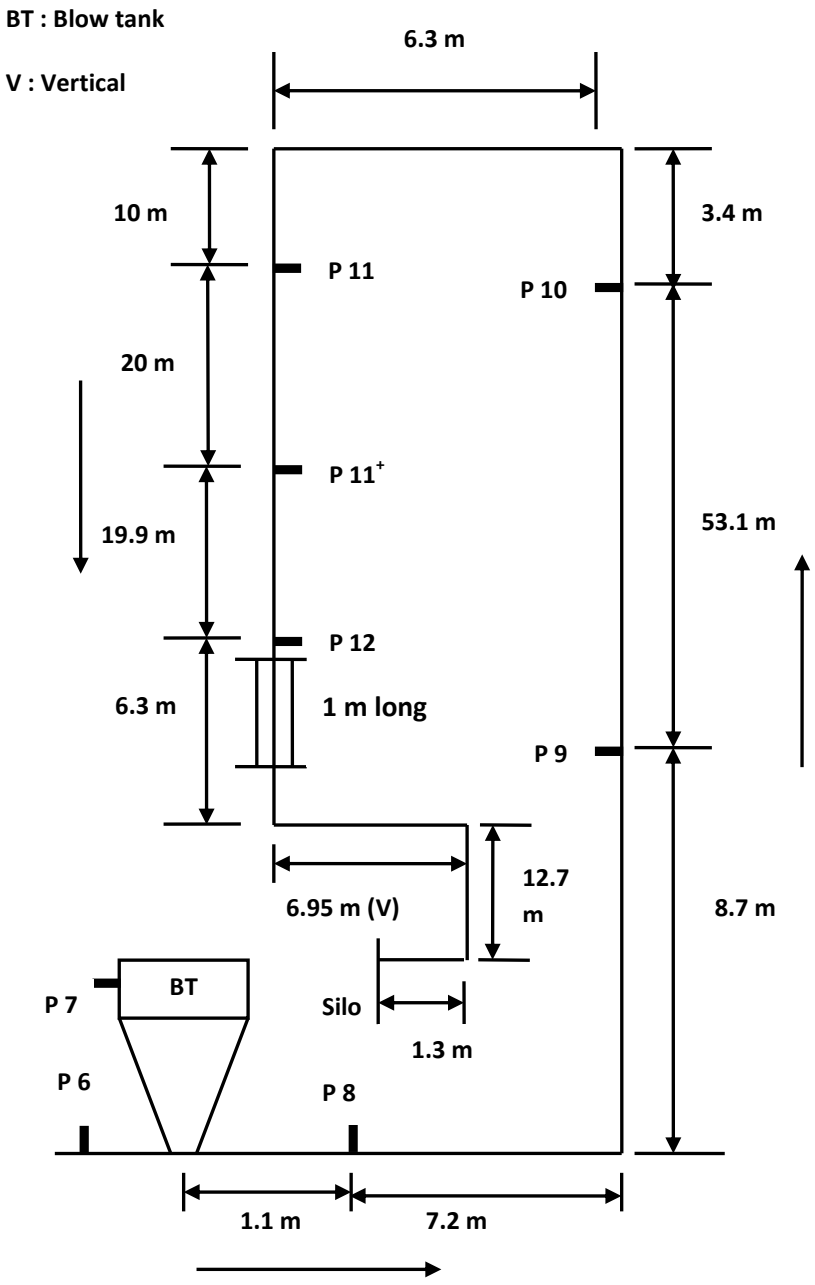

Figure A3: Layout of the 69 mm I.D. × 148 m long test rig for white powder

Programme for calculating total pipe line pressure drop

Horizontal straight section L1: 1st section from exit		
Pipe cross sectional area	m2	0.0037
solid loading ratio (m*)		55.556
Exit Condition		
density of air at exit	kg/m3	1.204
superficial air velocity at exit	m/s	15.544
Froude number at exit		18.893
Assumed Pressure loss	**kPa**	**6.608**
Entry Condition		
density of air at inlet	kg/m3	1.283
superficial air velocity at inlet	m/s	14.592
Froude number at inlet		17.736
Average Condition		
Average air density	kg/m3	1.244
Air velocity at average condition	m/s	15.053
Air viscosity at average condition	Pa.S	***0.000018***
Reylonds Number for average condition		***71115.908***
Froude Number for average condition		***18.297***
vs/Vfm		***0.9971***
vs (particle velocity)	m/s	***15.0094***
Solid friction factor (λs) for average condition		***0.0045***
Air only friction factor (λf) for average condition		***0.019***
Pressure drop for average condition	**kPa**	***6.608***
Pressure difference	kPa	**0.000**
Pressure at entry to the section	kPa (g)	***6.608***
Pressure at entry to the section	kPa (a)	107.933
Bend B1		
Air density at bend outlet	kg/m3	1.283
Air velocity at bend outlet	m/s	14.592
RB/r = Radius of curvature of bend/ pipe radius		28.986
Reynolds number (Re)		71115.908
Re. {r/RB}^2		84.646
Air only friction factor through bend (λfb)		0.550
Solid friction factor at bend outlet		1.301
Pressure drop due to solid + air through bend	kPa	3.862
Total pressure drop due to bend	**kPa**	**3.862**
Pressure at the entry of bend	kPa (g)	***10.471***
Pressure at the entry of bend	kPa (a)	111.796
Vertical lift loss due to elevation H		
Pipe cross sectional area	m2	0.0037

solid loading ratio (m*)		55.556
Exit Condition		
density of air at exit	kg/m3	1.329
superficial air velocity at exit	m/s	14.088
Froude number at exit		17.124
Assumed Pressure loss	**kPa**	**10.080**
Entry Condition		
density of air at inlet	kg/m3	1.449
superficial air velocity at inlet	m/s	12.923
Froude number at inlet		15.707
Average Condition		
Average air density	kg/m3	1.389
Air velocity at average condition	m/s	13.481
Air viscosity at average condition	Pa.S	0.000018
Reylonds Number for average condition		71115.908
Froude Number for average condition		16.385
vs/Vfm		0.9971
vs (particle velocity)	m/s	13.4413
Solid friction factor (λs) for average condition		***0.0047***
Air only friction factor (λf) for average condition		0.019
Pressure drop due to friction for average condition through lift of 'h'	**kPa**	**3.594**
Pressure drop due to Elevation of materials through evelation of 'H'	**kPa**	**6.487**
Total pressure loss through the elevation	**kPa**	**10.080**
Pressure difference	kPa	**0.000**
Pressure at entry to the section	kPa (g)	***20.551***
Pressure at entry to the section	kPa (a)	121.876
Bend B2		
Air density at bend outlet	kg/m3	1.449
Air velocity at bend outlet	m/s	12.923
RB/r = Radius of curvature of bend/ pipe radius		28.986
Reynolds number (Re)		71115.908
Re. {r/RB}^2		84.646
Air only friction factor through bend (λfb)		0.550
Solid friction factor at bend outlet		1.073
Pressure drop due to solid + air through bend	kPa	3.420
Total pressure drop due to bend	**kPa**	**3.420**
Pressure at the entry of bend	kPa (g)	***23.971***
Pressure at the entry of bend	kPa (a)	125.296
Horizontal straight section L2		
Pipe cross sectional area	m2	0.0037
solid loading ratio (m*)		55.556
Exit Condition		

density of air at exit	kg/m3	1.489
superficial air velocity at exit	m/s	12.570
Froude number at exit		15.279
Assumed Pressure loss	**kPa**	**40.589**
Entry Condition		
density of air at inlet	kg/m3	1.972
superficial air velocity at inlet	m/s	9.495
Froude number at inlet		11.540
Average Condition		
Average air density	kg/m3	1.730
Air velocity at average condition	m/s	10.818
Air viscosity at average condition	Pa.S	0.000018
Reylonds Number for average condition		71115.908
Froude Number for average condition		13.149
vs/Vfm		0.9971
vs (particle velocity)	m/s	***0.0536***
Solid friction factor (λs) for average condition		0.0161
Air only friction factor (λf) for average condition		0.019
Pressure drop for average condition	**kPa**	**40.589**
Pressure difference	kPa	**0.000**
Pressure at entry to the section	kPa (g)	***64.561***
Pressure at entry to the section	kPa (a)	165.886
Horizontal straight section L3		
Pipe cross sectional area	m2	0.0037
solid loading ratio (m*)		55.556
Exit Condition		
density of air at exit	kg/m3	1.972
superficial air velocity at exit	m/s	9.495
Froude number at exit		11.540
Assumed Pressure loss	**kPa**	**12.151**
Entry Condition		
density of air at inlet	kg/m3	2.116
superficial air velocity at inlet	m/s	8.847
Froude number at inlet		10.753
Average Condition		
Average air density	kg/m3	2.044
Air velocity at average condition	m/s	9.159
Air viscosity at average condition	Pa.S	0.000018
Reylonds Number for average condition		71115.908
Froude Number for average condition		11.132
vs/Vfm		0.9971
vs (particle velocity)	m/s	9.1324
Solid friction factor (λs) for average condition		***0.0055***
Air only friction factor (λf) for average condition		0.019

Pressure drop for average condition	**kPa**	**12.151**
Pressure difference	kPa	**0.000**
Pressure at entry to the section	kPa (g)	***76.711***
Pressure at entry to the section	kPa (a)	178.036
Bend B3		
Air density at bend outlet	kg/m3	2.116
Air velocity at bend outlet	m/s	8.847
RB/r = Radius of curvature of bend/ pipe radius		28.986
Reynolds number (Re)		71115.908
Re. {r/RB}^2		84.646
Air only friction factor through bend (λfb)		0.550
Solid friction factor at bend outlet		0.588
Pressure drop due to solid + air through bend	kPa	2.342
Total pressure drop due to bend	**kPa**	**2.342**
Pressure at the entry of bend	kPa (g)	***79.053***
Pressure at the entry of bend	kPa (a)	180.378
Horizontal straight section L4		
Pipe cross sectional area	m2	0.0037
solid loading ratio (m*)		55.556
Exit Condition		
density of air at exit	kg/m3	2.144
superficial air velocity at exit	m/s	8.732
Froude number at exit		10.613
Assumed Pressure loss	**kPa**	**1.846**
Entry Condition		
density of air at inlet	kg/m3	2.166
superficial air velocity at inlet	m/s	8.643
Froude number at inlet		10.506
Average Condition		
Average air density	kg/m3	2.155
Air velocity at average condition	m/s	8.687
Air viscosity at average condition	Pa.S	0.000018
Reylonds Number for average condition		71115.908
Froude Number for average condition		10.559
vs/Vfm		0.9971
vs (particle velocity)	m/s	8.6620
Solid friction factor (λs) for average condition		***0.0056***
Air only friction factor (λf) for average condition		0.019
Pressure drop for average condition	**kPa**	**1.846**
Pressure difference	kPa	**0.000**

Pressure at entry to the section	kPa (g)	***80.899***
Pressure at entry to the section	kPa (a)	182.224
Bend B4		
Air density at bend outlet	kg/m3	2.166
Air velocity at bend outlet	m/s	8.643
RB/r = Radius of curvature of bend/ pipe radius		28.986
Reynolds number (Re)		71115.908
Re. {r/RB}^2		84.646
Air only friction factor through bend (λfb)		0.550
Solid friction factor at bend outlet		0.567
Pressure drop due to solid + air through bend	kPa	2.288
Total pressure drop due to bend	**kPa**	**2.288**
Pressure at the entry of bend	kPa (g)	***83.187***
Pressure at the entry of bend	kPa (a)	184.512
Horizontal straight section L5		
Pipe cross sectional area	m2	0.0037
solid loading ratio (m*)		55.556
Exit Condition		
density of air at exit	kg/m3	2.193
superficial air velocity at exit	m/s	8.536
Froude number at exit		10.375
Assumed Pressure loss	**kPa**	**13.730**
Entry Condition		
density of air at inlet	kg/m3	2.356
superficial air velocity at inlet	m/s	7.945
Froude number at inlet		9.657
Average Condition		
Average air density	kg/m3	2.275
Air velocity at average condition	m/s	8.230
Air viscosity at average condition	Pa.S	0.000018
Reylonds Number for average condition		71115.908
Froude Number for average condition		10.003
vs/Vfm		0.9971
vs (particle velocity)	m/s	8.2059
Solid friction factor (λs) for average condition		***0.0058***
Air only friction factor (λf) for average condition		0.019
Pressure drop for average condition	**kPa**	**13.730**
Pressure difference	kPa	**0.000**
Pressure at entry to the section	kPa (g)	***96.917***
Pressure at entry to the section	kPa (a)	198.242
Horizontal straight section L6		

Pipe cross sectional area	m2	0.0037
solid loading ratio (m*)		55.556
Exit Condition		
density of air at exit	kg/m3	2.356
superficial air velocity at exit	m/s	7.945
Froude number at exit		9.657
Assumed Pressure loss	**kPa**	**13.255**
Entry Condition		
density of air at inlet	kg/m3	2.514
superficial air velocity at inlet	m/s	7.447
Froude number at inlet		9.051
Average Condition		
Average air density	kg/m3	2.435
Air velocity at average condition	m/s	7.688
Air viscosity at average condition	Pa.S	0.000018
Reylonds Number for average condition		71115.908
Froude Number for average condition		9.344
vs/Vfm		0.9971
vs (particle velocity)	m/s	7.6655
Solid friction factor (λs) for average condition		***0.0060***
Air only friction factor (λf) for average condition		0.019
Pressure drop for average condition	**kPa**	**13.255**
Pressure difference	kPa	**0.000**
Pressure at entry to the section	kPa (g)	***110.171***
Pressure at entry to the section	kPa (a)	211.496
Bend B5		
Air density at bend outlet	kg/m3	2.514
Air velocity at bend outlet	m/s	7.447
RB/r = Radius of curvature of bend/ pipe radius		28.986
Reynolds number (Re)		71115.908
Re. {r/RB}^2		84.646
Air only friction factor through bend (λfb)		0.550
Solid friction factor at bend outlet		0.447
Pressure drop due to solid + air through bend	kPa	1.971
Total pressure drop due to bend	**kPa**	**1.971**
Pressure at the entry of bend	kPa (g)	***112.142***
Pressure at the entry of bend	kPa (a)	213.467
Horizontal straight section L7		
Pipe cross sectional area	m2	0.0037
solid loading ratio (m*)		55.556
Exit Condition		

density of air at exit	kg/m3	2.537
superficial air velocity at exit	m/s	7.378
Froude number at exit		8.968
Assumed Pressure loss	**kPa**	**2.330**
Entry Condition		
density of air at inlet	kg/m3	2.565
superficial air velocity at inlet	m/s	7.299
Froude number at inlet		8.871
Average Condition		
Average air density	kg/m3	2.551
Air velocity at average condition	m/s	7.338
Air viscosity at average condition	Pa.S	0.000018
Reylonds Number for average condition		71115.908
Froude Number for average condition		8.919
vs/Vfm		0.9971
vs (particle velocity)	m/s	7.3168
Solid friction factor (λs) for average condition		***0.0061***
Air only friction factor (λf) for average condition		0.019
Pressure drop for average condition	**kPa**	**2.330**
Pressure difference	kPa	**0.000**
Pressure at entry to the section	kPa (g)	***114.473***
Pressure at entry to the section	kPa (a)	215.798
Acceleartion Pressure Loss at Feed Point		
Pipe cross sectional area	m2	0.0037
density of air at feed point	kg/m3	2.565
superficial air velocity at exit	m/s	7.299
solid loading ratio (m*)		55.556
Accelation pressure loss	**kPa**	**7.591**
Pressure at Feed point	kPa (g)	***122.063***
Pressure at Feed point	kPa (a)	223.388
Pressure drop contributed by Horizontal straight pipes	**kPa**	**90.509**
Pressure drop contributed by Vertical pipes + Bends + Entry losses	**kPa**	**31.554**
Total Pressure drop for the entire pipe	**kPa**	**122.063**